Characterisation of astrocyte diversity in the multiple sclerosis motor cortex



Sydney Alexandra Yee

Keble College
University of Oxford

A thesis submitted for the degree of
Doctor of Philosophy

Trinity Term, 2022

Abstract

Multiple sclerosis (MS) is a chronic inflammatory demyelinating disease of the central nervous system where neurodegeneration often leads to irreversible disability. Clinical and pathological heterogeneity is the rule, with genetic (e.g. *HLA-DRB1*15* status) and environmental factors playing important roles. The mechanisms underlying such heterogeneity remain elusive. Astrocytes, which are involved in MS pathogenesis, are an attractive candidate to contribute to such variation in MS pathology due to their complex functions in health and disease. Recent progress has also challenged the conventional view that astrocytes represent a homogenous population, indicating that astroglial diversity may underscore MS heterogeneity.

In this thesis, we undertake a quantitative neuropathological analysis of GFAP+ and ALDH1L1+ astrocyte subpopulations in the motor cortex of a large cohort of human post-mortem MS cases genotyped at the *HLA-DRB1*15* locus. We find that GFAP+ and ALDH1L1+ astrocytes represent distinct subpopulations that differ in their distribution along the motor cortex and in their relationships with MS pathological outcomes. GFAP+ astrocytes show a greater extent of reactivity in the MS motor cortex, especially in areas of demyelination and in younger *HLA-DRB1*15*+ cases. In contrast, MS ALDH1L1+ astrocytes associate with neuronal density and macrophage/microglial inflammation, a relationship not seen in cases carrying the *HLA-DRB1*15* allele. These astrocyte subpopulations also vary in their relationship with surrogate markers of blood-brain barrier dysfunction with decreasing perivascular GFAP+ astrocyte expression and increasing perivascular ALDH1L1+ astrocyte expression in MS. Given the histopathological differences between the two astrocyte markers, we also perform proteomics using laser capture microdissection coupled to mass spectrometry to probe the deep proteome of GFAP+ and ALDH1L1+ astrocyte subpopulations. Protein expressions show clear differences between GFAP+ and ALDH1L1+ astrocytes. In MS cases, GFAP+ astrocytes abundantly express immune-related proteins compared to ALDH1L1+ astrocytes, which associate with protein expression changes related to synaptic vesicle clustering and voltage-gated potassium channels. Immune-related proteins in astrocyte subpopulations are impacted by the carriage of the *HLA-DRB1*15* allele.

Altogether, our data implicate astrocyte subpopulation diversity as a contributing factor of MS heterogeneity. We suggest that GFAP+ astrocytes have relatively detrimental roles, whilst ALDH1L1+ astrocytes have relatively protective roles in MS. This thesis highlights the pressing need to understand the role of astrocyte diversity in MS so that selective targets amenable to therapeutic modulation may be identified and halt the devastating outcomes of MS.

Dedication

For my grandparents, Eva & Philip Shu and Margery & Albert Yee, who made the courageous choice to emigrate to Canada. All of this was made possible because of your dedication and personal sacrifices. Thank you.

Acknowledgement

This thesis would not be possible without the invaluable support and encouragement of those around me. Your support has made a substantial impact of who I am today, and I cannot express my appreciation enough.

First and foremost, I want to thank my supervisors, Gabriele DeLuca and Roman Fischer, for their continuous support, patience, and expertise throughout my DPhil journey. It has been an incredibly rewarding experience working with you both. Your enthusiasm for science has been inspiring, and I look forward to continuing our mentorship as I embark on the next phase of my academic career.

Likewise, special thanks go to the following individuals: (1) to Simon Davis for the mass spectrometry acquisition, processing, and guidance on the downstream analysis; (2) to Jonathan Pansieri for your optimism, scientific insight, and thought-provoking discussions; and (3) to Margaret Esiri for your excellent advice and critical analysis. It has been a privilege getting to know you all, and I thank you for always being willing to lend me your time.

I also wish to express my gratitude to all the members of the DeLuca and Fischer group, past and present, who have been extremely helpful and an absolute pleasure to work with. Many thanks to these wonderful colleagues, including Marco Pisa, Bryan Adriaanse, Max Crane, Alex Waldman, Adele Smart, Richard Yates, Catherine Foster, Jonny Attwood, Lucy Bland, Josh Frost, Estefania Simones, Ruth Geraldes, Darragh O'Brien, Iolanda Vendrell, Andreas Damianou, and Phil Charles. Wherever our future endeavours might take us, I sincerely hope this is just the beginning of lifelong camaraderie and scholastic conversation.

Furthermore, I would like to acknowledge the generous support of the Commonwealth Scholarship Commission and Canadian Centennial Scholarship Fund, as well as all the donors and their families at the UK MS Society Tissue Bank, who have made this DPhil possible.

To David, Jacinta, Lina, José, Joseph, Jack, Heike, Emily, Emi, Kate, and others, thank you. Near or far, our friendship has been a huge source of laughter, comfort, and love during my DPhil. Words cannot describe how grateful I am to have crossed paths with such compassionate, kind-hearted people.

Finally, a massive thank you to my incredible family. To my parents, Norman Yee and Margaret Shu, I thank you for your unwavering support, continual interest in my passions, and unconditional love. I am beyond proud to be your daughter. Equally as important, thank you Everett, for always being there for me. You are the best sibling one could ever ask for.

Statement of Originality

I declare that, unless otherwise stated, this thesis is entirely my own work and describes my own research.

S. A. Yee
Keble College, Oxford

Table of Contents

List of Figures 1
List of Tables 3
Abbreviations 4
1 Introduction 6
1.1 An Overview of Multiple Sclerosis 6
1.1.1 Clinical course 6
1.1.2 Epidemiology and risk factors 8
1.1.2.1 Environmental and lifestyle risk factors 9
1.1.2.2 Genetic risk factors 9
1.1.3 Pathogenesis 10
1.1.4 Pathological features 11
1.1.4.1 Demyelination and lesion burden 11
1.1.4.1.1 Pathological features of white matter lesions 11
1.1.4.1.2 Pathological features of grey matter lesions 12
1.1.4.2 Neuronal and axonal loss 13
1.2 Astrocyte Biology and their Role in Health and Multiple Sclerosis 14
1.2.1 Astrocyte morphology 17
1.2.2 The role of the astrocyte in vascular integrity and disruption 18
1.2.2.1 Properties of perivascular astrocytes in adult health 19
1.2.2.2 Perivascular astrocyte dysregulation in multiple sclerosis 20
1.2.3 Interactive signalling between astrocytes and microglia 21
1.2.3.1 Astrocyte-microglia crosstalk in adult health 21
1.2.3.2 Inflammatory modulation and propagation via astrocyte-microglia crosstalk in multiple sclerosis 22
1.2.4 Astrocyte modulation of neuronal integrity 23
1.2.4.1 Astroglial provision of neurotrophic support in adult health 23
1.2.4.2 Astroglial promotion of neurotoxicity in multiple sclerosis 24
1.3 Molecular Tools to Study Astrocytes in Multiple Sclerosis 25
1.3.1 Current astrocyte protein markers 29
1.3.2 Characterising astrocytes using mass spectrometry-based proteomics 30
1.3.2.1 Proteomic approaches and strategies to study human tissues 31
1.3.2.2 Proteome profiles of astrocytes in MS 32
1.4 Overview of Thesis 34

2 Subpopulations of astrocytes and their antagonistic relationships with motor cortical pathology in progressive multiple sclerosis 35

2.1 Introduction 35

2.2 Materials and Methods 36

2.2.1 Study population 36

2.2.2 Immunohistochemistry 36

2.2.3 Data analyses 37

2.2.3.1 Quantification of global astrocyte expression in the motor cortex 37

2.2.3.2 Assessment of astrocyte features in the motor cortex 38

2.2.4 Statistical analyses 40

2.3 Results 41

2.3.1 Demographics and pathological features 41

2.3.2 Validation of semi-quantitative astrocyte score 42

2.3.3 Topographical differences of motor cortical astrocyte subpopulations in MS and control cases 43

2.3.4 Cortical astrocyte subpopulations are differentially expressed in the GM and WM of MS and controls cases 46

2.3.4.1 Distribution and extent of cortical astrocyte expression 46

2.3.4.2 Astrocyte processes 47

2.3.4.3 Quantity of astrocyte cell bodies 48

2.3.4.4 Astroglial soma reactivity 48

2.3.5 Features of MS motor cortical astrocyte subpopulations differ from controls 50

2.3.5.1 GFAP+ astrocyte expression 50

2.3.5.2 ALDH1L1+ astrocyte expression 50

2.3.6 NAGM cortical astrocyte subpopulations show opposite features with ageing depending on *HLA-DRB1*15* status 51

2.3.6.1 Influence of *HLA-DRB1*15* genotype on cortical astrocyte subpopulations 51

2.3.6.2 Influence of age at death on genotype for cortical astrocyte subpopulations 52

2.3.7 Astrocyte subpopulations are differentially related to MS motor cortical pathology 55

2.3.7.1 Brain weight 55

2.3.7.2 Demyelination 55

2.3.7.3 Neuronal density in NAGM 56

2.3.7.4 Macrophage/microglia expression in NAGM 60

2.4 Discussion 61

3 Perivascular astrocyte subpopulations and their relationships with vessel integrity in the multiple sclerosis motor cortex 66

3.1 Introduction 66

3.2 Materials and Methods 67

3.2.1 Study population 67

3.2.2 Immunohistochemistry and immunofluorescence 67

3.2.3 Data analyses 70

3.2.3.1 Quantification of NAGM perivascular astrocytes 70

3.2.3.2 Quantification of endothelial expression 71

3.2.3.3 Assessment of NAGM vessel integrity 72

3.2.3.4 Assessment of astrocyte relationships with vessel integrity 73

3.2.4 Statistical analyses 75

3.3 Results 75

3.3.1 Demographics 75

3.3.2 Validation of binarised score for vessel integrity and perivascular astrocytes 77

3.3.3 Perivascular expression of astrocyte subpopulations in NAGM 78

3.3.3.1 Perivascular astrocyte expression is altered in MS compared to controls 79

3.3.3.2 Genotype influences perivascular astrocyte expression within MS .. 80

3.3.3.3 Vessel size does not influence presence of perivascular astrocyte expression in MS 81

3.3.3.4 Perivascular GFAP+ astrocytes relate to AQP4+ astrocyte expression, whilst perivascular ALDH1L1+ astrocytes do not 82

3.3.4 Vascular landscape in NAGM 84

3.3.4.1 Endothelial expression differs between MS and controls 84

3.3.4.2 Genotype does not impact endothelial expression 84

3.3.5 Vessel integrity in NAGM 85

3.3.5.1 Fibrinogen distribution is altered in MS compared to controls 85

3.3.5.2 Tight junction morphology is preserved in MS and controls 87

3.3.5.3 Relationships between metrics of vessel integrity differ in MS 88

3.3.6 Perivascular astrocyte relationships with markers of vessel integrity 90

3.3.6.1 Perivascular astrocyte subpopulations differ in their relationships with fibrinogen deposition 90

3.3.6.2 Perivascular astrocyte subpopulations differ in their relationship with tight junctions 92

3.4 Discussion 94

4 The distinct proteome profiles of astrocyte subpopulations in the multiple sclerosis motor cortex 99

4.1 Introduction 99

4.2 Materials and Methods 100

4.2.1 Study population 100

4.2.2 Optimisation of the formalin-fixed paraffin-embedded tissue workflow 100

4.2.3 Immunohistochemistry 102

4.2.4 Laser capture microdissection and SP3 digestion of astrocytes 103

4.2.5 Mass spectrometry data analyses 104

4.2.5.1 Data-dependent acquisition workflow 105

4.2.5.2 Data-independent acquisition workflow 106

4.2.6 Statistical analyses 106

4.2.6.1 Quality control processing 107

4.2.6.2 Differential expression analyses 108

4.2.6.3 Function and global pathway analysis 108

4.3 Results 109

4.3.1 Demographics 109

4.3.2 FFPE workflow 111

4.3.3 Proteomic quality control 112

4.3.4 Influence of astrocyte subtype, disease, and genotype status on protein group IDs 114

4.3.4.1 Astrocyte subtype versus disease status 114

4.3.4.2 Astrocyte subtype versus genotype status 116

4.3.5 Proteome profiles of GFAP+ astrocytes differ from ALDH1L1+ astrocytes 118

4.3.5.1 Identification of astrocyte subtype proteomes 118

4.3.5.2 Protein expression differences between GFAP+ and ALDH1L1+ astrocytes 121

4.3.6 Proteome profiles differ between MS and controls in astrocyte subtypes 123

4.3.6.1 Proteome profile of GFAP+ astrocytes 123

4.3.6.2 Proteome profile of ALDH1L1+ astrocytes 125

4.3.6.3 Proteome profile of GFAP+/ALDH1L1+ astrocytes 127

4.3.7 *HLA-DRB1*15* status influences the proteome profiles of astrocyte subtypes 129

4.3.7.1 Proteome profile of GFAP+ astrocytes 129

4.3.7.2 Proteome profiles of ALDH1L1+ astrocytes 130

4.3.7.3 Proteome profiles of GFAP+/ALDH1L1+ astrocytes 131

4.3.8 Discussion 131

5 Overview and Future Perspectives 139

5.1 Thesis Summary 139

5.1.1 GFAP+ and ALDH1L1+ astrocytes represent distinct astroglial subpopulations, which differentially relate to MS pathological outcome 140

5.1.1.1 GFAP+ astrocytes act as perpetrators of MS pathology 140

5.1.1.2 ALDH1L1+ astrocytes act as protectors of MS pathology 141

5.1.1.3 Astrocyte subpopulation composition is important for astrocyte diversity in MS 142

5.1.2 *HLA-DRB1*15* influences GFAP+ and ALDH1L1+ astrocyte subpopulations in MS 142

5.2 Study Limitations 144

5.3 Future Work 146

5.3.1 Pathological validation of astroglial subpopulation protein group IDs and their relationship with known pathological outcomes in MS 146

5.3.2 Evaluate the cell-cell interactions of astrocyte subpopulations with neurons and microglia in MS 148

5.3.3 Investigating the spatial relationships and functional mechanisms of perivascular astrocyte subpopulations with vessel integrity in MS 149

5.4 Concluding Thoughts 151

Appendix 152

References 166

List of Figures

Chapter 1

Figure 1.1. The disease course of MS. 8
Figure 1.2. Classification of grey matter lesions in the MS motor cortex. 13
Figure 1.3. Overview of common astrocyte functions in health. 15
Figure 1.4. Possible mechanisms of astrocytes influencing the CNS in health and MS. 16

Chapter 2

Figure 2.1. Semi-quantitative scoring of GFAP+ and ALDH1L1+ astrocyte expression in the motor cortex. 39
Figure 2.2. Topography of GFAP+ and ALDH1L1+ astrocytes in the MS motor cortex. 45
Figure 2.3. Extent and distribution of GFAP+ and ALDH1L1+ astrocytes in the MS motor cortex. 47
Figure 2.4. The influence of age on genotype status for GFAP+ astrocyte in NAGM in the MS motor cortex. 53
Figure 2.5. GFAP+ astrocyte expression in lesional, perilesional, and corresponding NAGM of the MS motor cortex. 56
Figure 2.6. Summary of relationships for GFAP+ and ALDH1L1+ astrocytes with NeuN+ neurons, CD68+ or IBA1+ macrophage/microglia, and TMEM119+ microglia in the motor cortex. 58
Figure 2.7. The influence of age on MS genetic status for relationships between GFAP+ and ALDH1L1+ astrocytes, neuronal density and macrophage/microglia expression in the motor cortex. 59

Chapter 3

Figure 3.1. Assessment of perivascular astrocyte expression in the MS motor cortex. 71
Figure 3.2. Binary assessment of NAGM vessel integrity. 73
Figure 3.3. Binary assessment of NAGM perivascular astrocyte expression. 74
Figure 3.4. Perivascular expression of GFAP+ and ALDH1L1+ astrocytes in NAGM of the motor cortex. 79
Figure 3.5. Changes to perivascular GFAP+ and ALDH1L1+ astrocyte expression in NAGM of the MS motor cortex. 80
Figure 3.6. Perivascular AQP4+ astrocyte expression in the NAGM of the MS motor cortex. 83
Figure 3.7. CD31/34+ endothelial expression in motor cortical NAGM. 85
Figure 3.8. Extent and distribution of fibrinogen+ expression in motor cortical NAGM. 87
Figure 3.9. Relationship between ZO-1+ tight junctions and fibrinogen+ expression in MS cortical NAGM. 89
Figure 3.10. The relationship between perivascular astrocytes and fibrinogen deposition in the MS NAGM cortex. 91
Figure 3.11. Relationship between perivascular astrocytes and ZO-1+ tight junctions in the MS NAGM cortex. 93

Chapter 4

Figure 4.1. IHC directed LCM of GFAP+, GFAP+/ALDH1L1+, and ALDH1L1+ astrocytes in NAGM motor cortex. 104
Figure 4.2. Summary of downstream proteomic analyses workflow. 107
Figure 4.3. Influence of fixation and slide-type on the number of proteins identified with LCM-directed mass spectrometry. 112
Figure 4.4. The number of samples for differential expression analysis after quality control filtering. 113
Figure 4.5. Influence of disease status and astrocyte subtype on the protein group IDs in all samples. 115
Figure 4.6. Influence of genotype status and astrocyte subtype on the protein group IDs in MS samples. 117
Figure 4.7. Differential expression of astrocyte subtypes in MS and control samples. 120
Figure 4.8. Differentially expressed protein groups between GFAP+ and ALDH1L1+ astrocytes in MS and controls. 122
Figure 4.9. Differential expression of GFAP+ astrocytes in MS. 124
Figure 4.10. Differential expression of ALDH1L1+ astrocytes in MS. 126
Figure 4.11. Differential expression of GFAP+/ALDH1L1+ astrocytes in MS. 128
Figure 4.12. Enriched protein group IDs of astrocyte subtypes in *HLA-DRB1*15*+ compared to *HLA-DRB1*15*- samples. 130

List of Tables

Chapter 1

Table 1.1. Overview of common immunohistochemical markers for astrocytes in the adult human CNS. 27

Chapter 2

Table 2.1. Details of antibodies used in IHC methods.....37
Table 2.2. Clinical details of MS and control cohort. 42
Table 2.3. Reliability of GFAP+ and ALDH1L1+ semi-quantitative scoring.....43
Table 2.4. Comparison between NAGM and NAWM for GFAP+ and ALDH1L1+ expression in the motor cortex of MS and control cases.....49
Table 2.5. The influence of *HLA-DRB1*15* genotype on GFAP+ and ALDH1L1+ astrocyte expression in motor cortical NAGM. 51
Table 2.6. The relationships between ALDH1L1+ astrocyte expression, age on *HLA-DRB1*15* genotype, and demyelination in the MS motor cortex. 54

Chapter 3

Table 3.1. Details of antibodies used in IHC and IF methods. 69
Table 3.2. Clinical features of the cohort used for the IHC analyses of Chapter 3. 76
Table 3.3. Clinical features of the cohort used for IF analyses.....77
Table 3.4. Reliability of perivascular GFAP+, ALDH1L1+, fibrinogen+, and ZO-1+ semi-quantitative scoring.....78
Table 3.5. The impact of vessel size on perivascular astrocyte expression in control, MS, *HLA-DRB1*15*-, and *HLA-DRB1*15*+ cases. 81

Chapter 4

Table 4.1. Details of antibodies used in IHC methods for Chapter 4.....102
Table 4.2. Clinical features of the cohort used in IHC analyses of Chapter 3. 110

Appendix

Table S4.1. The DIA segment widths used for mass-spectrometry analysis of LCM-targeted astrocytes. 152
Table S4.2. Differentially expressed protein groups between LCM-targeted GFAP+ and ALDH1L1+ astrocytes in MS and control samples. 153
Table S4.3. Differential protein expression of LCM-targeted GFAP+ astrocytes between MS and control samples. 155
Table S4.4. Differential protein expression of LCM-targeted ALDH1L1+ astrocytes between MS and control samples. 159
Table S4.5. Differential protein expression of LCM-targeted GFAP+/ALDH1L1+ astrocytes between MS and control samples. 163

Abbreviations

15-	*HLA-DRB1*15-*
15+	*HLA-DRB1*15+*
ALDH1L1	aldehyde dehydrogenase 1 L1
ANOVA	analysis of variance
AP	alkaline phosphatase
AQP4	aquaporin 4
ATP	adenosine triphosphate
BBB	blood-brain barrier
BH	Benjamini and Hochberg
CD	cluster of differentiation
CNS	central nervous system
CRISPER	clustered regularly interspaced short palindromic repeats
CSF	cerebrospinal fluid
DAB	3,3'-diaminobenzidine
DDA	data-dependent acquisition
DIA	data-independent acquisition
DNA	deoxyribonucleic acid
DTT	dithiothreitol
EAAT	excitatory amino acid transporter
EAE	experimental autoimmune encephalomyelitis
EBV	Epstein-Barr virus
EDTA	ethylenediaminetetraacetic acid
FDR	false discovery rate
FFPE	formalin-fixed paraffin-embedded
FOV	field of view
GABA	gamma amino butyric acid
GEE	general estimating equation
GFAP	glial fibrillary acidic protein
GM	grey matter
GWAS	genome-wide association studies
HLA	human leukocyte antigen
HRP	horseradish peroxidase
IAA	iodoacetamide
IBA1	ionized calcium binding adaptor molecule 1
IF	immunofluorescence
IHC	immunohistochemistry
IL	interleukin
iPSC	induced pluripotent stem cell
LacCer	lactosylceramide
LC-MS/MS	liquid-chromatography tandem mass spectrometry

Abbreviations *continued…*

LCM	laser capture microdissection
LPS	lipopolysaccharide
MHC	major histocompatibility complex
MRI	magnetic resonance imaging
MS	multiple sclerosis
NAGM	normal-appearing grey matter
NAWM	normal-appearing white matter
NeuN	neuronal nuclei
NF	nuclear factor
OPC	oligodendrocyte precursor cell
PCA	principal component analysis
PLP	proteolipid protein
PPMS	primary progressive MS
REC	research ethics code
RIPA	radioimmunoprecipitation assay buffer
RNA	ribonucleic acid
RRMS	relapsing remitting MS
SEM	standard error of the mean
SNP	single nucleotide polymorphism
SP3	single pot solid-phase enhanced sample preparation
SPMS	secondary progressive MS
TMEM119	transmembrane protein 119
UEA-1	ulex europaeus agglutinin 1
UK	United Kingdom
WM	white matter
ZO-1	zonula occludens-1

1 Introduction

1.1 An Overview of Multiple Sclerosis

Multiple sclerosis (MS) is a chronic inflammatory, demyelinating, and degenerative disease of the central nervous system (CNS). It is the leading cause of non-traumatic disability in young adults, posing a major personal and socioeconomic burden[1,2]. The causes of MS are largely unknown, but general consensus suggests that an interplay of genetic and environmental factors play an important role[3,4]. Presentation of MS is heterogenous, making it difficult to ascertain the pathological substrates of neurological dysfunction. Therefore, our knowledge of factors associated with MS outcome is limited.

1.1.1 Clinical course

MS typically affects young adults, with disease onset presenting around age 30-years old[5]. Diagnosis is based on the presentation of the dissemination demyelinating lesions in space and time, often with magnetic resonance imaging (MRI)[6]. Numerous clinical symptoms are present in MS, including motor impairments, disturbances to both sensory and visual systems, fatigue, pain, and cognitive decline[7]. Although clinical manifestations and disease course are highly variable amongst affected individuals, most of MS patients present with relapsing-remitting MS (RRMS; **Figure 1.1**)[8].

RRMS is characterised by intermittent episodes of neurologic dysfunction followed by spontaneous partial or complete recovery. There is substantial variation in relapse frequency, although the interval between relapses increases with advancing disease[9]. Within 20 years of disease onset, most RRMS patients

develop secondary progressive MS (SPMS), during which permanent and progressive disability occurs[8,10]. Although some evidence suggests that a higher rate of relapses in early disease stages associates with an increased risk of permanent disability[11], there are no specific symptoms exclusively related to the transition from RRMS to SPMS[12].

A subset of MS patients (~10-15%) experience primary progressive MS (PPMS), where deterioration begins from the onset of disease and recovery periods are absent[8,13]. The average disease onset in PPMS typically peaks in the 4th decade of life and is slightly more common in men than RRMS or SPMS[14,15]. However, the pathological features, mechanisms, and therapeutic responses between PPMS and SPMS have substantial overlap, which has led to the suggestion of merging PPMS and SPMS as a progressive MS phenotype[16].

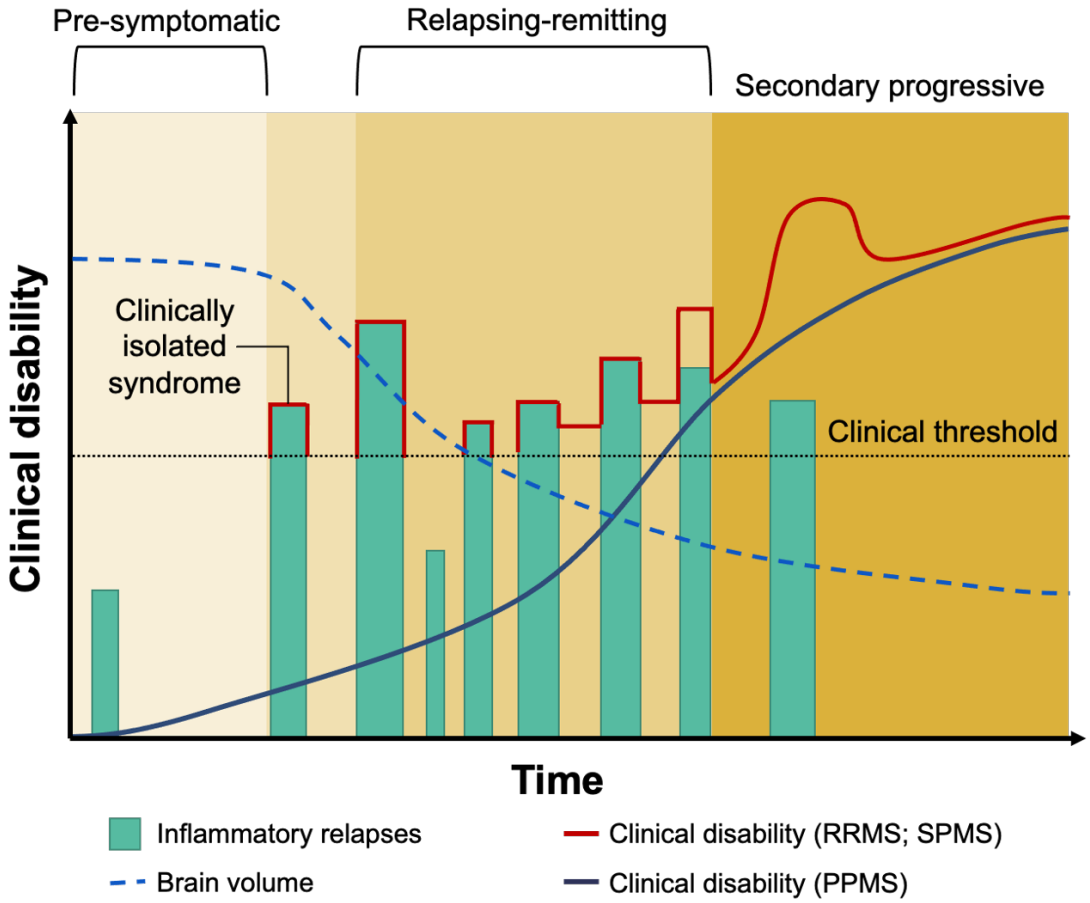


Figure 1.1. The disease course of MS. Although the presentation of MS is heterogenous, general clinical courses have been recognised. RRMS, the most common form of MS, is characterised by an initial episode of neurological dysfunction (clinically isolated syndrome), followed by a remission period of clinical recovery and then episodic bouts of relapse and remission (solid red line). Relapses coincide with inflammatory demyelination and increase in frequency over the disease course (teal rectangle). Most RRMS patients will develop SPMS, which is characterised by progressive, irreversibly disability and neuroaxonal loss (blue dashed line), independent of relapse. A subset of patients with MS are diagnosed with PPMS, where progression occurs from disease onset (solid blue line).

1.1.2 Epidemiology and risk factors

The global rates of MS are highly variable. There are substantial geographic differences, with the incidence of MS increasing with distance from the equator, even amongst countries with comparable medical infrastructure[2]. MS is also more common in females than males by at least two times[5]. The current

consensus indicates that MS onset likely occurs when a genetically predisposed individual is exposed to unknown environmental trigger(s), although it remains unknown if a single or multiple triggers cause MS[3,4].

1.1.2.1 Environmental and lifestyle risk factors

Many environmental and lifestyle factors can contribute to the risk of MS. Epstein-Barr virus (EBV) infection, particularly in adolescence and young adulthood, is one of the most well-established risk factors for MS[3,17,18]. In a recent longitudinal analysis, MS risk increased 32-fold post-EBV infection[17]. Genetic and molecular analysis of the role of EBV in MS has suggested that molecular mimicry may lead to the transformation of immune cell-types[18]. Although these findings suggest that EBV exposure can contribute to the development of MS, it is not clear if EBV is sufficient to cause MS.

Other MS risk factors include lack of sun exposure (low vitamin D levels) and smoking[3,4]. For example, epidemiological observations on the effect of both latitude and month-of-birth for MS risk has been attributed to sunlight exposure, a major determinant of vitamin D levels, which tends to decrease with increasing latitudes[19,20].

1.1.2.2 Genetic risk factors

In addition to environmental risk factors, genetic susceptibility is considered an important risk factor for MS. The prevalence of familial MS is around 13% for all MS phenotypes, with the risk of recurrence increasing with the percentage of genetic sharing[21,22].

Genome-wide association studies (GWAS) have identified over 200 gene variants for MS, most of which encode molecules involved in immune functions[23]. Polymorphisms in the human leukocyte antigen (*HLA*) genes exert the largest genetic contribution to MS susceptibility, where carriage of the extended *HLA* class II haplotype, namely *HLA-DRB1*15*, confers the greatest risk factor for developing MS[23]. The *HLA-DRB1*15* allele is also thought to influence MS disease severity as MS carriage of *HLA-DRB1*15* associates with lower age of onset[24], worse disability[25], greater cognitive impairment[26], and more severe inflammation and demyelination throughout the neuraxis[27,28].

1.1.3 Pathogenesis

Two hypotheses, the "outside-in" and "inside-out" paradigms, have been proposed to explain the pathogenesis of MS[29]. In the "outside-in" paradigm, infiltration of peripheral immune cells in response to an external trigger generates a CNS immune response. In contrast, the "inside-out" paradigm proposes that secondary autoimmune reactions respond to an unknown primary CNS degenerative or dysfunctional process. Regardless of the model, activated immune cells remain a consistent feature and thus, are considered a prominent cause of damage in MS[30,31]. Activated immune cells are also present outside demyelinated areas in normal-appearing grey matter (NAGM) and normal-appearing white matter (NAWM), suggesting that immune response may represent the earliest stage of lesion development[32,33]. Of note, immune cells, such as microglia, do not only exacerbate inflammation but can also suppress inflammation and limit tissue damage by clearing debris and pruning dysfunctional cells[34].

1.1.4 Pathological features

The neuropathology of MS is complex. Characteristic hallmarks include chronic inflammation of the parenchyma and meninges, demyelination, varying degrees of neuroaxonal loss, and reactivity of glial cells[35]. Given this, neuropathologic assessment continues to be fundamental to our understanding of MS pathogenesis by providing substantial insights into the cellular and subcellular changes that are currently beyond the resolution of conventional *in vivo* neuroimaging techniques.

1.1.4.1 Demyelination and lesion burden

1.1.4.1.1 Pathological features of white matter lesions

Changes to white matter (WM) occur in all MS subtypes regardless of disease stage. Lesion location is variable, but there is a predilection for the optic nerve, brainstem, cerebellum, periventricular WM, and spinal cord[36]. Demyelinated areas have been broadly classified as active, mixed active-inactive, and inactive lesions based on expression pattern of associated immune cells[37,38]. In active WM lesions, there is blood-brain barrier (BBB) breakdown, accumulation of myelin-containing macrophages and microglia, lymphocyte infiltration, and reactive glial cells. This pro-inflammatory response contributes to neuroaxonal and oligodendrocyte loss. Over time, the activated macrophages and microglia become limited to the perimeter of the lesion (mixed active-inactive lesion), leaving the centre nearly devoid of immune cell types and depleted of mature oligodendrocytes (inactive lesion). Newly formed oligodendrocyte precursor cells (OPCs) may work towards re-establishing damaged and lost myelin sheaths[38]; although, remyelination is variable and decreases with disease duration[37]. Glial

scarring produced by reactive astrocytes is often present with lesion progression. Although this glial scarring may prevent further demyelination, it can also hinder the CNS' capacity for remyelination by preventing OPCs entry into the demyelinated area, leaving the area vulnerable to neuroaxonal damage and loss[39,40].

1.1.4.1.2 Pathological features of grey matter lesions

Although MS has traditionally been considered a WM disease, increasing evidence has identified grey matter (GM) changes as an important feature of MS pathology[41-43]. GM lesions can occur in the cerebral cortex, deep GM, and spinal cord[42,44]. In the cerebral cortical GM pathology, four major cortical lesion subtypes have been accepted for histological classification as common demyelinating lesions: type I (leukocortical), which extend from the deep cortical layers into the subcortical WM; type II (intracortical), which are typically small and perivascular; type III (subpial), which extend from the pial surface to cortical layers II-IV; and type IV, which extend from the pial surface to the grey/white matter boundary (**Figure 1.2**)[42]. Subpial lesions are the most common subtype, with affected regions often spanning multiple adjacent gyri. Unlike WM lesions, immune-cell infiltrates and activated macrophage/microglia in GM lesions are typically less prominent[42]. Given this difference, it has been proposed that the pathogenesis of GM lesions may differ from WM lesion pathogenesis. The association of lesions with meningeal inflammation has led to the hypothesis that GM lesion formation is a consequence of cytotoxic diffusion from the cerebrospinal fluid (CSF) into the CNS[45]. However, not all subpial lesions associate with meningeal inflammation[28].

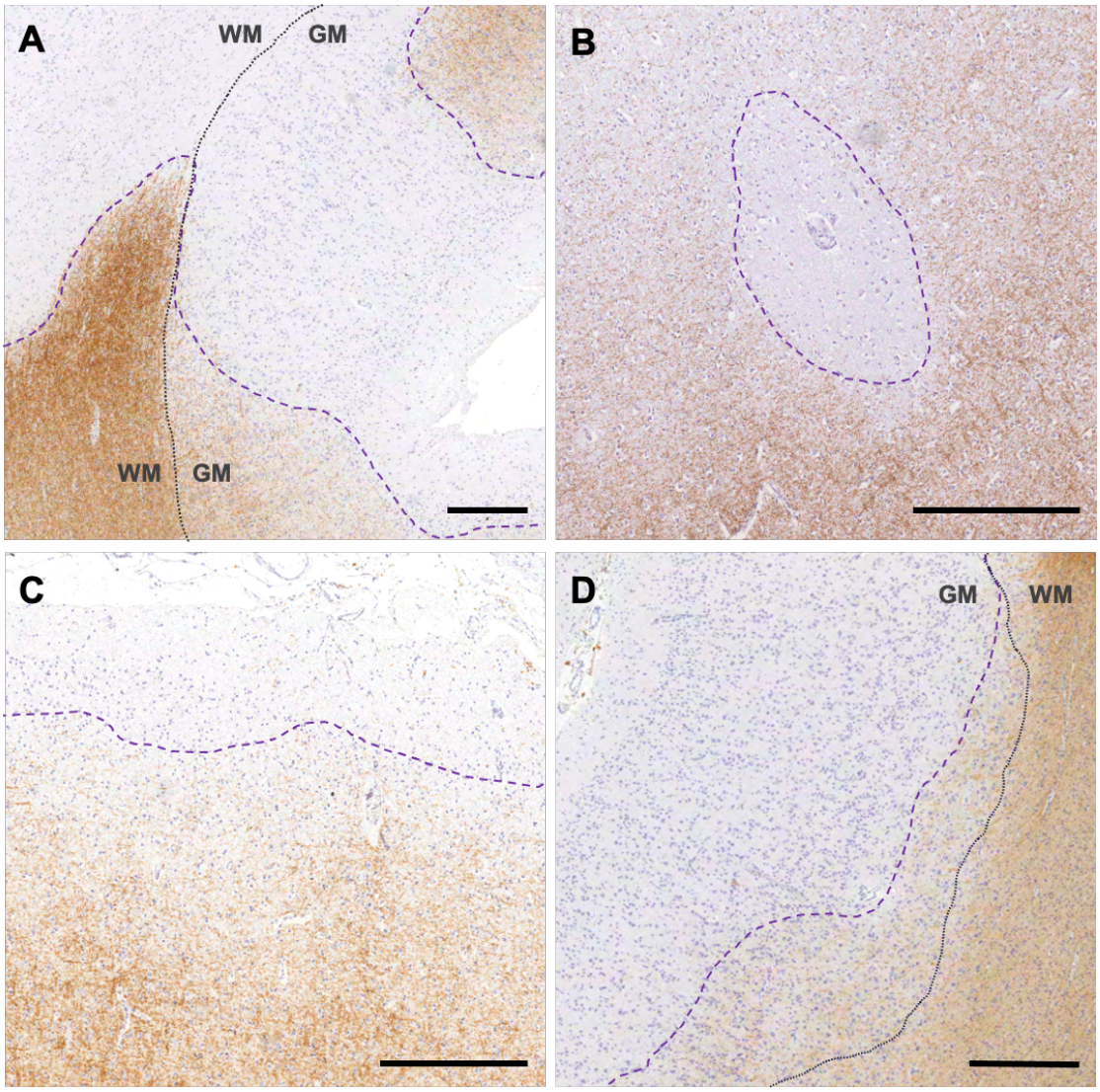


Figure 1.2. Classification of grey matter lesions in the MS motor cortex. There are four types of cortical lesions defined by Bö et al. (2003). Type I (leukocortical) lesions extend through both GM and WM (**A**). Type II (intracortical) lesions are typically small and perivascular (**B**). Type III (subpial) lesions are the most common and can extend over several gyri (**C**). Type IV span the full cortical depth without affecting the WM (**D**). Sections imaged here were immunolabeled with proteo-lipid protein (PLP) and counterstained with Harris Haematoxylin to identify cortical matters. Dotted line = white-grey matter boundary; Purple dashed line = lesion boundary. Bar represents 500μm. GM = grey matter; WM = white matter.

1.1.4.2 Neuronal and axonal loss

Neuroaxonal damage and loss, which occurs throughout the neuraxis in varying degrees, have been identified as an important correlate of disability in MS[46].

However, the mechanisms that underlie neuroaxonal loss in MS are not well understood. Axonal and neuronal injury can occur in non-lesional areas suggesting that neuroaxonal loss in MS can also be independent of demyelination[47,48]. In contrast, inflammation, which is present in all forms of MS, has been linked with the extent of neuroaxonal damage in MS[37]. Transcriptional profiling of human microglia also reports MS-associated metabolic changes in NAGM and NAWM, suggesting that dysregulation of immune function could be an early contributor to downstream neuroaxonal pathology[49].

Although the presence of axonal loss is a well-established feature of MS pathology[47,50], evidence of neuronal loss in the MS cerebral cortex has been more ambiguous. Data on the magnitude of neuronal loss in the MS cerebral cortex has been highly variable, and displays heterogeneity between different cortical regions[51-53]. Restriction of neuronal loss to the upper cortical layers has indicated that selective neuronal vulnerability plays a role in MS, which may contribute to the variable nature of MS cortical neuronal loss[54]. Despite no overall reduction in neuronal density between MS and controls, inhibitory synapses show a selective loss in the MS cerebral cortex[52].

1.2 Astrocyte Biology and their Role in Health and Multiple Sclerosis

A growing body of evidence has shown that non-neuronal cells, known as glia, play an important role in MS pathology throughout all stages of MS disease[55]. Once thought to be purely supportive for neurons, glial cells, such as astrocytes, have since been recognised as a major contributor to CNS diversity and an active determinant of CNS health (**Figure 1.3**).

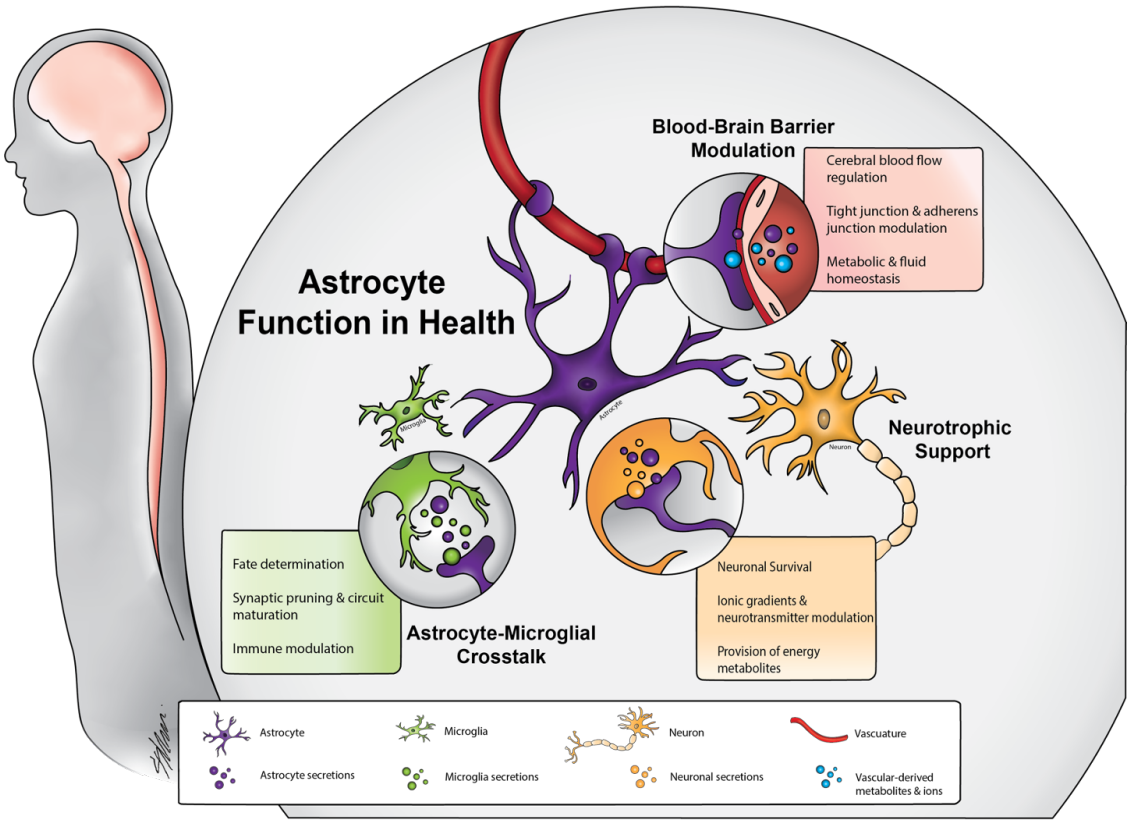


Figure 1.3. Overview of common astrocyte functions in health. Amongst the many functions attributed to astrocytes, astroglial interactions with vasculature, namely the BBB, microglia, and neurons, are central to maintaining appropriate homeostasis in the CNS. Key examples of astrocyte function in these systems are highlighted here. Red box = vasculature; Green box = microglia; Orange box = neurons.

Astrocytes are the most abundant glial cells in the CNS. Their ubiquitous network is ideally positioned to execute multiple functions integral to neurological function in health, such as modulating vessel integrity, interacting with immune cells, and providing trophic support for neurons (**Figure 1.3**).

However, astrocytes are also key modulators in the inflammatory pathway of the CNS and likely contribute to MS pathogenesis[56]. Astrocytes undergo significant molecular and cellular changes in disease, which greatly impact the brain's microenvironment (**Figure 1.4**). In MS, astrocytes have been associated with neuroprotection, including the release of anti-inflammatory molecules[57], inhibition

of further demyelination[58], and secretion of factors responsible for cellular repair and regeneration[59]. Inversely, astrocytes in MS are also associated with neurotoxicity, including the release of pro-inflammatory factors[60], exacerbation of BBB dysfunction[61], and recruitment of cytotoxic factors into the CNS[62,63]. With much of the focus on the traditional immune cells of the CNS, the field of astrocytes in MS has been relatively neglected, and thus, many of these astroglial changes in MS remains to be explored.

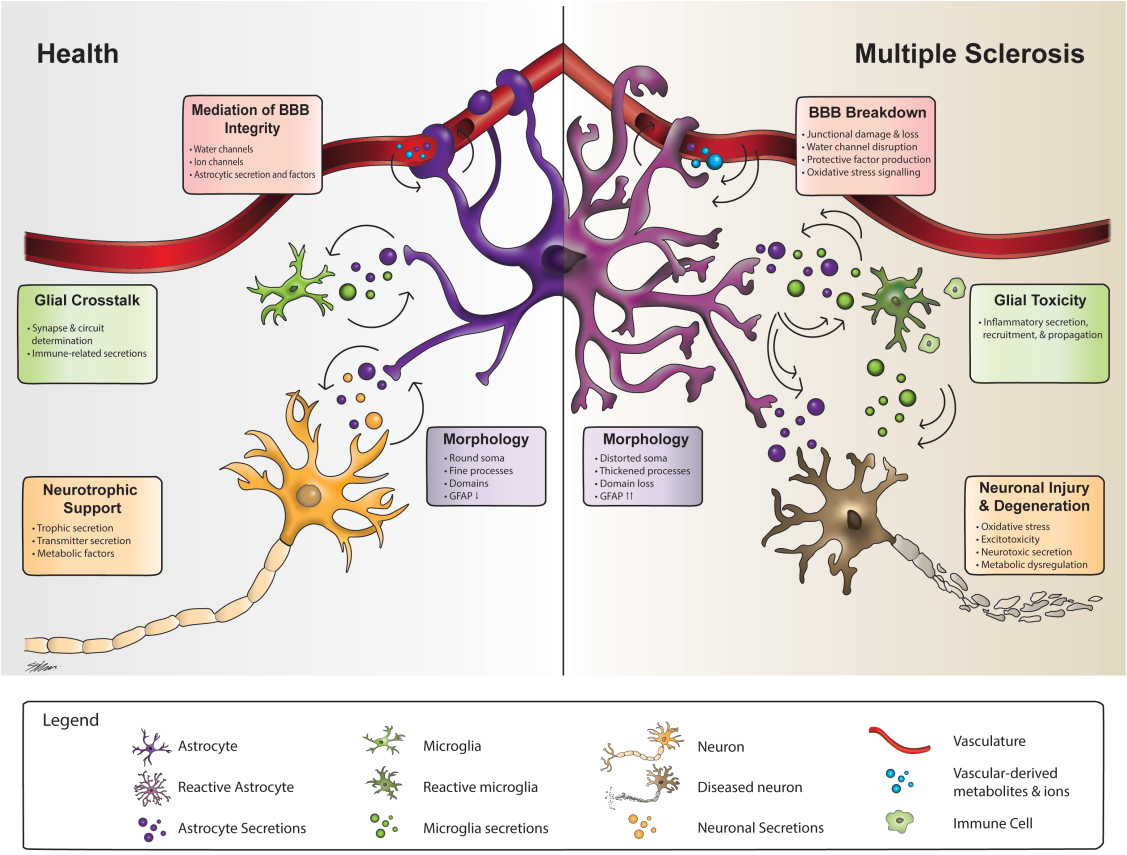


Figure 1.4. Possible mechanisms of astrocytes influencing the CNS in health and MS. In health, astrocytes contribute to the homeostasis of the CNS microenvironment by coordinating vessels, microglia, and neurons. In MS, astrocytes can become reactive, undergoing morphological and functional changes. Astroglial dysregulation at vascular sites can allow cytotoxic materials to freely enter the CNS and further weaken the BBB. Astrocyte-microglia interactions can also enhance cytotoxic inflammation, which can result in neuronal damage and subsequent cell death. Red box = vasculature; Green box = microglia; Orange box = neurons; Purple box = morphology.

1.2.1 Astrocyte morphology

Studies on astrocytes date to the late 19th century, with the term “astrocyte” (or “astrocyten”) coined by Michael von Lenhossék in the 1890s[64]. Although initially defined based on the star-shaped morphology, histological studies from William Lloyd Andriezen, Camillo Golgi, and Santiago Ramón y Cajal alluded to their complex and heterogeneous nature[64,65]. With the advent of advanced microscopy, histological techniques, and “-omic” technologies, such as proteomics, astrocytes have since been acknowledged as the most heterogeneous glial cell[66].

Astrocyte diversity extends across the CNS, displaying morphological and functional features that reflect the surrounding circuitry. Numerous astrocyte subpopulations and region-specific specialised cells belonging to the astrocyte family, such as cerebellar Bergmann glia and retinal Müller cells, have been identified[67]. Despite this considerable diversity, astrocytes have largely been categorised into two main classes: protoplasmic and fibrous astrocytes. Protoplasmic astrocytes localise to the GM and display bushy processes that extend from a relatively round soma, whereas fibrous astrocytes are present in the WM and exhibit longitudinally oriented long and thin processes that extend from a more elongated soma[67,68].

Human astrocytes display species-specific features, increasing morphological complexity with mammalian order[69-71]. Humans and higher-order primates also have greater astrocyte subtype and subpopulation diversity. Characterisation of astrocytes in the human cerebral cortex has identified GM interlaminar and GM

varicose projection astrocytes, which are only present in higher-order primates[68,70,72]. Both subtypes span across neighbouring astrocyte domains, terminating in the interstitial space or on vasculature several cortical layers away from their soma[71].

In MS, astrocytes also undergo morphological changes, including soma enlargement, thickening of processes, loss of territorial domains, and multi-nucleation[73,74]. These changes are context-specific and vary according to disease stage and CNS region[55]. In active MS lesions, astrocytes display enlarged or hypertrophic soma with abnormal processes. Astrocytes will occasionally express prominent nuclei and may contain myelin or cellular debris in their cytoplasm[59]. Reactive astrocytes with fragmented nuclear inclusions (Creutzfeldt-Peters cells) can also be found[75]. As lesions progress from active to inactive, astrocytes can form tightly organised fibres or glial scars[76]. The astrocytes within inactive lesions have small soma and little cytoplasm expression, which are accompanied by long, thin processes[77]. NAGM and NAWM astrocytes typically exhibit similar features to astrocytes in non-neurological disease[78]. However, astrocytes, especially in peri-lesional regions, can undergo morphological changes in normal-appearing regions, including hypertrophic morphology and thickened processes[79].

1.2.2 The role of the astrocyte in vascular integrity and disruption

The CNS has a vascular system that is distinct from the rest of the body. Specialised endothelial cells, possessing tight junctional proteins, are closely juxtaposed by astrocyte endfeet and pericytes to create a highly dynamic

interface known as the BBB. The BBB filters requisite molecules and regulates ionic gradients to protect the CNS from imbalances, toxins, pathogens, and foreign materials[80]. Astrocyte endfeet are a key component of the vascular system. They directly link blood vessels to neurons and are also essential for regulating barrier properties of the CNS endothelial cells[81]. Therefore, perivascular astrocytes play a crucial role in vascular health and may be an important contributor to MS pathology.

1.2.2.1 Properties of perivascular astrocytes in adult health

Astrocyte modulation of vascular properties is essential to maintaining homeostasis of the CNS environment. Studies on endothelial and astrocyte co-cultures have demonstrated astrocytes can enhance barrier properties[82,83]. Indeed, astrocytes modulate the physical barrier tightness by regulating the organisation and integrity of tight junctional proteins, cell adhesion molecules, ion channels, and receptors of endothelial cells[80]. For example, astrocytic secretion of the morphogen sonic hedgehog interacts with endothelial hedgehog receptors to strengthen tight junctions and enhance the barrier function of CNS vessels[84,85].

Astrocytes also regulate flux across CNS vasculature by creating fluid and solute gradients. The endfeet, which vary in dimension based on vessel diameter, are enriched with specialised water channels, known as aquaporins, and inwardly rectifying potassium channels to maintain water and ion homeostasis[86,87]. Emphasis rests on the main aquaporin isoform, aquaporin 4 (AQP4), due to its relationship with inflammatory demyelinating diseases[88]. Its localisation to perivascular endfeet and uniform distribution across the cerebral cortex makes

AQP4+ astrocytes well suited to mediate osmotic homeostasis and extracellular space volume[89,90].

1.2.2.2 Perivascular astrocyte dysregulation in multiple sclerosis

In MS, astrocytes can negatively impact the integrity of the CNS vasculature via endfeet detachment[91], degradation of endothelial barrier proteins[92], and recruitment of pro-inflammatory factors[93]. However, not all astrocytes are detrimental to the BBB and may support vessels in MS[94]. For example, the changes to AQP4+ astrocyte expression are highly variable in MS[91]. Subsets of active and inactive MS lesions show decreased AQP4+ expression[95,96], whilst other active and inactive WM lesions show increased AQP4+ expression[97,98]. Areas of AQP4+ loss may reflect endfeet retraction from the vasculature, whilst areas of increased AQP4+ may be a protective mechanism for a weakened BBB. Altogether, these results highlight heterogeneous properties of astrocytes, which may contribute to the varying degrees of BBB breakdown present in MS lesions[95].

Astrocytes are also associated with many metrics used to assess vessel integrity, including large serum proteins[99] and endothelial tight junctions[100]. For example, fibrinogen, a glycoprotein often used as a surrogate marker of vessel permeability, has been localised to astroglial processes[99,101]. Fibrinogen deposition is considered a potent activator of the immune system and associates with inflammation, demyelination, and neuronal loss in MS[99]. Although fibrinogen co-localises with the astrocyte endfeet[99,102], the role of fibrinogen on astrocyte expression and their corresponding relationship with BBB breakdown is poorly understood. Work in mice has shown that fibrinogen can influence astrocytes

towards a more reactive phenotype[103], which may cause further dysregulation of the endfeet and upregulation of astrocyte-mediated immune cell infiltration into the CNS. These findings highlight the influence of fibrinogen deposition on astrocyte dysfunction and the role of astrocyte reactivity in MS disease propagation.

1.2.3 Interactive signalling between astrocytes and microglia

In addition to regulating the vasculature, astroglial communication with other glial cells, including microglia, is also crucial for CNS health. In particular, astrocytes and microglia are components of the neurovascular unit, making the communication between the two cells important for relaying signals between neurons and the blood supply. CNS phagocytosis and immune response are primary functions of microglia, which complement the work of astrocytes to modulate CNS inflammation, defend against invaders, and clear diseased or damaged cells. Therefore, the bidirectional communication between astrocytes and microglia is vital to health, and its dysfunction can directly impact MS outcome.

1.2.3.1 Astrocyte-microglia crosstalk in adult health

The essential role of the molecular dialogue between astrocytes and microglia begins in early development. This bidirectional communication contributes to synapse formation and pruning through signalling molecules, such as cytokines[104]. Astrocyte-microglia crosstalk modulates circuit maturation with both cells continuously scanning the CNS environment to regulate neural activity[105,106].

Other pathways by which astrocyte-microglia crosstalk act on include the modulation of CNS inflammation through the secretion of multiple cytokines and inflammatory mediators[107]. Due to the intrinsically close connection with normal immune function, it is difficult to disentangle the difference between astrocyte-microglia crosstalk in health versus disease. Therefore, immune-related communication between astrocytes and microglia will be outlined in the context of MS.

1.2.3.2 Inflammatory modulation and propagation via astrocyte-microglia crosstalk in multiple sclerosis

Astrocyte-microglia crosstalk may contribute to the primary inflammation observed in MS pathogenesis through the secretion of various cytokines and chemokines[56]. They can also activate each other to promote toxic inflammation[108]. Following classical immune challenge with lipopolysaccharide (LPS), microglia secretion of cytokines can induce the pro-inflammatory "A1" astrocyte phenotype, which is associated with reduced viability of neurons and oligodendrocytes. These astrocytes also demonstrate increased complement expression in actively demyelinating lesions and closely associate with macrophage/microglia expression[56].

Furthermore, several inflammatory pathways, such as purinergic signalling, are mediated by astrocyte-microglial communication and may contribute to MS pathology. Both astrocytes and microglia possess purinergic receptors, which may enable both cell types to work together to release pro-inflammatory factors

such as IL-1ß[109,110]. Therefore, these findings suggest that astrocyte-microglia crosstalk can use purinergic signalling to propagate the cytotoxic immune response and subsequent tissue damage observed in MS.

1.2.4 Astrocyte modulation of neuronal integrity

Although astrocytes and microglia provide neuronal support, astrocytes likely play a more dominant role in everyday neuronal function because of their more consistent interactions with neurons. Unlike microglia, which patrol the CNS to detect modifications in their environment, astrocytes are more positionally stable. Astrocytes establish spatially constant networks, known as the tripartite synapse, with neurons. Their processes contact neuronal spines and terminals to directly respond and influence synaptic development and survival, neurotransmission, and neural metabolites. Consequently, astrocyte-neuronal interactions have implications not only for health but also for disease. Although inflammation is the primary feature of MS, neurodegeneration is considered an underlying cause of irreversible disability in the disease[46,111]. Thus, the study of astrocyte communication with neurons is critical to our understanding of the pathological underpinnings of MS pathogenesis.

1.2.4.1 Astroglial provision of neurotrophic support in adult health

Astrocytes can influence neuronal survival by secreting neurotrophic factors responsible for regulating survival, growth, and morphological plasticity[112,113]. They are also crucial to the development of efficient synapses[114-116]. Indeed, induced pluripotent stem cell (iPSC) models show that neurons in astrocyte-neuronal co-cultures undergo faster synaptic maturation and more robust

signalling than neuronal cultures alone[117]. In addition, astrocytes can mediate neuron-neuron communication through the astrocyte-specific transporters that modulate the ion gradients and neurotransmitter concentration. Of key importance are the astroglial excitatory amino acid transporters, EAAT-1 and -2. EAAT-1 and EAAT-2 facilitate the movement of the neurotransmitter glutamate out of the synaptic space, which prevents the toxic build-up of glutamate[118]. Furthermore, astrocytes possess gliotransmitters, such as adenosine triphosphate (ATP) and D-serine, which allows astrocytes to communicate bi-directionally within the synapse and influence the neural networks[119].

Astrocytes can also ensure that neurons have regular access to metabolite and energy substrates. As predominantly glycolytic cells, astrocytes can produce lactate, which may be taken up by neurons for oxidative metabolism[120]. Although further investigation is required to confirm the specific function in human systems, it is thought that this astrocyte-neuron metabolic trafficking is essential for long-term memory formation[121].

1.2.4.2 Astroglial promotion of neurotoxicity in multiple sclerosis

The changes to astrocyte pathology in MS lesions and its association with inflammatory infiltrates make the astrocyte a key suspect in mediating neuronal injury and loss in MS. Astrocytes can produce a wealth of neurotoxic factors that can promote oxidative stress, excitotoxicity, and metabolic dysregulation in MS[122]. Furthermore, astrocytes may influence neurodegeneration in MS via dysregulated glutamate trafficking. Excess glutamate can drive excitotoxicity and contribute to MS neurodegeneration[123]. Studies have indicated that astrocytes

have a reduced capacity to uptake glutamate under inflammatory conditions, which leaves MS neurons vulnerable to excitotoxicity[124,125]. Despite the evidence for glutamate-induced excitotoxicity in MS neurodegeneration, clinical trials utilising glutamate-inhibiting compounds have been disappointing, with limited efficacy on brain atrophy[126,127].

Emerging evidence also suggests that the astrocyte-neuron metabolic shuttling is impaired in MS[125]. Of the many mechanisms that could underlie lactate-derived astrocyte secretion, research has focused on the lactosylceramide (LacCer) pathway due to its role in inflammation and demyelination in MS[108,128,129]. Dysregulation of the LacCer pathway in an animal model of MS, experimental autoimmune encephalomyelitis (EAE), demonstrates reduced lactate secretion from astrocytes, and associates with impaired recovery, increased axonal loss, and demyelination[108,128]. This reduction of astroglial-secreted lactate may leave neurons with reduced energy substrates and therefore, susceptible to injury and death[108].

1.3 Molecular Tools to Study Astrocytes in Multiple Sclerosis

Although progress has been made to understand astrocytes and their properties, information remains relatively limited concerning how astrocytes function or interact with other cells. A major bottleneck to progressing our understanding of astrocytes in human health and disease is the paucity of reliable tools and limited techniques available to study adult human astrocytes. Studies on human CNS cells, especially in disease states, are typically restricted to post-mortem tissue. Post-mortem studies can provide important insights into the morphological,

spatial, and topographical features of human astrocytes, although direct functional information is lost. In contrast, cell culture can probe the functional properties of human astrocytes but often lack the complex cell-to-cell interactions found in whole tissues.

The development of more targeted molecular markers and improved genetic and transcriptomic techniques, has greatly facilitated our ability to understand the human astrocyte. Indeed, establishing astrocyte-specific gene databases has already identified a wide range of astrocyte populations[130,131] (**Table 1.1**). These databases provide an opportunity to better target astrocytes, which will be necessary if we are to elucidate human astrocyte functions in health and disease.

Table 1.1. Overview of common immunohistochemical markers for astrocytes in the adult human CNS. Abbreviations: OL = oligodendrocyte; NPC = neural progenitor cell.

Gene (Protein)	Labelled Cells	Astroglial Localisation	Functional Property
Aldh1l1 **(ALDH1L1)**	Astrocyte + OL	• Soma • Fine processes	Oxidoreductase involved in folate metabolism[132]
Aqp4 **(AQP4)**	Astrocyte + ependymal cell	• Endfeet	Water channel[133]
C3 **(C3)**	Astrocyte +	• Soma • Major processes	Complement pathway[56]
Cd44 **(CD44)**	Astrocyte + OL	• Soma • Fine processes	Cell surface glycoprotein involved in cell-cell and cell-matric interactions[134]
Gjb6 **&** ***Gja1*** **(CX30 & CX43)**	Astrocyte + OL+ NPCs	• Soma • Endfeet	Gap junction protein[135]
Gfap **(GFAP)**	Astrocyte + NPCs	• Soma • Major processes	Intermediate filament involved in cytoskeleton[136]
Glul **(Glutamine synthetase)**	Astrocyte + OL	• Soma • Major processes	Enzyme involved in nitrogen metabolism[62]
Ndrg2 **(NDRG2)**	Astrocyte + NPCs	• Soma • Fine processes	Cell proliferation inhibitor and cell differentiation and apoptosis promotor[137-139]

1/2

***Table 1.1**. Continued…*

Gene (Protein)	Labelled Cells	Astroglial Localisation	Functional Property
***S100b* (S100ß)**	Astrocyte + OL+ NPCs	• Soma • Some processes	Calcium binding protein[140]
***Slc1a3* & *Slc1a2* (EAAT-1 & EAAT-2)**	Astrocyte + OL + NPCs + endothelial cell	• Fine processes	Glutamate transporter[141]
***Slc6a11* (GAT3)**	Astrocyte + NPCs	• Major processes	Terminates the action of GABA via high affinity sodium-dependent reuptake[142]
***Sox9* (SOX9)**	Astrocyte + NPCs + ependymal cell	• Nucleus	Transcription factor important for development and glial fate[143]
***Vim* (VIMENTIN)**	Astrocyte + NPCs+ endothelial cell	• Soma • Fine Processes	Intermediate filament protein[144]

2/2

1.3.1 Current astrocyte protein markers

Intermediate filament protein, glial fibrillary acidic protein (GFAP), is the most widely used astrocyte marker and has provided the basis for foundational work on astrocyte function. It was first identified in the post-mortem brains of MS cases and isolated from an MS plaque consisting of fibrous astrocytes and demyelinated axons[145]. GFAP is a major contributor to the cytoskeleton and thus, clearly defines astroglial soma and processes[62]. However, GFAP+ labelling fails to capture the fine processes of astrocytes and is preferentially expressed in the WM over GM[146,147]. Moreover, GFAP+ expression can be present in other CNS cells, such as neurons[148,149]. Given the limitations of GFAP+ labelling, other astrocyte markers have also been identified (**Table 1.1**)[131,150]. Common GFAP alternatives include AQP4, EAAT-1 and EAAT-2, and calcium-binding protein S100ß. Of interest, aldehyde dehydrogenase-1 L1 (ALDH1L1) is a folate enzyme shown to be a specific and ubiquitous marker of astrocytes[147]. Transgenic mice under the control of the ALDH1L1 promotor demonstrate expression in more than 90% of astrocytes in the hippocampal regions and, unlike GFAP+ labelling, show ALDH1L1+ expression of the finer astrocyte processes[151].

Using a combination of molecular markers to characterise astrocyte phenotypes can facilitate a complete understanding of astroglial properties. A limitation common to all known astrocyte markers is the lack of specificity and ability to capture all astrocytes[150]. Although ALDH1L1+ is considered a pan-specific astrocyte marker, its expression in human tissues is not as widespread as reported in rodent models[62,132]. Moreover, the expression pattern of astrocyte markers can vary, which suggests that different astrocyte markers label different

astroglial subpopulations or phenotypes[56]. This astrocyte diversity is crucial to consider when characterising astrocytes in pathological conditions and for data interpretation, as many studies often use only GFAP+ to label astrocytes[150]. Indeed, GFAP+ labelling is routinely used as a marker of astrocyte reactivity due to its upregulation across many CNS disorders, early response to injury, and sensitivity to environmental changes[150]. A common mistake is interpreting changes to GFAP+ expression as proliferation or loss of astrocytes rather than a change in phenotype[152]. One strategy to understand astrocyte changes in disease is to dissociate reactive astrocytes from non-reactive astrocytes using co-labelling of two astrocyte markers[152]. Using a non-reactive or quiescent astrocyte marker, such as ALDH1L1, in tandem with GFAP+ labelling, we can better understand astrocyte properties in disease.

1.3.2 Characterising astrocytes using mass spectrometry-based proteomics

The increasing prevalence of "-omic" technologies, including genomics, transcriptomics, and proteomics, has advanced our understanding of astrocytes and their role in health and disease. "-Omic" technologies often identify key molecular markers for pathway identification, which can be functionally validated via technologies, such as human iPSC cultures[153]. Bulk approaches, such as proteomics, are relatively unbiased allowing for the identification of new molecular targets. These bulk approaches can also be run in parallel with immunohistochemistry (IHC) or laser capture microdissection (LCM) to maintain spatial information[154].

1.3.2.1 Proteomic approaches and strategies to study human tissues

Proteomics, the large-scale study of proteins, has been of particular interest due to its potential for early disease diagnosis, identification of better therapeutic targets, and development of novel treatments. A benefit of proteomics rests on its ability to provide a more comprehensive understanding of molecular and cellular functions, which can be further targeted with methods like LCM to isolate specific cell populations from heterogeneous tissue. Given that proteins and peptides can reflect changes in physiological states, proteomic analysis of human materials is important to advancing our understanding of native molecular mechanisms and disease pathophysiology.

Currently, there are two main approaches to proteomics: top-down and bottom-up proteomics. Both approaches have a general workflow of proteins or peptide separation using techniques such as high-performance liquid chromatography, identification via technologies such as tandem mass spectrometry, and interpretation of biological relevance using bioinformatics[155,156]. Although the top-down approach allows for identifying intact proteins, it remains technically challenging, especially for complex biological samples[156]. Therefore, bottom-up proteomics has been the method of choice for studying human tissues and materials[157].

However, bottom-up workflows typically require sample homogenisation and digestion. Because distinct cell populations contribute an unknown amount of cellular constituents to a given tissue lysate, information regarding protein and spatial localisation is lost. LCM, a technique for isolating specific subpopulations

of tissue cells, has greatly facilitated our ability to target specific cell populations within their heterogeneous tissue. LCM approaches can also be used in conjunction with co-labelling IHC or immunofluorescence (IF) techniques, which is particularly useful for targeting cell-specific subpopulations. Many sample types can undergo LCM, from live cells to formalin-fixed paraffin-embedded (FFPE) tissues, which is crucial for human studies where available sample types are limited[59,158].

1.3.2.2 Proteome profiles of astrocytes in MS

Advances in proteomics, have been of particular interest in MS research due to its potential for biomarker identification, improved understanding of disease pathogenesis, and identification of targets for future therapies and treatments[156]. Much of the MS proteomic research has focused on CSF, serum, or other biofluids due to their relatively easy accessibility and suitability for clinical use[155,159]. However, biofluid proteomics lacks the cellular and spatial nuances present in whole tissues, limiting its generalisability into MS pathophysiology.

Proteomic analysis of post-mortem brain tissue has the potential to characterise the molecular neuropathology of MS of specific cell types. However, proteomic studies in MS tissue samples are limited[156]. Most of the LCM-directed proteomic work in MS tissues has focused on lesions, identifying protein group functions related to the cell cycle, synaptic transmission, myelin, cell metabolism, and immune responses[160,161]. Although many of these protein group IDs map to astrocytes and neuron origin[63,162], proteomic analysis of specific cell types, including astrocytes, in MS has been relatively neglected.

Furthermore, much of our understanding of the molecular signatures of human astrocytes from MS tissues is based on genomic and transcriptomic studies[59,157]. LCM-targeted astrocytes from human CNS tissues express transcriptomic signatures related to oxidative stress, apoptosis, inflammation, iron metabolism, and glutamate transport[62,157], suggesting that distinct molecular profiles underlie astrocyte subpopulations and their corresponding functional diversity. Indeed, EAE animal models demonstrate transcriptional differences between astrocyte subtypes, which show distinct functional responses associated with MS pathological outcomes such as inflammation and neurotoxicity[163]. Given the diverse transcriptomic signatures expressed by astrocytes, characterisation of the proteome in astrocyte subpopulations may provide greater insight into the heterogeneous contributions and responses of astrocytes in MS.

1.4 Overview of Thesis

This thesis focuses on the contributions of astrocyte diversity on pathological outcomes in MS. The overall hypothesis of this thesis is that astrocyte phenotype and subpopulation diversity influences MS inflammatory neurodegeneration, which may act in a genotype-dependent manner.

To address this overarching hypothesis, the specific aims of this thesis are as follows:

1. To characterise astrocyte subpopulation morphology, topography, and relationships with MS pathological outcomes in the MS motor cortex using quantitative neuropathological methods.
2. To evaluate perivascular astrocyte subpopulation relationships with vessel permeability in the MS motor cortex using quantitative neuropathological methods.
3. To establish an FFPE LCM-based proteomic workflow and to identify proteome signatures of LCM-targeted astrocyte subpopulations in the MS motor cortex.

This thesis aims to improve our understanding of astrocyte extent, distribution, and contribution to motor cortical pathology in MS and its relationship with the genetic risk factor, *HLA-DRB1*15*. We achieve this using quantitative neuropathology and LCM-directed proteomics. Using a combined pathologic and proteomic approach, we advance our understanding of astrocyte subpopulations and their diverse roles in MS cerebral cortical pathology.

2 Subpopulations of astrocytes and their antagonistic relationships with motor cortical pathology in progressive multiple sclerosis

2.1 Introduction

Cortical tissue injuries in functionally relevant areas, such as the motor cortex, are key contributors to the progression to permanent disability in MS[28,164,165]. Inflammation and neurodegeneration are common features of the MS motor cortex, of which the severity of MS pathological outcome relates to *HLA-DRB1*15* status[28,52]. Focus on the traditional immune cells of the CNS has revealed an impact of inflammation on neuronal survival in MS[52], but little is known about other modulators of inflammation and cell survival, such as astrocytes.

This chapter evaluates the extent and distribution of astrocytes using GFAP+ and ALDH1L1+ markers in a post-mortem MS cohort genotyped for *HLA-DRB1*15*. We provide evidence that distinct astrocyte subpopulations are present in the MS motor cortex and are influenced by the *HLA-DRB1*15* genotype. Astrocyte subpopulations display divergent topographical patterns with GFAP+ biased towards WM expression and ALDH1L1+ expression dominant in the GM. In addition to these topographical distinctions, we show that GFAP+ and ALDH1L1+ astrocytes have opposing relationships with demyelination, neuronal counts, and immune cells. Overall, these findings suggest astrocyte subpopulation differences at both the topographical and functional level, which furthers our understanding of how astrocytes influence MS pathogenesis.

2.2 Materials and Methods

2.2.1 Study population

A human autopsy cohort of pathologically confirmed MS cases (*n*=47) and age- and sex-matched non-neurological controls (*n*=10) derived from the UK MS tissue bank, Imperial College, London was used. The materials used had ethics approval (Research Ethics Code [REC] 08/MRE09/31+5) according to the UK Human Tissue Act 2006.

Each MS case had DNA available for genetic analysis of the *HLA-DRB1*15* locus (*15*-: *n*=26; *15*+: *n*=21) and all cases had fixed material available for detailed pathologic characterisation. Cases in this cohort were part of a previous study of genetic-pathology correlations in the MS motor cortex, which were used to correlate known MS pathological outcomes[28,52,99].

2.2.2 Immunohistochemistry

Serial 6µm-thick FFPE sections of the motor cortex were used. Based on the pre-established method described by Yates et al. (2015), motor cortical sections were labelled with primary antibodies for astrocytes (GFAP, Dako; ALDH1L1, Abcam), myelin (PLP, BioRad), neurons (NeuN, Millipore), microglia/macrophages (IBA1, Wako; CD68, Dako), and resident microglia (TMEM119, Sigma) using 3,3'-diaminobenzidine IHC (DAB: Dako REAL™ EnVision™ Detection System, Agilent; K500711-2; **Table 2.1**). Sections were counterstained with Harris Haematoxylin (Lecia, 3801560E). IHC sections were imaged and visualised using AxioVision software (v4.9.1, ZEISS) and digitally scanned using Aperio

ScanScope AT Turbo system (Leica Biosystems) at 400X magnification for downstream analyses.

Table 2.1. Details of antibodies used in IHC methods.

Primary Antibodies				
Name	**Manufacture**	**Catalogue Number**	**Host**	**Dilution**
ALDH1L1	Abcam	ab177463	Rabbit monoclonal	1/4000
CD68	Dako	M0876	Mouse monoclonal	1/100
GFAP	Dako	Z0334	Rabbit polyclonal	1/6000
IBA1	Wako	019-19741	Rabbit polyclonal	1/1000
NeuN	Millipore	MAB377	Mouse monoclonal	1/400
PLP	BioRad	MCA839G	Mouse monoclonal	1/1000
TMEM119	Sigma	HPA051870	Rabbit polyclonal	1/1500

2.2.3 Data analyses

2.2.3.1 Quantification of global astrocyte expression in the motor cortex

Global astrocyte expression was quantified in pre-defined DAB stained trajectories using established methods[28]. Trajectories were placed perpendicular to the motor cortical surface and spaced at pre-specified intervals. Each trajectory had two fields of views (FOVs) denoted per GM layer, except for layer III, which had four FOVs due to its larger and heterogeneous nature. In addition to the fourteen GM FOVs, four WM FOVs were captured. Astrocyte expression was quantified as positively labelled pixel density (pixels/mm^2) using a semi-automatic

colour-based extraction in MATLAB software (vR2019a). Only trajectories with all six cortical GM layers and WM present were considered.

FOVs were denoted as normal-appearing, lesional, or perilesional based on adjacent PLP-stained sections. To control for region-biases, lesional and perilesional FOVs were only compared to normal-appearing FOVs of the corresponding GM or WM areas. Lesions were defined as areas of complete demyelination, and perilesions were defined as the first normal-appearing region outside of the lesion[42].

2.2.3.2 Assessment of astrocyte features in the motor cortex

A semi-quantitative score was devised to address specific features of astrocytes along the same FOVs outlined above. The strength of immune-positive staining in the glial processes, cell quantity, and cell reactivity was assessed in each FOV as follows: 0 (absent), 1 (weak), 2 (moderate), or 3 (strong) (**Figure 2.1**). We defined glial processes as either granular or fibrous extensions. Cell body reactivity was based on the extent of hypertrophy or loss of spherical shape[150]. Scores were validated for reliability within rater (test-retest) and between two independent raters (interrater reliability) using Kendall's Coefficient of Concordance (W) on a subset of test cases (n=30).

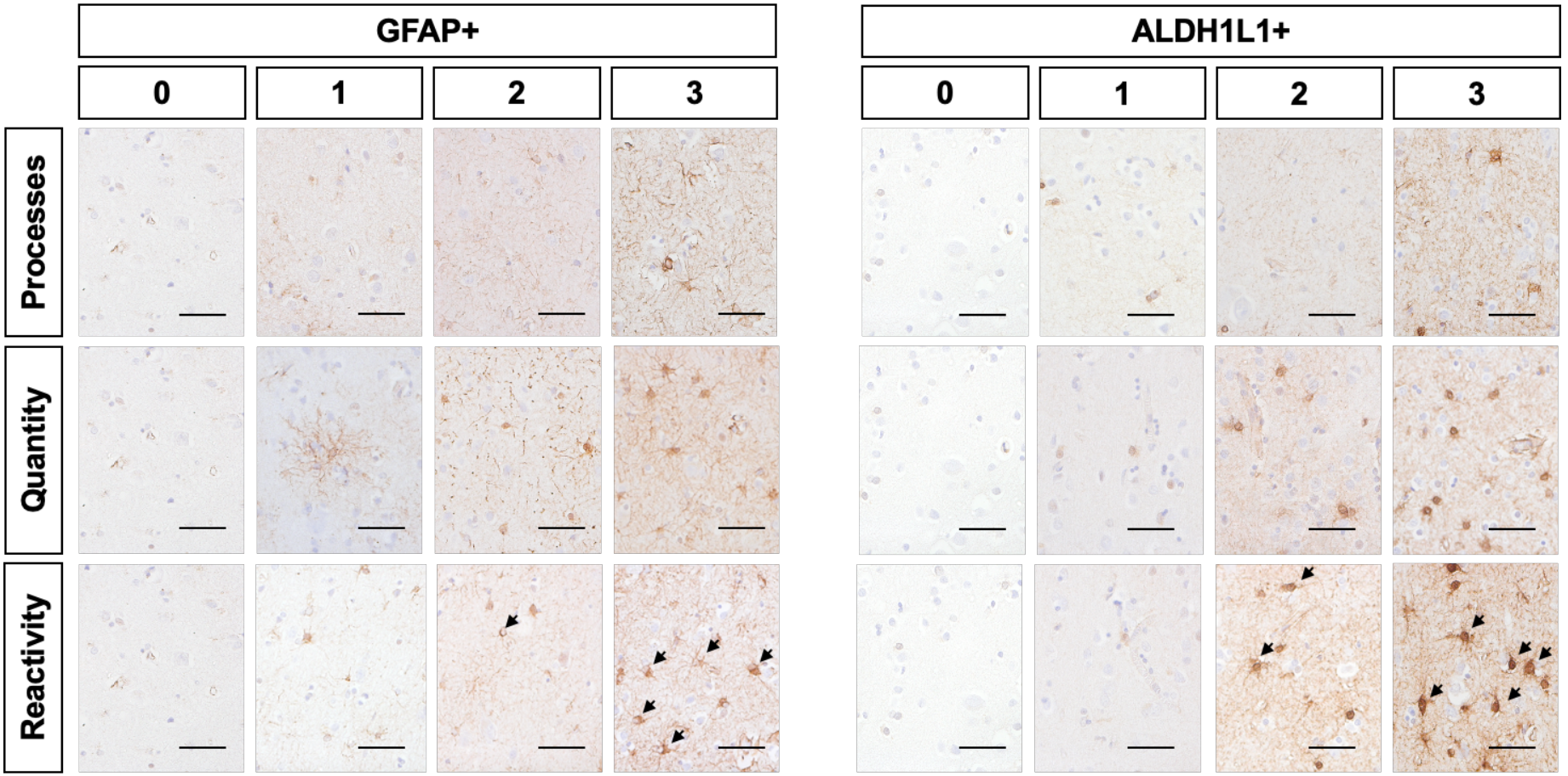


Figure 2.1. Semi-quantitative scoring of GFAP+ and ALDH1L1+ astrocyte expression in the motor cortex. For each FOV, the strength of astrocyte immunopositive labelling was assessed in the glial processes, cell body quantity, and reactivity of cell bodies. We defined cell body reactivity as hypertrophy or complete breakdown of spherical shape (arrows). GFAP+ and ALDH1L1+ staining were analysed in each component on a scale of 0 (absent), 1 (weak), 2 (moderate), or 3 (strong). Scale bar = 500μm.

2.2.4 Statistical analyses

Statistics were calculated and graphed using SPSS software (v27; IBM) and Prism software (v9; GraphPad). All tests of hypotheses were carried out using two-sided tests, and $p \leq .05$ was considered significant. Data normalities were assessed with the Shapiro-Wick test. Backwards elimination was performed to remove any covariates (age; post-mortem interval; sex) that did not significantly contribute to the model.

Curve-estimation regression models were fitted to assess the line of best fit for astrocyte patterns in cortical GM layers and WM. To account for intra-subject variability, generalised estimating equation (GEE) models were used to evaluate astroglial GM and WM differences within MS and control cases. General linear models were used to assess the influence of MS, *HLA-DRB1*15* status, and age on astrocyte expression. Overall models for genotype status also underwent pairwise comparisons to identify specific *15*- vs *15*+ relationships. To assess the influence of demyelination, GEE models were applied to measure astrocyte changes in lesional and perilesional areas within MS cases. Astroglial correlations with neuronal and macrophage/microglia outcomes were assessed using Spearman's rank correlation coefficient, which were corrected for multiple comparisons using the Benjamini and Hochberg (BH) method[166]. To ensure covariates did not influence significant associations, data deemed significant were normalised using the Two-Step procedure[167-169] and controlled for covariates using partial correlations.

2.3 Results

2.3.1 Demographics and pathological features

Clinical details of the cases used in this study are found in **Table 2.2**, as previously described[28,52,99]. 80.9% of our MS cases were classified as SPMS (*n*=38), with 8.5% being PPMS (*n*=4) and 2.1% being RRMS (*n*=1). The clinical course was unknown for 4 MS cases.

Brain weight was decreased in MS compared to controls (MS: 1157.0 ± 120.4g; Control: 1341.0 ± 203.1g; $p<.0001$). However, brain weight was not influenced by genotype (*15*-: 1152.2 ± 137.1g; *15*+: 1163.3 ± 101.1g; $p=.860$). MS cases had a median age of 62-years old, which were younger than the median age of 76-years old in control cases ($p=.005$). Genetic status did not influence the median age at death (*15*-: 58-years old; *15*+: 66-years old; $p=.380$). In our MS cohort, we classified younger cases as those equal to or below the median age of 62-years old (*15-: n*=15, *15+: n*=9) and older cases as those above the median age of 62-years old (*15*-: *n*=11, *15*+: *n*=12). MS disease duration was 30.20 years and was not influenced by genotype ($p=.749$).

Concerning motor cortical demyelination, 51.0% (24/47) of MS cases demonstrated motor cortical lesions in the pre-defined trajectories. Of the 34 cortical lesions recorded in our MS cohort, 85.3% (29/34) were subpial (Type III), 8.8% (3/34) spanned the full cortical depth (Type IV), 5.9% (2/34) were leukocortical (Type I), and none were intracortical (Type II), according to established criteria[42]. Subpial lesions typically involved multiple gyri and did not extend beyond layers I-III. Cortical plaques were chronic inactive, except for one

leukocortical lesion, which had macrophage/microglial activation at the lesion border. No demyelination was observed in control cases. Motor cortical lesion data were part of previously published work[28].

Table 2.2. Clinical details of MS and control cohort. Values represent the mean unless stated otherwise. F = female; M = male; N/A = not applicable.

	MS (*n*=47)	***HLA-DRB1*15-* (*n*=26)**	***HLA-DRB1*15+* (*n*=21)**	**Control (*n*=10)**
Age of death (yrs)	62.9 (range:40-92)	61.5 (range: 43-86)	64.8 (range: 40-92)	76.7 (range: 68-91)
Duration of disease (yrs)	30.9 (range:11-58)	29.0 (range: 12-56)	31.7 (range: 12-58)	N/A
Sex	F = 34, M = 13	F = 20, M = 6	F = 14, M = 7	F = 6, M = 4
Clinical course	PPMS = 4 RRMS = 1 SPMS = 38 Unknown = 4	PPMS = 1 RRMS = 1 SPMS = 21 Unknown = 3	PPMS = 3 RRMS = 0 SPMS = 17 Unknown = 1	N/A
Brain weight (g)	1157.0 (range: 894-1380)	1151.8 (range: 894-1380)	1163.2 (range:1000-1364)	1350.3 (range: 1072-1628)
Post-mortem interval (hrs)	18.1 (range:7-38)	18.2 (range: 8-28)	18.1 (range: 7-38)	26.3 (range:10-52)

2.3.2 Validation of semi-quantitative astrocyte score

Validation of semi-quantitative method showed a test-retest and interrater reliability greater than 75%, which was deemed sufficient for assessment of the entire cohort (**Table 2.3**).

Table 2.3. Reliability of GFAP+ and ALDH1L1+ semi-quantitative scoring. Semi-quantitative scores were assessed for reliability using Kendall's Coefficient of Concordance (W) on a subset of test cases (*n*=30). Data consider the concordance of two independent raters (interrater reliability) and test-retest of a single rater. There was no reliability data for GFAP processes layer I due to unanimous agreement between raters. Blue indicates significant ($p \leq .05$).

		GFAP+		ALDH1L1+	
		Kendall's W	***p*-value**	**Kendall's W**	***p*-value**
Processes	**Layer I**	N/A	N/A	.937	.0001
	Layer II	.890	.0001	.984	.0001
	Layer III	.876	.0001	.976	.0001
	Layer IV	.889	.0001	.983	.0001
	Layer V	.836	.0001	.967	.0001
	Layer VI	.878	.0001	.951	.0001
	WM	.902	.0001	.981	.0001
Quantity	**Layer I**	.795	.0001	.887	.0001
	Layer II	.807	.0001	.811	.0001
	Layer III	.859	.0001	.835	.0001
	Layer IV	.844	.0001	.822	.0001
	Layer V	.789	.0001	.808	.0001
	Layer VI	.893	.0001	.931	.0001
	WM	.917	.0001	.978	.0001
Reactivity	**Layer I**	.859	.0001	.938	.0001
	Layer II	.794	.001	.929	.0001
	Layer III	.793	.0001	.890	.0001
	Layer IV	.861	.0001	.887	.0001
	Layer V	.811	.0001	.905	.0001
	Layer VI	.891	.0001	.937	.0001
	WM	.841	.0001	.980	.0001

2.3.3 Topographical differences of motor cortical astrocyte subpopulations in MS and control cases

In our MS and control cohort, we observed GFAP+ interlaminar, varicose projection, and protoplasmic astrocytes in the GM, as previously shown[71]. A thick border marked the glia limitans, followed by a dense network of astroglial processes in layer I (**Figure 2.2A**). Interlaminar astrocytes, identified by their

needle-like extensions, were located in layer II and extended into the beginning of layer III. Around non-capillary GM vessels, there was a concentration of GFAP+ expression, including the contacts of many GFAP+ endfeet and cell bodies (**Figure 2.2B**). GFAP+ endfeet also contacted GM capillaries, which were occasionally contacted by the long processes of varicose projection astrocytes. GFAP+ astrocytes in GM layers III-IV were typical of protoplasmic astrocytes – bushy with clearly defined somas (**Figure 2.2C**). Cell body expression at the GM-WM boundary was prominent. WM GFAP+ mainly was localised to the processes organised in compact, relatively parallel strands (**Figure 2.2D**). As seen in the GM, WM fibrous GFAP+ astrocytes also had endfoot contacts with vasculature.

GM ALDH1L1+ expression was localised to the astrocyte soma. These well-defined cell bodies were occasionally accompanied by diffuse processes (**Figure 2.2G**). A thin, pale border marked the glia limitans, followed by a stretch of immunoreactivity in layer I (**Figure 2.2E**). Immunopositive labelling was present at the start of layer II and extended throughout the rest of the GM. Unlike GFAP+ perivascular expression, ALDH1L1+ was absent around non-capillary GM vessels (**Figure 2.2F**). This perivascular expression was restricted to non-capillary vessels, as ALDH1L1+ endfeet contacts were present around GM capillaries. ALHD1L1+ cell body expression was also concentrated at the GM-WM border. In the WM, ALDH1L1+ expression was localised to the astrocyte soma and had minimal-to-no processes (**Figure 2.2H**). However, ALDH1L1+ endfeet were present around WM vasculature.

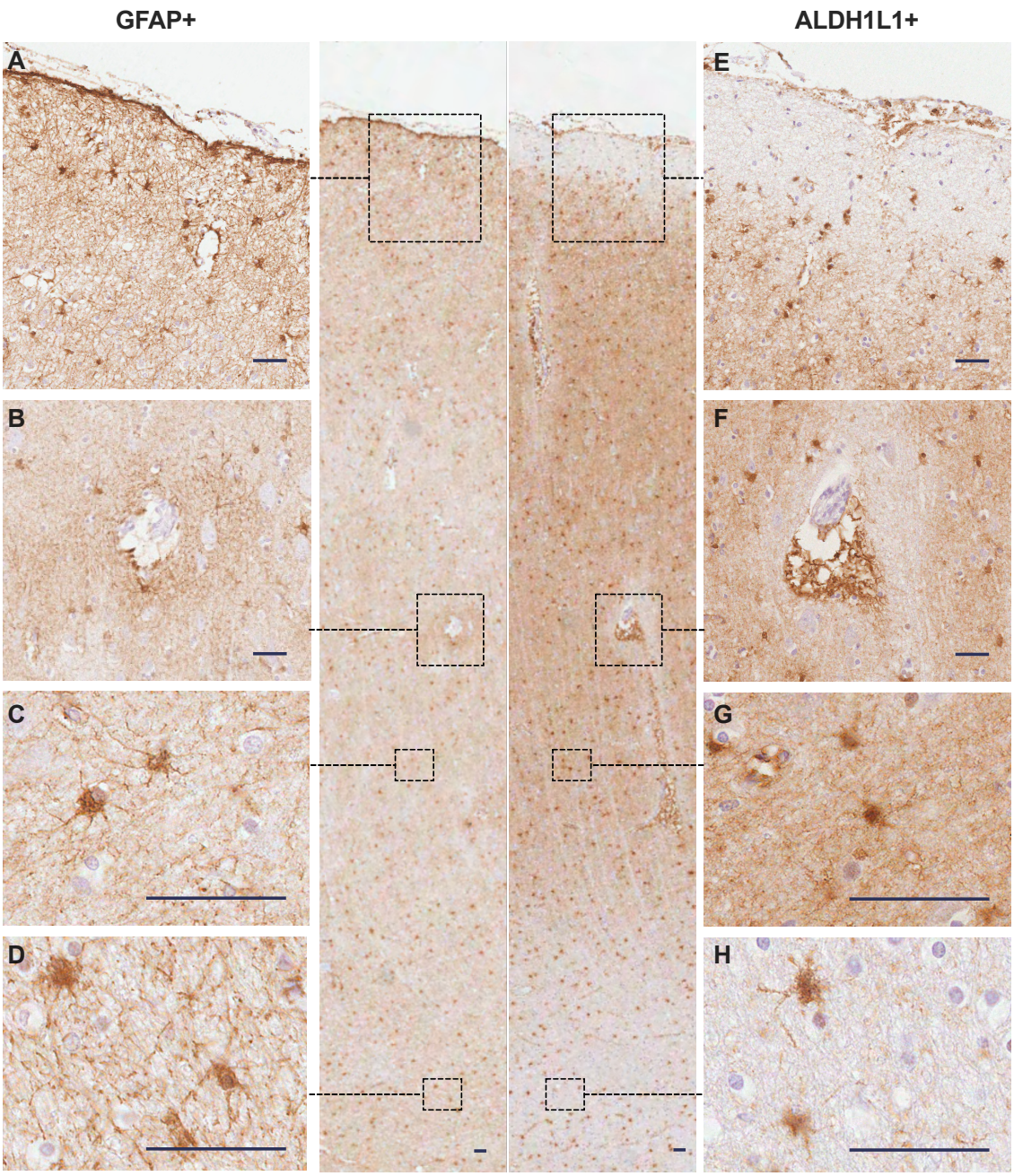


Figure 2.2. Topography of GFAP+ and ALDH1L1+ astrocytes in the MS motor cortex. GFAP+ expression was localised to processes and the soma, which was concentrated at the glia limitans (**A**) and NAGM vessels (**B**). NAGM GFAP+ astrocytes displayed bushy morphology (**C**), whilst NAWM GFAP+ astrocytes were organised along compact parallel strands (**D**). In contrast, ALDH1L1+ expression was primarily absent at the glia limitans (**E**) and NAGM vessels (**F**). ALDH1L1+ astrocytes in NAGM (**G**) and NAWM (**H**) had strong soma labelling with occasional diffuse extensions. Scale bar = 50μm.

2.3.4 Cortical astrocyte subpopulations are differentially expressed in the GM and WM of MS and controls cases

2.3.4.1 Distribution and extent of cortical astrocyte expression

In both MS and control cases, global GFAP+ astrocyte expression was greatest in NAGM layer I and NAWM. The lowest global GFAP+ astrocyte expression was in NAGM layers III-V. Indeed, curve-estimation in MS and control cases displayed an upward quadratic curve across NAGM layers to NAWM (MS, R^2=.627, p<.0001; Control, R^2=.568, p<.0001; **Figure 2.3A**). In MS, global GFAP+ astrocyte expression was greater in NAWM than NAGM, although this was not observed in control cases (MS: p<.0001; Control: p=.383; **Table 2.4**).

Inversely, global ALDH1L1+ astrocyte expression for MS and control cases was highest in NAGM layers II-IV and lowest expression in NAGM layer I and NAWM. This distribution across the cortex showed a downward quadratic curve in MS and control cases (MS, R^2=.132, p<.0001; control, R^2=.160, p=.003, **Figure 2.3B**). Further, MS and controls had greater global ALDH1L1+ astrocyte expression in NAGM than NAWM (MS and Control: p<.0001; **Table 2.4**)

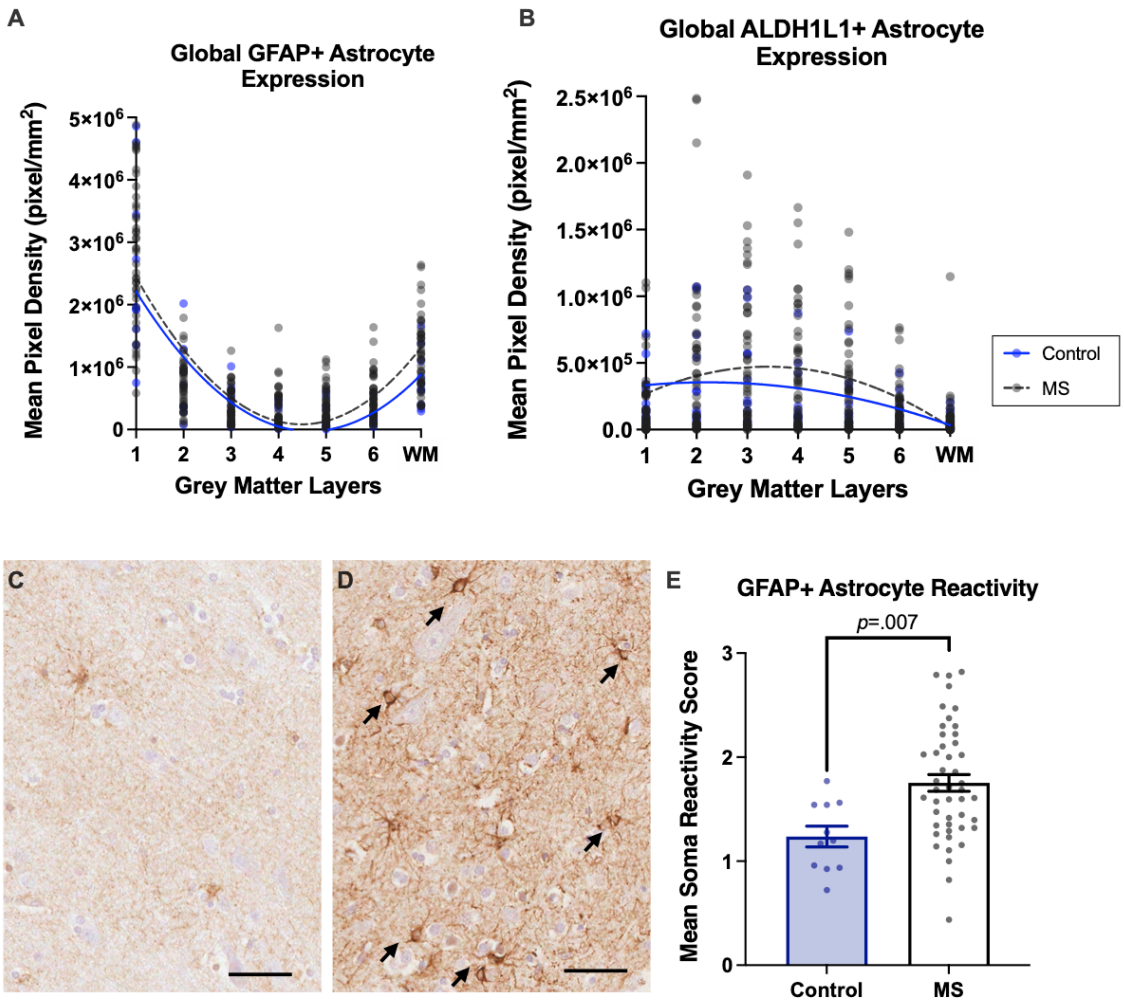


Figure 2.3. Extent and distribution of GFAP+ and ALDH1L1+ astrocytes in the MS motor cortex. Quantitation of global GFAP+ and ALDH1L1+ expression in MS and controls demonstrated opposing distribution with peak GFAP+ expression in NAGM layer I and NAWM (**A**). In contrast, ALDH1L1+ expression peaked in NAGM layers II-IV (**B**). NAGM GFAP+ astrocytes showed relatively spherical somas with fine extending processes (**C**). In addition to thickened processes, the soma of reactive GFAP+ astrocytes was distorted and had a hollow-like appearance (arrows; **D**). GFAP+ astrocyte reactivity was greater in MS compared to control cases (**E**). Scale bar = 50μm. Error bars represent ±SEM.

2.3.4.2 Astrocyte processes

In line with our global astrocyte expression findings, GFAP+ processes in MS and control cases were greater in NAWM than NAGM (MS and Controls: $p<.0001$;

Table 2.4). Conversely, ALDH1L1+ processes in MS and controls were greater in NAGM compared to NAWM (MS and Controls: $p<.0001$; **Table 2.4**).

2.3.4.3 Quantity of astrocyte cell bodies

Scores for soma quantity in MS and controls were also greater in NAWM than NAGM in GFAP+ (MS and Control: $p<.0001$;**Table 2.4**). In contrast, ALDH1L1+ soma quantity in MS cases were greater in NAGM than NAWM, whilst control case ALDH1L1+ soma quantity scores did not differ between GM and WM (MS: $p<.0001$; Control: $p=.541$;**Table 2.4**).

2.3.4.4 Astroglial soma reactivity

GFAP+ soma reactivity was greater in MS NAWM than NAGM ($p=.002$; **Table 2.4**). However, there was no difference between NAGM and NAWM for ALDH1L1+ cell body reactivity in MS ($p=.141$; **Table 2.4**). These relationships were also seen in control cases (GFAP: $p<.0001$; ALDH1L1: $p=.116$; **Table 2.4**).

Table 2.4. Comparison between NAGM and NAWM for GFAP+ and ALDH1L1+ expression in the motor cortex of MS and control cases.

		GFAP+			ALDH1L1+		
		NAGM	**NAWM**	***p*-value**	**NAGM**	**NAWM**	***p*-value**
MS	**Global Expression (pixel/mm^2)**	$8.1x10^5 \pm 4.1x10^5$	$1.2x10^6 \pm 5.9x10^5$	<.0001	$3.6x10^5 \pm 3.7x10^5$	$8.0x10^4 \pm 1.7x10^5$	<.0001
	Processes	2.2 ± 0.5	2.8 ± 0.4	<.0001	1.8 ± 0.9	0.6 ± 0.7	<.0001
	Soma Quantity	1.9 ± 0.5	2.4 ± 0.5	<.0001	2.3 ± 0.6	1.9 ± 1.0	<.0001
	Soma Reactivity	1.7 ± 0.6	2.1 ± 0.6	.002	1.8 ± 0.7	1.6 ± 1.0	.141
Control	**Global Expression (pixel/mm^2)**	$7.0x10^5 \pm 4.2x10^5$	$8.0x10^5 \pm 4.6x10^5$	.383	$2.9x10^5 \pm 2.5x10^5$	$6.9x10^4 \pm 7.1x10^4$	<.0001
	Processes	2.0 ± 0.7	2.6 ± 0.3	<.0001	1.8 ± 0.7	0.8 ± 0.5	<.0001
	Soma Quantity	1.6 ± 0.6	2.7 ± 0.3	<.0001	2.1 ± 0.7	2.2 ± 0.5	.541
	Soma Reactivity	1.2 ± 0.4	2.0 ± 0.6	<.0001	1.5 ± 0.6	1.7 ± 0.8	.116

2.3.5 Features of MS motor cortical astrocyte subpopulations differ from controls

2.3.5.1 GFAP+ astrocyte expression

In NAGM, global GFAP+ astrocytes expression did not differ between MS and control cases (p=.433). However, global GFAP+ astrocyte expression in NAWM was greater in MS than controls (p=.044). The specific astrocytic features, processes and soma quantity, did not differ between MS and controls in NAGM (Processes: p=.082; Quantity: p=.073). Processes and soma quantity scores in NAWM regions also showed no difference between MS and controls (Processes: p=.560; Quantity: p=.058). However, GFAP+ soma reactivity in NAGM was greater in MS compared to controls (p=.007; **Figure 2.3C-E**). In NAWM, GFAP+ reactivity did not differ between MS or control cases (p=.106).

2.3.5.2 ALDH1L1+ astrocyte expression

For both NAGM and NAWM, global ALDH1L1+ astrocyte expression in NAGM did not differ between MS and control cases (NAGM: p=.532; NAWM: p=.172). There was no difference between ALDH1L1+ astrocyte processes, soma quantity or soma reactivity in NAGM regions (Processes: p=.798; Quantity: p=.299; Reactivity: p=.455). This was also observed in NAWM (Processes: p=.421; Quantity: p=.795; Reactivity: p=.903).

2.3.6 NAGM cortical astrocyte subpopulations show opposite features with ageing depending on *HLA-DRB1*15* status

2.3.6.1 Influence of *HLA-DRB1*15* genotype on cortical astrocyte subpopulations

There was no influence of *HLA-DRB1*15* status on NAGM global GFAP+ astrocyte expression, processes, soma quantity, or soma reactivity (Global Expression: p=.355; Processes: p=.111; Quantity: p=.390; Reactivity: p=.107; **Table 2.5**). Similarly, genotype status did not influence NAGM global ALDH1L1+ astrocyte expression, processes, soma quantity, nor soma reactivity (Global expression: p=.591; Processes: p=.794; Quantity: p=.371; Reactivity: p=.441; **Table 2.5**).

Table 2.5. The influence of *HLA-DRB1*15* genotype on GFAP+ and ALDH1L1+ astrocyte expression in motor cortical NAGM. Reported p-values are the result of pairwise comparisons between *15*- and *15*+ cases.

		HLA-DRB1*15-	***HLA-DRB1*15+***	***p*-value**
GFAP+	**Global Expression (pixel/mm^2)**	$7.7x10^5 \pm 4.2x10^5$	$8.7x10^5 \pm 3.9x10^5$	.355
	Processes	2.1 ± 0.5	2.3 ± 0.5	.111
	Soma Quantity	1.9 ± 0.6	2.0 ± 0.5	.390
	Soma Reactivity	1.6 ± 0.5	1.9 ± 0.5	.107
ALDH1L1+	**Global Expression (pixel/mm^2)**	$3.4x10^5 \pm 3.3x10^5$	$3.9x10^5 \pm 4.2x10^5$	.591
	Processes	1.7 ± 0.9	1.8 ± 0.9	.794
	Soma Quantity	2.3 ± 0.7	2.4 ± 0.4	.371
	Soma Reactivity	1.7 ± 0.7	1.9 ± 0.6	.441

2.3.6.2 Influence of age at death on genotype for cortical astrocyte subpopulations

Given the influence of *HLA-DRB1*15* genotype on NAGM pathological features of MS in our cohort[28], we conducted assessment of GFAP+ and ALDH1L1+ astrocyte expression based on genotype to further probe differences between these two astrocyte markers.

In *HLA-DRB1*15*- cases, age only influenced GFAP+ astrocyte soma quantity (**Figure 2.4A-B**). Older *HLA-DRB1*15*- cases had greater GFAP+ soma quantity scores than their younger *HLA-DRB1*15*- counterparts (p=.005; **Figure 2.4B**). Age did not influence global GFAP+ astrocyte expression, processes, or soma reactivity in *HLA-DRB1*15*- cases (Global Expression: p=.358; Processes: p=.079; Reactivity: p=.076; **Figure 2.4A-B**).

In contrast, age impacted many features of GFAP+ astrocyte expression in *HLA-DRB1*15*+ (**Figure 2.4C-D**). Younger *HLA-DRB1*15*+ cases had greater global GFAP+ astrocyte expression, processes scores, and soma reactivity scores than older *HLA-DRB1*15*+ cases (Global Expression: p=.002; Processes: p=.011; Reactivity: p=.040; **Figure 2.4C-D**). GFAP+ soma quantity in *HLA-DRB1*15*+ cases were not affected by age (p=.197; **Figure 2.4D**).

Age did not influence NAGM ALDH1L1+ astrocyte expression in either *HLA-DRB1*15*- nor *HLA-DRB1*15*+ cases (**Table 2.6**).

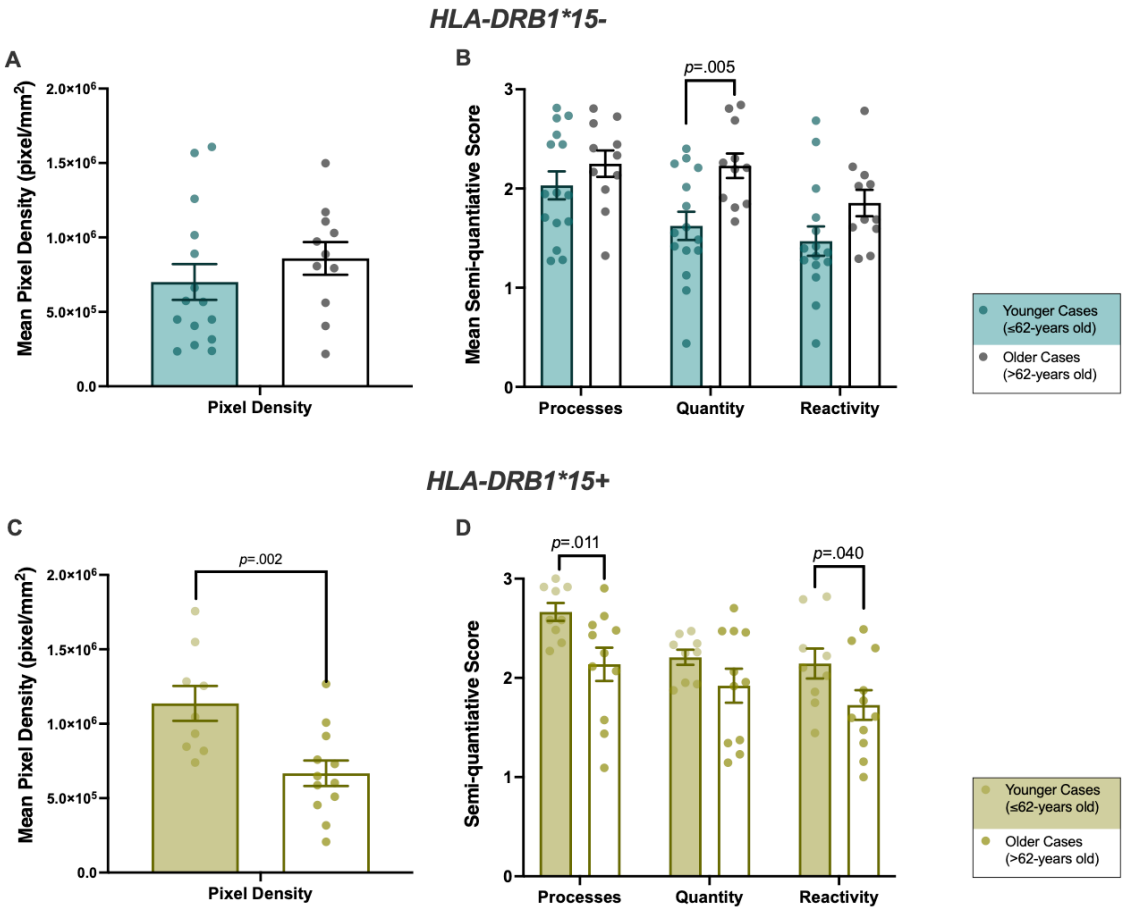


Figure 2.4. The influence of age on genotype status for GFAP+ astrocyte in NAGM in the MS motor cortex. For *HLA-DRB1*15-* cases, we saw no influence of age on global GFAP+ astrocyte expression, processes, or soma reactivity (**A-B**). Older *HLA-DRB1*15-* (>62-years old) cases had more GFAP+ cell bodies than their younger counterparts (≤62-years old; **B**). Inversely, *HLA-DRB1*15+* had greater global GFAP+ expression, processes, and soma reactivity than their younger counterparts (**C**). Age did not affect the number of GFAP+ cell bodies in *HLA-DRB1*15+* cases (**D**). Error bars represent ±SEM.

Table 2.6. The relationships between ALDH1L1+ astrocyte expression, age on *HLA-DRB1*15* genotype, and demyelination in the MS motor cortex. Age was based on the MS median age of 62-years old. Demyelination assessed in lesional, perilesional, and corresponding NAGM.

			Global Expression (pixel/mm^2)	Processes	Soma Quantity	Soma Reactivity
Age	***15-***	**Younger (≤62-years old)**	$3.0x10^5 \pm 3.2x10^5$	1.6 ± 0.9	2.2 ± 0.7	1.6 ± 0.7
		Older (>62-years old)	$3.8x10^5 \pm 3.6x10^5$	1.9 ± 1.0	2.4 ± 0.7	1.8 ± 0.8
		***p*-value**	**.141**	**.449**	**.396**	**.386**
	15+	**Younger (≤62-years old)**	$4.5x10^5 \pm 4.3x10^5$	1.9 ± 1.0	2.5 ± 0.2	1.9 ± 0.7
		Older (>62-years old)	$3.5x10^5 \pm 4.2x10^4$	1.8 ± 0.8	2.4 ± 0.5	1.9 ± 0.7
		***p*-value**	**.625**	**.255**	**.301**	**.198**
Demyelination	**Lesion vs NAGM**	**Lesion**	$1.3x10^7 \pm 4.5x10^6$	2.2 ± 0.7	2.3 ± 0.6	2.2 ± 0.7
		NAGM	$1.3x10^7 \pm 3.8x10^6$	2.3 ± 0.8	2.3 ± 0.6	2.2 ± 0.7
		***p*-value**	**.707**	**.079**	**.867**	**.595**
	Perilesion vs NAGM	**Perilesion**	$1.4x10^7 \pm 5.0x10^6$	2.5 ± 0.9	2.6 ± 0.6	2.1 ± 0.6
		NAGM	$1.4x10^7 \pm 3.5x10^6$	2.7 ± 0.6	2.5 ± 0.6	2.1 ± 0.6
		***p*-value**	**.876**	**.192**	**.702**	**.724**

2.3.7 Astrocyte subpopulations are differentially related to MS motor cortical pathology

2.3.7.1 Brain weight

There was no relationship between brain weight and NAGM GFAP+ astrocyte expression or between brain weight and ALDH1L1+ astrocyte expression (GFAP+: r=-.240, p=.109; ALDH1L1+: r=.110; p=.466).

2.3.7.2 Demyelination

The expression pattern of GFAP+ astrocytes differed in lesional and perilesional regions from the corresponding NAGM (**Figure 2.5**). GFAP+ processes and soma reactivity were greater in lesional areas than in corresponding NAGM (Processes: p=.003; Reactivity: p=.047; **Figure 2.5C**). Similarly, perilesions had greater GFAP+ processes and soma reactivity than corresponding NAGM (Processes: p=.017; Reactivity: p=.029; **Figure 2.5F**). Global GFAP+ expression and soma quantity were comparable between lesional areas and corresponding NAGM (Global Expression: p=.220; Quantity: p=.374; **Figure 2.5B-C**). This was similarly observed between perilesions and corresponding NAGM (Global Expression: p=.294; Quantity: p=.094; **Figure 2.5E-F**).

No relationships were found between ALDH1L1+ astrocyte expression and demyelination (**Table 2.6**).

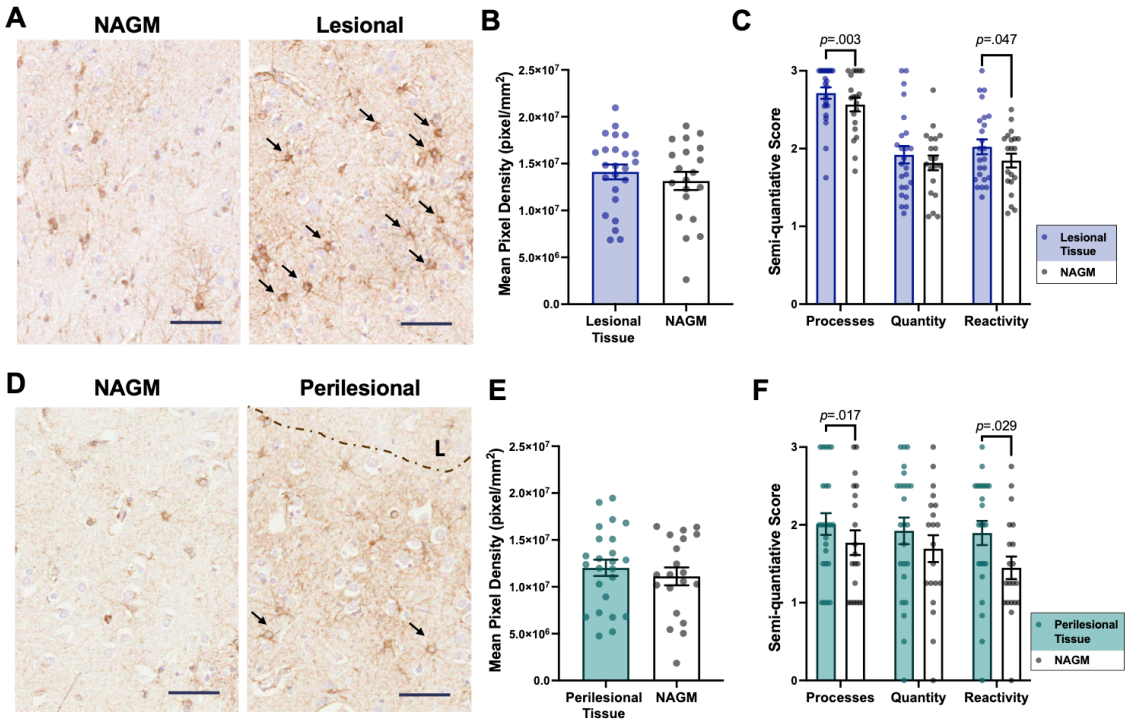


Figure 2.5. GFAP+ astrocyte expression in lesional, perilesional, and corresponding NAGM of the MS motor cortex. GFAP+ astrocytes displayed thickened processes and distorted, hollow somata indicative of reactivity in lesional compared to NAGM (arrows; **A**). Although global GFAP+ astrocyte expression and soma quantity were comparable between lesional and corresponding NAGM (**B-C**), GFAP+ processes and reactivity scores were greater in lesional compared to corresponding NAGM (**C**). GFAP+ astrocytes had similar reactive features in perilesional areas (arrows; L = lesion; **D**). Global GFAP+ astrocyte expression and cell body quantity were comparable between perilesional and corresponding NAGM (**E-F**). Perilesional areas had greater GFAP+ processes and soma reactivity than corresponding NAGM (**F**). Scale bar = 50μm. Error bars represent ±SEM.

2.3.7.3 Neuronal density in NAGM

No relationship between GFAP+ and NeuN+ density was found regardless of disease, genotype, or age status (**Figure 2.6-Figure 2.7**).

NAGM ALDH1L1+ astrocyte density positively associated with NeuN+ neuron density in MS cases (r=.457, p=.001; **Figure 2.6**). This relationship was restricted to *HLA-DRB1*15*- cases (*15*-: r=.540, p=.004; *15*+: r=.358, p=.121; **Figure 2.6**).

Investigation of the influence of age depending on the genetic status revealed that the positive association with NeuN+ was only observed in older *HLA-DRB1*15-* and not observed in the younger *15-* counterparts (Older: r=.918, p<.0001; Younger: r=.482, p=.069; **Figure 2.7**). Age did not influence *HLA-DRB1*15+* cases (Younger: r=.533, p=.139; Older: r=.145, p=.670; **Figure 2.7**). In controls, there was also no relationship between ALDH1L1+ astrocytes NeuN+ neurons (r=.714, p=.071; **Figure 2.6**).

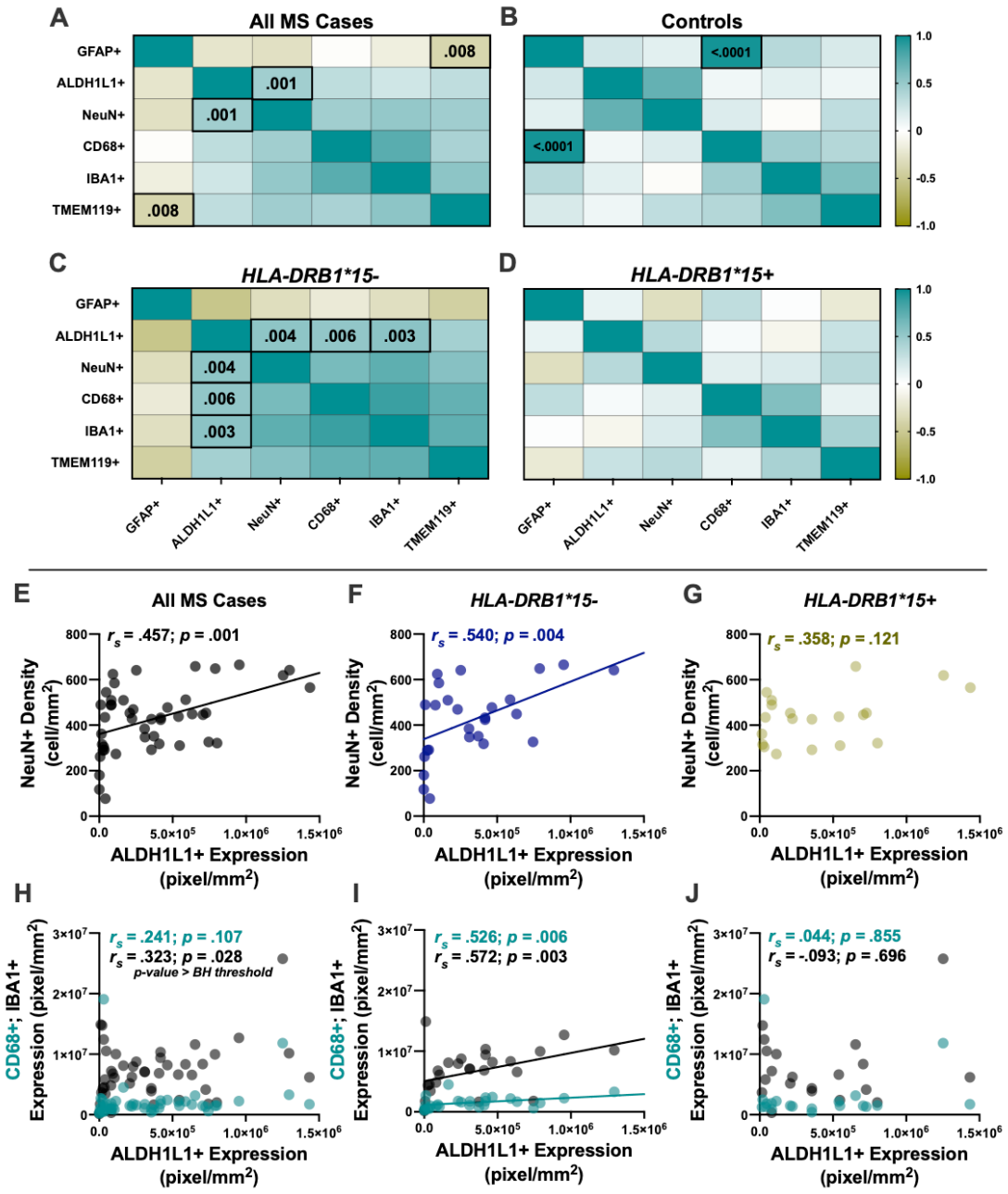


Figure 2.6. Summary of relationships for GFAP+ and ALDH1L1+ astrocytes with NeuN+ neurons, CD68+ or IBA1+ macrophage/microglia, and TMEM119+ microglia in the motor cortex. Relationships were assessed in NAGM of MS (**A**) and control cases (**B**). MS cases were also segregated by *HLA-DRB1*15* status (**C-D**). Spearman's correlation showed a positive relationship between ALDH1L1+ and NeuN+ density in MS cases, which was restricted to *HLA-DRB1*15-* cases (**E-G**). In MS, there was no relationship between ALDH1L1+ and CD68+ or IBA1+ (**H**). However, there was an influence of genotype where ALDH1L1+ positively correlated with CD68+ or IBA1+ density in *HLA-DRB1*15-* cases only (**I-J**). Only *p*-values that met the BH threshold were considered significant (*p*-value < BH threshold). Matrix legend: Values represent *p*-value; Colour bar represent Spearman's *r*-value where teal is positive and yellow is negative.

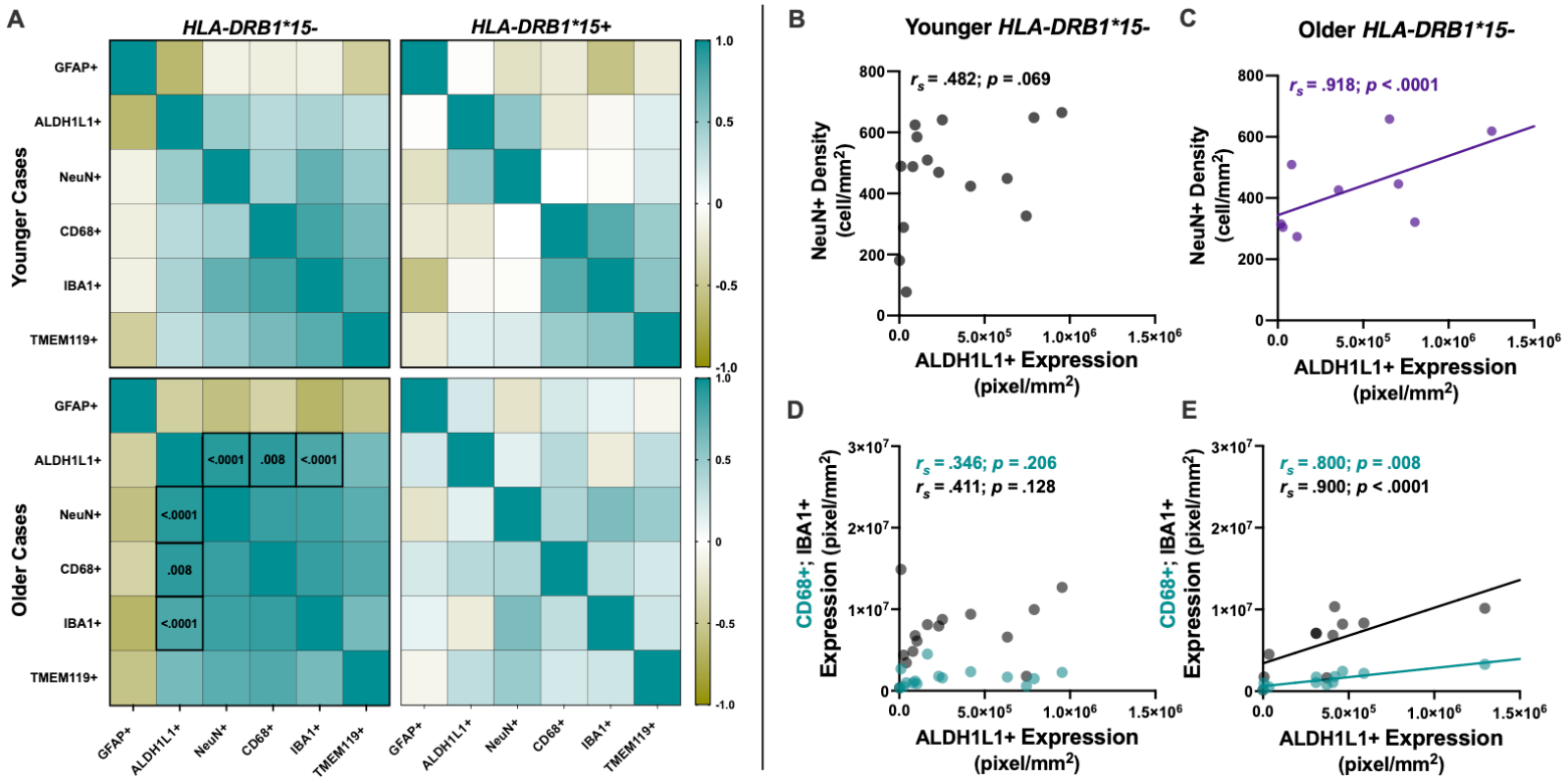


Figure 2.7. The influence of age on MS genetic status for relationships between GFAP+ and ALDH1L1+ astrocytes, neuronal density and macrophage/microglia expression in the motor cortex. Correlation matrices depict the relationships for GFAP+ and ALDH1L1+ astrocytes with NeuN+ neurons, CD68+ or IBA1+ macrophages/microglia, and TMEM119+ microglia in younger (≤62-years old) and older (>62-years old) MS within segregated by *HLA-DRB1*15* genotype (**A**). ALDH1L1+ astrocytes only associated with NeuN+, CD68+, and IBA1+ in older *HLA-DRB1*15-* cases (**B-E**). Multiple comparisons were corrected using the BH method. Matrix legend: Values represent *p*-value; Colour bar represents Spearman's *r*-value where teal is positive and yellow is negative.

2.3.7.4 Macrophage/microglia expression in NAGM

GFAP+ astrocyte expression negatively correlated with TMEM119+ microglia in MS cases (r=-.389, p=.008; **Figure 2.6**). However, genotype or age was not influenced by this relationship (**Figure 2.6**-**Figure 2.7**). In MS, markers of macrophage/microglia inflammation, CD68+ and IBA1+, did not associate GFAP+ astrocytes and were not impacted by genotype or age (**Figure 2.6-Figure 2.7**). Control cases had no relationship between GFAP+ and IBA1+ or TMEM119+, although there was a positive relationship between GFAP+ and CD68+ density (r=.964; p<.0001;**Figure 2.6**).

In MS, ALDH1L1+ astrocyte expression did not correlate with CD68+ nor IBA1+ (CD68+: r=.241, p=.107; IBA1+: r=.323, p=.028 [p-value > BH threshold]; **Figure 2.6**). However, ALDH1L1+ astrocyte expression positively correlated with both CD68+ and IBA1+ microglia/macrophages in *HLA-DRB1*15*- cases (CD68+: r=.526, p=.006; IBA1+: r=.572, p=.003; **Figure 2.6**). This relationship was not observed in *HLA-DRB1*15*+ cases (CD68+: r=.044, p=.855; IBA1+: r=-.093, p=.696; **Figure 2.6**). In addition, the ALDH1L1-CD68+ and ALDH1L1-IBA1+ relationship in *HLA-DRB1*15*- cases were influenced by age (**Figure 2.7**). A positive relationship was restricted to older *HLA-DRB1*15*- cases (CD68+: r=.800, p=.008; IBA1+: r=.900; p<.0001; **Figure 2.7**). No relationship in younger *HLA-DRB1*15*- cases was observed (CD68+: r=.346, p=.206; IBA1+: r=.411; p=.128; **Figure 2.7**). ALDH1L1+ astrocytes did not associate with TMEM119+ microglia in MS regardless of genotype or age (**Figure 2.6-Figure 2.7**). Control cases had no relationships between ALDH1L1+ astrocytes and CD68+, IBA1+, nor TMEM119+ (**Figure 2.6**).

2.4 Discussion

Understanding the morphological and functional astrocyte changes that contribute to MS pathological outcomes is key to unravelling the complexities of MS heterogeneity. In this chapter, we demonstrate that there are two astrocyte subpopulations, GFAP+ and ALDH1L1+ astrocytes, in our cohort of human post-mortem motor cortex. These astrocyte subpopulations show topographical differences with preferential expression of GFAP+ in NAWM and ALDH1L1+ in NAGM. We also report that these two subpopulations have divergent relationships in MS, relating to outcomes of demyelination, cortical neuronal density and macrophage/microglia inflammation. GFAP+ astrocyte reactivity increases in MS NAGM, especially in younger *HLA-DRB1*15*+ cases, and is also greater in areas of demyelination. ALDH1L1+ astrocytes are correlated with neuronal density and macrophage/microglial inflammation in MS NAGM, a relationship not seen in cases carrying the *HLA-DRB1*15* allele. These findings present GFAP+ astrocytes as possible contributors to pathological harm and ALDH1L1+ astrocytes as mediators of neurotrophic support. Overall, this work highlights the heterogeneous contributions astrocyte subpopulations may have on MS pathology.

Astrocyte subpopulations are considered the main contributor to astroglial heterogeneity, which differs in molecular profile, cytoarchitecture, and function[56,152,163]. We observe distinct topographical differences across the MS and control motor cortex between GFAP+ and ALDH1L1+ astrocytes (**Figure 2.2**). Our data show that GFAP+ astrocyte expression is concentrated at critical boundary zones, including the subpial matter and GM-WM boundary (**Figure**

2.2). Given the importance of these boundaries against potentially neurotoxic CSF milieu and deleterious products of inflammation[170], our observations suggest that GFAP+ astrocytes contribute to barrier function in the cortex. Indeed, GFAP is thought to be necessary for BBB integrity and WM architecture[171], which may explain the preferential GFAP+ expression in the subpial, specifically glia limitans and WM regions (**Figure 2.3**).

In contrast, ALDH1L1+ astrocyte expression is predominantly in the cortical GM (**Figure 2.3**), which corresponds to the density of motor neurons across the cortical layers. Our findings suggest that ALDH1L1+ astrocytes may provide neurotrophic support, which is a critical astroglial role in disease[56]. Although ALDH1L1 has been identified as a comprehensive astrocyte marker[147], little is known about its functional relevance in the adult human brain. Based on its role as a folate oxidoreductase, ALDH1L1+ astrocytes may be important to neuronal health by providing oxidative and metabolic support[172].

The divergent relationships between GFAP+ and ALDH1L1+ extend to astroglial relationships with several known pathological outcomes of MS, which is a principal finding of this study. Indeed, previous work has revealed that astroglial responses in chronic disease are largely due to changes in the composition or phenotype of astrocyte subpopulations rather than cell proliferation[152]. This may explain why GFAP+ reactivity, not quantity, is increased in MS compared to controls (**Figure 2.3**). In disease states, GFAP+ reactivity is a commonly found feature and can confer pathological harm[73,131,150,173]. We also show that GFAP+ astrocyte reactivity associates with *HLA-DRB1*15* status (**Figure 2.4**). GFAP+

astrocyte reactivity is increased in younger *HLA-DRB1*15*+ cases, supporting the notion that younger age and MS carriage of MS *HLA-DRB1*15* relate to worse pathological outcomes[28]. Previous work has indicated that *HLA-DRB1*15* influences the expression of antigen-presentation on immune cells[174], which may induce astrocyte reactivity in MS[175,176]. This suggests that our cohort's increased GFAP+ astrocyte reactivity may reflect a phenotypic response to the increased inflammation associated with the *HLA-DRB1*15* haplotype. Our data also indicate that the GFAP+ astrocytes observed in our cohort may possess a more harmful phenotype, contributing to worse MS pathological outcomes.

We also find that GFAP+ astrocytes are associated with demyelination (**Figure 2.5**), which is in line with previous studies[60,91,177]. GFAP+ astrocyte reactivity is greater in lesional and perilesional areas than in corresponding NAGM, suggesting that GFAP+ astrocyte reactivity may impact the integrity of cortical myelin in MS[171]. This relationship between GFAP+ astrocyte reactivity and demyelination supports our topographical observations, as GFAP+ astrocyte expression was exaggerated in areas where cortical pathology is typically present (**Figure 2.3**). As mediators of vascular integrity[171] and immune cell signalling[56], dysfunctional GFAP+ astrocytes in MS may heighten cortical susceptibility to local inflammation resulting in demyelination.

We also observe an inverse relationship between GFAP+ astrocytes and microglia in MS, irrespective of genotype status (**Figure 2.6**). Microglia and immune cell upregulation are important features of MS pathology and can induce astrocyte reactivity in disease states to drive MS lesion formation and

inflammatory cytotoxicity[56,63]. Although little is known about the astrocyte-microglia relationship in MS NAGM, GFAP+ astrocytes may influence microglia expression towards a more inflammatory subpopulation or phenotype[63,178]. This may explain the inverse association between GFAP+ astrocytes and microglia, which warrants further investigation. Moreover, our results highlight the subtle cellular changes undergone by MS NAGM and suggest that GFAP+ astrocytes prime the NAGM before the recruitment and presence of inflammatory cells contribute to cortical lesion development.

Interestingly, our data suggest that ALDH1L1+ astrocytes play a different role in MS. Indeed, our results indicate that GFAP+ astrocytes may contribute to disease severity and pathology, whilst ALDH1L1+ astrocytes may support and protect against disease progression. ALDH1L1+ astrocytes do not differ between lesions and NAGM regions (**Table 2.6**), suggesting that ALDH1L1+ astrocyte expression is independent of demyelination. We also find a positive correlation between neurons and macrophage/microglia with ALDH1L1+ astrocytes, which is restricted to older *HLA-DRB1*15*- cases (**Figure 2.7**). Based on our results, we suggest that ALDH1L1+ astrocytes may have a beneficial role in disease states, which is influenced by genetic *HLA-DRB1*15* status. Although little is known about ALDH1L1+ astrocyte function in the adult human brain, studies show that ALDH1L1+ astrocytes are important to neuronal health[172] and neurotrophic support, which is a critical astroglial role in disease[56]. Considering the dual protective and toxic role both astrocytes and microglia have in disease states[107], these findings support a beneficial role of ALDH1L1+ astrocytes for neuronal survival.

In summary, we demonstrate that the extent and distribution of ALDH1L1+ and GFAP+ astrocytes differ from one another across the motor cortex. We show that the *HLA-DRB1*15* allele influences these two subpopulations in MS. Our data suggest that GFAP+ astrocytes associate with pathological harm and ALDH1L1+ astrocytes relate to protection in MS, aligning with the proposed dual role astrocytes play in pathological states. This work highlights the crucial need to understand the functional properties of GFAP+ and ALDH1L1+ subpopulations, which will aid in deciphering how these subpopulations contribute to MS pathology. In particular, the distinct perivascular features and association with the severity of MS pathologic outcome by these two astrocyte subpopulations suggest that perivascular astrocyte diversity may be important determinants of MS vascular integrity. Given the relevance of vascular breakdown to MS inflammatory degeneration, investigating the perivascular feature of GFAP+ and ALDH1L1+ astrocytes in MS would be pertinent to unravelling the mechanisms behind cortical pathology. Moreover, future work on the mechanisms underlying the influence of *HLA-DRB1*15* on astrocytes and their cell-cell interaction with cortical neurons and macrophage/microglia inflammation is needed. This will help identify key targets against inflammatory degeneration and, therefore, permanent disability in MS.

3 Perivascular astrocyte subpopulations and their relationships with vessel integrity in the multiple sclerosis motor cortex

3.1 Introduction

Astrocytes, along with endothelial tight junctions and pericytes, play an essential role in barrier function[80]. However, perivascular astrocytes and their interaction with vessel integrity in the MS cortex are poorly understood.

Chapter 2 showed that astrocyte subpopulations differentially associate with motor cortical pathological outcomes in MS. Specifically, we found distinct perivascular patterns, where GFAP+ astrocytes clustered around vessels, whilst ALDH1L1+ astrocytes were absent. These relationships between astrocyte subpopulations and the vasculature are relevant to MS, given the importance of vessel breakdown in MS pathogenesis and the detrimental impact of dysfunctional astrocytes on vessel barrier function[91,179]. Therefore, we hypothesise that distinct perivascular astrocyte subpopulations relate to changes in the integrity of the MS vasculature of the motor cortex.

In this chapter, we evaluate perivascular GFAP+ and ALDH1L1+ astrocyte expression patterns and their association with metrics of vessel integrity in the MS motor cortex. We report diverging changes to perivascular astrocyte subpopulations in MS compared with controls, where the presence of GFAP+ expression decreases and ALDH1L1+ expression increases. Our findings show that extravascular fibrinogen+ increases in the MS cortex, despite relative

preservation of zonula occludens-1 (ZO-1+) tight junctions, suggesting complex changes to MS vascular integrity. Moreover, our data implicate perivascular ALDH1L1+ astrocytes in a relationship with extravascular fibrinogen and tight junctional integrity, but not perivascular GFAP+ astrocytes. This work highlights the important contributions distinct perivascular astrocyte subpopulations have on vascular-related changes and aims to expand our understanding of cortical vascular disruption in MS.

3.2 Materials and Methods

3.2.1 Study population

A subset of cases selected from our cohort described in Chapter 2 was used (MS: *n*=20, Control: *n*=10). These cases were based on the extremes of fibrinogen deposition, a surrogate of vascular breakdown, from previous work where *HLA-DRB1*15* status (*15*-: *n*=10; *15*+: *n*=10) and quantitative neuropathological outcomes were available for study[99]. All autopsy material was derived from the UK MS tissue bank, Imperial College, London and obtained with relevant ethics committee approval according to regulations outlined in the UK Human Tissue Act 2006 (REC: 08/MRE09/31+5).

3.2.2 Immunohistochemistry and immunofluorescence

Serial FFPE sections of motor cortex cut into 6µm-thick adjacent sections were used. Using IHC methods outlined in Chapter 2, IHC sections were labelled with primary antibodies for astrocytes (GFAP, Dako; ALDH1L1, Abcam; AQP4, Millipore), endothelium (CD31, Dako; CD34, Serotec), and fibrinogen (Abcam; **Table 3.1**). Antibodies were visualised using DAB substrate and sections were

counterstained with Harris Haematoxylin. Sections were digitally scanned using Aperio ScanScope AT Turbo system (Leica Biosystems) at 400x magnification.

To further investigate the relationships between perivascular astrocyte expression and vessel integrity in MS, a subset of cases underwent IF co-labelling (MS: *n*=8; Control: *n*=4). Due to the changes in MS perivascular astrocyte expression, cases were selected based on the extremes of perivascular ALDH1L1+ expression whilst controlling for age, sex, post-mortem interval, brain weight, disease duration, and clinical course. Four sets of triple-labelling IF were carried out between astrocytes (GFAP, Abcam; ALDH1L1, Abcam, ab177463), endothelium (UEA-1, Vectorlabs), and fibrinogen (Abcam) or tight junctions (ZO-1, Life Technologies; **Table 3.1**). Triple-labelling of endothelium (UEA-1), fibrinogen (Dako), and tight junctions (ZO-1) was also performed (**Table 3.1**). In brief, sections were baked at 60°C, rehydrated, and deparaffinised before autoclave-mediate antigen retrieval (Tris-EDTA, pH 9). IF was performed in Shandon™ Sequenza™ units (Thermo Scientific, 10098889). Primary antibodies were incubated overnight at 4°C and followed by corresponding fluorescent antibodies for imaging (**Table 3.1**). Hoechst 33342 was used as a positive nuclear stain (ThermoFisher Scientific, H1399). Autofluorescence was quenched with TrueBlack® Plus (Biotium; 23014-BT) and coverslipped with ProLong™ Glass Antifade Mountant (ThermoFisher Scientific; P36980). Fluorescent images were captured using an inverted confocal (Olympus Fluoview FV1200, UPLFN40XO NA:1.30 oil immersion objective)and were processed using FIJI ImageJ (v1.0).

Table 3.1. Details of antibodies used in IHC and IF methods.

Primary Antibodies				
Name	**Manufacture**	**Catalogue Number**	**Host**	**Dilution**
ALDH1L1	Abcam	ab177463	Rabbit monoclonal	1/4000 (IHC) 1/2000 (IF)
AQP4	Millipore	AB3594	Rabbit polyclonal	1/750 (IHC)
CD31	Dako	M082301-2	Mouse monoclonal	1/25 (IHC)
CD34	Serotec	MCAP547	Mouse monoclonal	1/50 (IHC)
GFAP	Abcam	ab4674	Chicken polyclonal	1/1000 (IF)
GFAP	Dako	Z0334	Rabbit polyclonal	1/6000 (IHC)
Fibrinogen	Abcam	ab4674	Mouse monoclonal	1/50 (IF)
Fibrinogen	Dako	A0080	Rabbit polyclonal	1/20000 (IF)
ZO-1	Life Technologies	339100	Mouse monoclonal	1/3000 (IF)
Conjugated Antibodies				
Name	**Manufacture**	**Catalogue Number**	**Host**	**Dilution**
DyLight 594 UEA-I	Vectorlabs	DL-1067	N/A	1/1000 (IF)
Secondary Antibodies				
Name	**Manufacture**	**Catalogue Number**	**Host**	**Dilution**
Donkey anti-Mouse IgG (H+L) Highly Cross-Adsorbed Secondary Antibody, Alexa Fluor Plus 488	Life Technologies	A32766	Donkey anti-mouse	1/500
Donkey anti-Rabbit IgG (H+L) Highly Cross-Adsorbed Secondary Antibody, Alexa Fluor Plus 647	Life Technologies	A32795	Donkey anti-rabbit	1/200
Goat anti-Chicken IgG (H+L) Highly Cross-Adsorbed Secondary Antibody, Alexa Fluor 647	Life Technologies	A21449	Goat anti-Chicken	1/200

3.2.3 Data analyses

3.2.3.1 Quantification of NAGM perivascular astrocytes

Astroglial perivascular assessment was based on the pre-defined areas described in Chapter 2, using QuPath v0.1.2[180]. Regions of interest (ROI: 2mm X 5mm) were overlaid with a 500μm X 500μm grid. The largest vessel for each grid space was selected and measured for the area (μm^2) of the lumen, perivascular space, and, where applicable, perivascular astrocyte expression (**Figure 3.1A**). Given the distinct expression patterns of GFAP+ and ALDH1L1+ astrocytes around non-capillary sized vessels, only perivascular astrocyte expression around vessels >20μm in luminal diameter was assessed[181,182]. Vessels included in the analysis also had to be cross-sectional, relatively spherical, and located >200μm from the tissue boundary or disrupted tissue.

The evaluation of perivascular astrocyte expression was based on the percentage of vessels with perivascular astrocyte expression (**Figure 3.1B-D**). We defined the percentage of vessels with perivascular astrocyte expression (*PV'*) as:

$$PV' = \left(\frac{A_P}{V_T}\right) \times 100\%$$

where A_p was the number of times perivascular astrocyte expression was present per case, and V_T was the total number of vessels per case. This criterion was used to control for the varying number of assessed vessel per case.

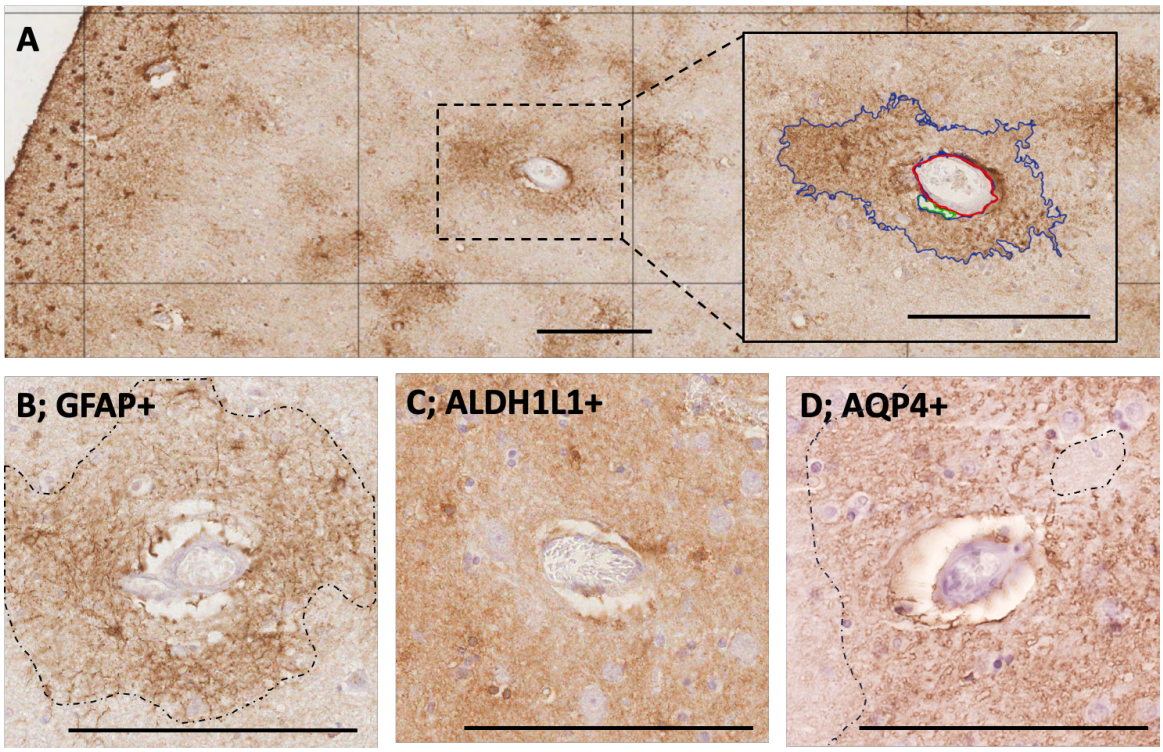


Figure 3.1. Assessment of perivascular astrocyte expression in the MS motor cortex. Evaluated vessels were based on regions of interest (2mm X 5mm) overlaid with a 500µm X 500µm grid (**A**). The largest vessel per grid square was selected and measured for the area for the lumen (red), luminal space (green), and astrocyte (blue) (inset in **A**). Perivascular astrocyte expression was identified based on the presence of astroglial processes and cell bodies for GFAP+ (**B**) ALDH1L1+ (**C**), or AQP4+ (**D**) around the entirety of a vessel. Scale bar = 200µm.

3.2.3.2 Quantification of endothelial expression

Endothelial expression was based on CD31/34+ labelling in motor cortical NAGM using the same pre-defined trajectories described in Chapter 2. Using a semi-automatic colour-based extraction in FIJI ImageJ software (v1.0), endothelial expression was determined based on the mean total vessel area per FOV (μm^2).

3.2.3.3 Assessment of NAGM vessel integrity

Vessel integrity of non-capillary and capillary vessels was assessed using IF sections labelled for fibrinogen+, ZO-1+ tight junctions, and UEA-1+ endothelium. Vessels included in the analysis had to be cross-sectional and located >200μm from the tissue boundary or any disrupted tissue. Based on established criteria[181,182], vessels with a diameter >20μm were categorised as non-capillary vessels and vessels with a diameter <6μm were categorised as capillaries. Classification of vessels between 6-20μm was not possible due to the lack of additional immunomarkers, and therefore, these vessels were excluded from the analysis.

A binary semi-quantitative score was devised to address fibrinogen and ZO-1+ tight junctional perivascular expression patterns. Intravascular fibrinogen+ received a score of 0, whilst extravascular fibrinogen+ expression received a score of 1 (**Figure 3.2**). As defined by others[100], relatively continuous ZO-1+ expression along UEA-1+ vessels was given a score of 0. In contrast, discontinuous or absent ZO-1+ expression received a score of 1 (**Figure 3.2**). Scores were validated for reliability within the rater (test-retest) and between two independent raters (interrater reliability) using Kendall's Coefficient of Concordance.

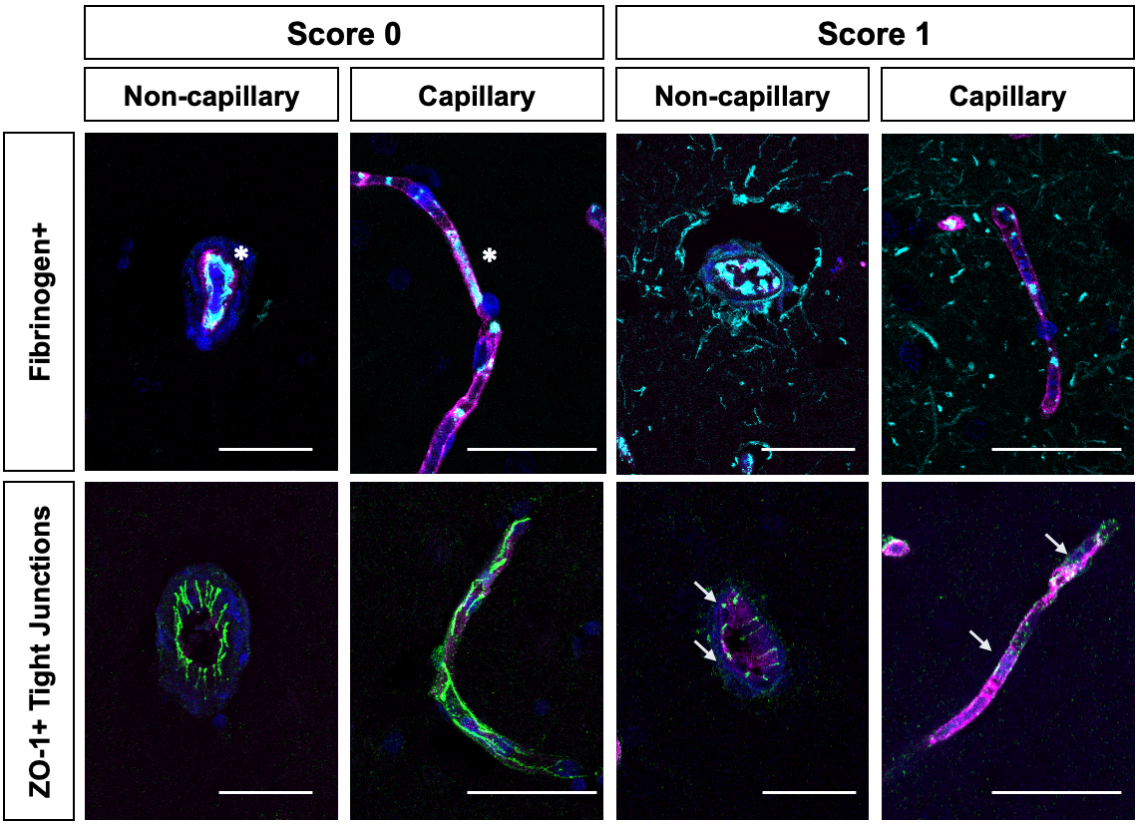


Figure 3.2. Binary assessment of NAGM vessel integrity. Representative images showing IF sections co-labelled for fibrinogen+ (cyan), ZO-1+ tight junctions (green), and UEA-1+ endothelium (magenta). Classification of vessels was based on size where non-capillaries were >20 µm and capillaries were <6 µm. Intravascular fibrinogen received a score of 0 (denoted by *), whilst extravascular fibrinogen received 1. Continuous vascular ZO-1+ expression was scored as 0, and sparse discontinuous ZO-1+ expression was scored as 1 (denoted by arrows). Nuclei were counterstained with Hoechst 33342 (blue). Scale bar = 50µm.

3.2.3.4 Assessment of astrocyte relationships with vessel integrity

Perivascular astrocyte relationships were assessed using IF sections labelled for astrocytes (GFAP+; ALDH1L1+), UEA-1+ endothelium, and fibrinogen or ZO-1+ tight junctions. Only non-capillary vessels were considered, as we did not observe expression pattern differences between GFAP+ and ALDH1L1+ around capillaries (Chapter 2). Perivascular astrocyte expression for IF sections was evaluated using a binary score of 0 (absence) or 1 (presence) of immunopositive

perivascular astrocyte expression (**Figure 3.3**). Scores were validated for reliability within the rater (test-retest) and between two independent raters (interrater reliability) using Kendall's Coefficient of Concordance. Sections were also assessed for vessel integrity using the binary method described above on perivascular fibrinogen+ and ZO-1+ expression (**Figure 3.2**).

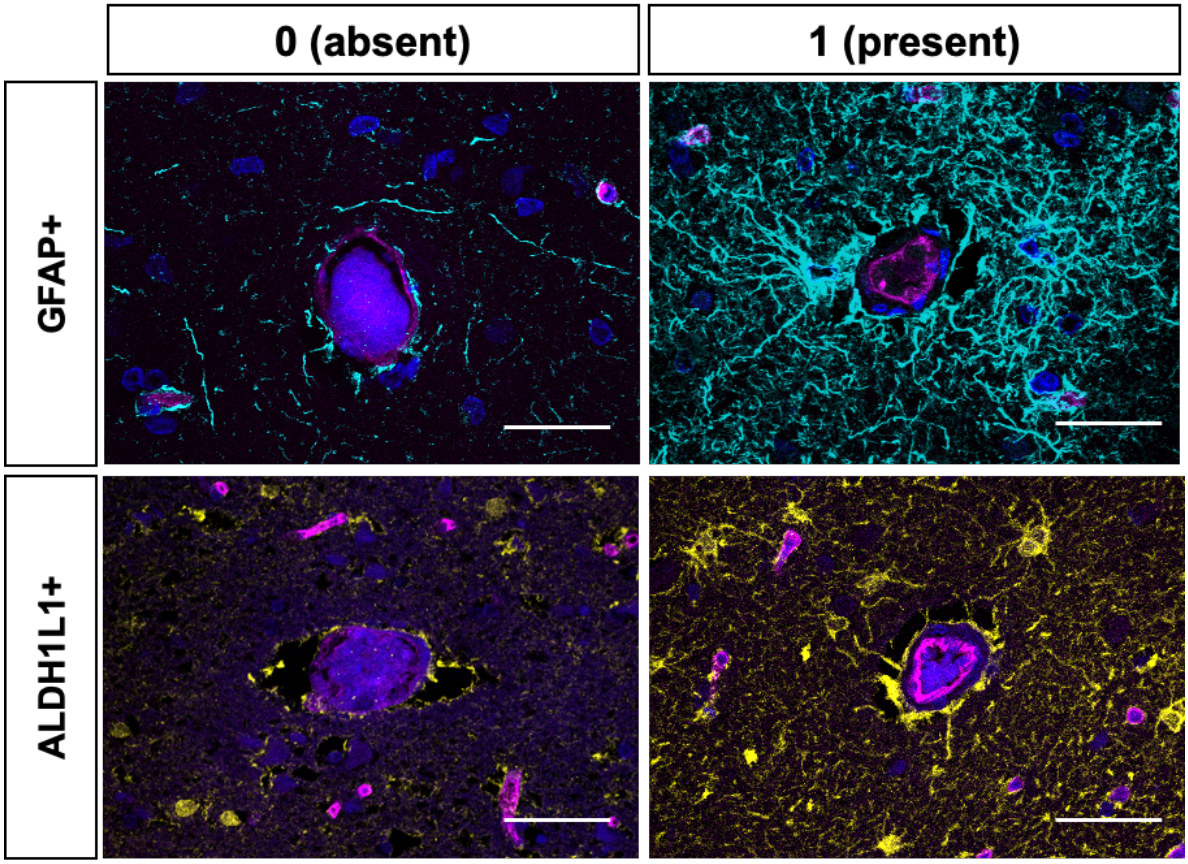


Figure 3.3. Binary assessment of NAGM perivascular astrocyte expression. Representative images showing IF sections co-labelled for astrocytes (GFAP+: cyan; ALDH1L1+: yellow) and UEA-1+ endothelium (magenta). Scores were based on the absence (score 0) or presence (score 1) of immunopositive perivascular astrocyte expression. Nuclei were counterstained with Hoechst 33342 (blue). Scale bar = 50μm.

3.2.4 Statistical analyses

Statistics were calculated and graphed using SPSS software (v27; IBM) and Prism software (v9; GraphPad). All hypotheses were carried out using two-sided tests, and $p \leq .05$ was considered significant. Data normalities were assessed with the Shapiro-Wick test. Backwards elimination was performed to remove any covariates (age; post-mortem interval; sex) that did not contribute to the model.

For analyses related to continuous perivascular astrocyte measures and vessel density, linear regression models were fitted to evaluate the influence of disease and *HLA-DRB1*15* status whilst controlling for age, sex, disease duration, and post-mortem interval, as appropriate. GEE models were used to evaluate the size of vessels with and without perivascular astrocyte expression, and to assess supra- and infragranular NAGM differences in endothelial expression. Binary logistic GEE models were used to compare the binary assessment of fibrinogen deposition and tight junctions in MS against controls. Categorical data within the disease group (MS; Control) were assessed using Fisher's Exact Test.

3.3 Results

3.3.1 Demographics

Clinical details of the cases used for the IHC analyses of this chapter are found in **Table 3.2**. The majority of MS cases were classified as SPMS (n=18) and the clinical course was unknown for 2 MS cases. **Table 3.3** outlines the clinical details. of the cases used for perivascular IF analysis. MS cases were SPMS (n=7) except for 1 MS case where the clinical course was unknown.

Table 3.2. Clinical features of the cohort used for the IHC analyses of Chapter 3. Covariates were assessed using Mann-Whitney (age; post-mortem interval; brain weight) and Fisher's Exact Test (sex). Values represent the mean unless otherwise stated. Abbreviations: F = female; M = male; N/A = not applicable.

	MS (*n*=20)	Control (*n*=10)	*p*-value	MS (*n*=20)		*p*-value
				*HLA-DRB1*15-* (*n*=10)	*HLA-DRB1*15+* (*n*=10)	
Age of death (yrs)	66 (range: 55-82)	77 (range: 68-91)	.007	64 (range: 55-82)	68 (range: 55-82)	.315
Sex (F:M)	16:4	3:7	.015	7:3	9:1	.582
Post-mortem interval (hrs)	16 (range: 7-25)	26 (range:10-52)	.031	17 (range: 9-25)	15 (range: 7-24)	.247
Brain weight (g)	1178 (range:1000-1380)	1350 (range: 1072-1628)	.009	1213 (range:1045-1380)	1146 (range: 1000-1272)	.211
Duration of disease (yrs)	31 (range: 12-50)	N/A	N/A	31 (range: 13-49)	32 (range: 12-50)	.971
Clinical course	SPMS=18 Unknown=2	N/A	N/A	SPMS=9 Unknown=1	SPMS=9 Unknown=1	N/A

Table 3.3. Clinical features of the cohort used for IF analyses. Covariates were assessed using Mann-Whitney (age; post-mortem interval; brain weight) and Fisher's Exact Test (sex). Values represent the mean unless otherwise stated. Abbreviations: F = female; M = male; N/A = not applicable.

	MS (*n*=8)	**Control (*n*=4)**	***p*-value**
Age of death (yrs)	68 (range: 57-82)	77 (range: 68-85)	.214
Sex (F:M)	7:1	0:4	.010
Post-mortem interval (hrs)	15 (range: 7-24)	31 (range:22-48)	.016
Brain weight (g)	1173 (range:1029-1280)	1398 (range: 1189-1628)	.073
Genotype (*15*-:*15*+)	4:4	N/A	N/A
Duration of disease (yrs)	29 (range: 12-47)	N/A	N/A
Clinical course	SPMS=7 Unknown=1	N/A	N/A

3.3.2 Validation of binarised score for vessel integrity and perivascular astrocytes

Validation of our binarised scoring method for vessel integrity and perivascular astrocyte expression in IF sections showed a test-retest and interrater reliability greater than 80%, which was deemed sufficient for assessment of the entire cohort (**Table 3.4**).

Table 3.4. Reliability of perivascular GFAP+, ALDH1L1+, fibrinogen+, and ZO-1+ semi-quantitative scoring. Semi-quantitative scores were assessed for reliability using Kendall's Coefficient of Concordance (W) on a subset of test images (*n*=24). Data consider concordance of two independent raters (interrater reliability) and test-retest of a rater.

Antibody	Kendall's W	p-value
GFAP+	.842	*p*<.0001
ALDH1L1+	.887	*p*<.0001
Fibrinogen+	.903	*p*<.0001
ZO-1+	.850	*p*<.0001

3.3.3 Perivascular expression of astrocyte subpopulations in NAGM

We have previously shown that NAGM perivascular GFAP+ and ALDH1L1+ astrocyte expression in MS and control cases displayed opposing immunolabelled patterns (Chapter 2). Perivascular GFAP+ expression was immunopositive for endfeet contacts and astroglial somata (**Figure 3.4**). In contrast, perivascular ALDH1L1+ presentation was immunonegative with minimal endfoot contacts (**Figure 3.4**).

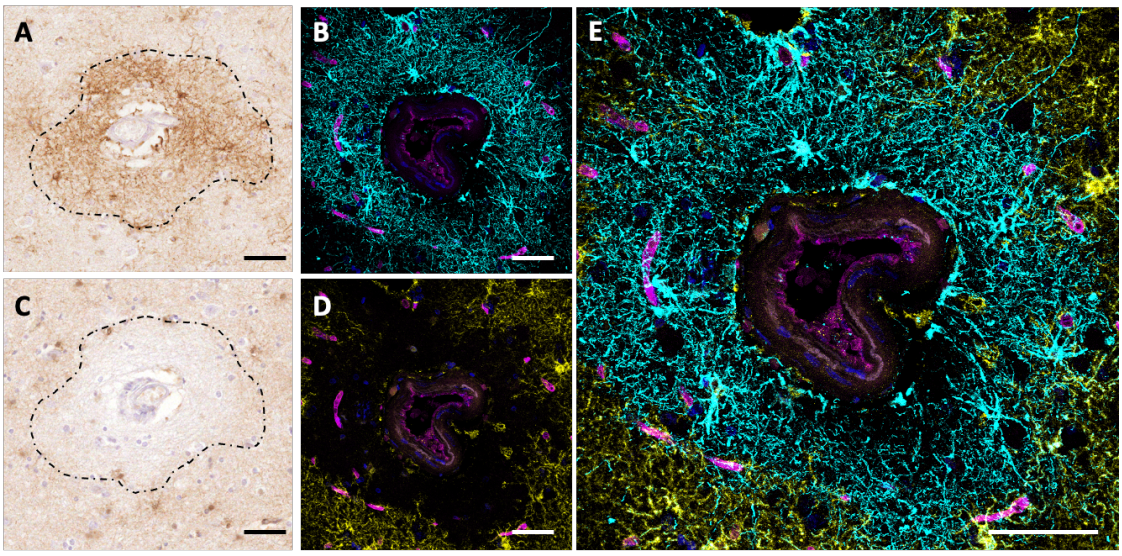


Figure 3.4. Perivascular expression of GFAP+ and ALDH1L1+ astrocytes in NAGM of the motor cortex. In both MS and control cases, GFAP+ perivascular expression displayed strong immunopositivity with many endfeet contacts on the vessel (**A-B**). Inversely, ALDH1L1+ was absent around vessels (**C-D**). Composite of perivascular astrocyte expression GFAP+ (cyan), ALDH1L1+ (yellow), and UEA-1+ endothelium (magenta) showed distinct astrocyte patterning between the two markers (**E**). IF nuclei were counterstained with Hoechst 33342 (blue). Scale bar = 50μm.

3.3.3.1 Perivascular astrocyte expression is altered in MS compared to controls

The percentage of vessels with perivascular GFAP+ astrocyte expression was decreased in MS compared to controls (MS: 30.9 ± 15.7%; Control: 53.4 ± 21.0%; *p*=.003; **Figure 3.5A-B**). In contrast, the percentage of vessels with perivascular ALDH1L1+ astrocyte expression was increased in MS compared to controls (MS: 75.7 ± 25.2%; Control: 39.3 ± 26.6%; *p*=.001; **Figure 3.5D-E**).

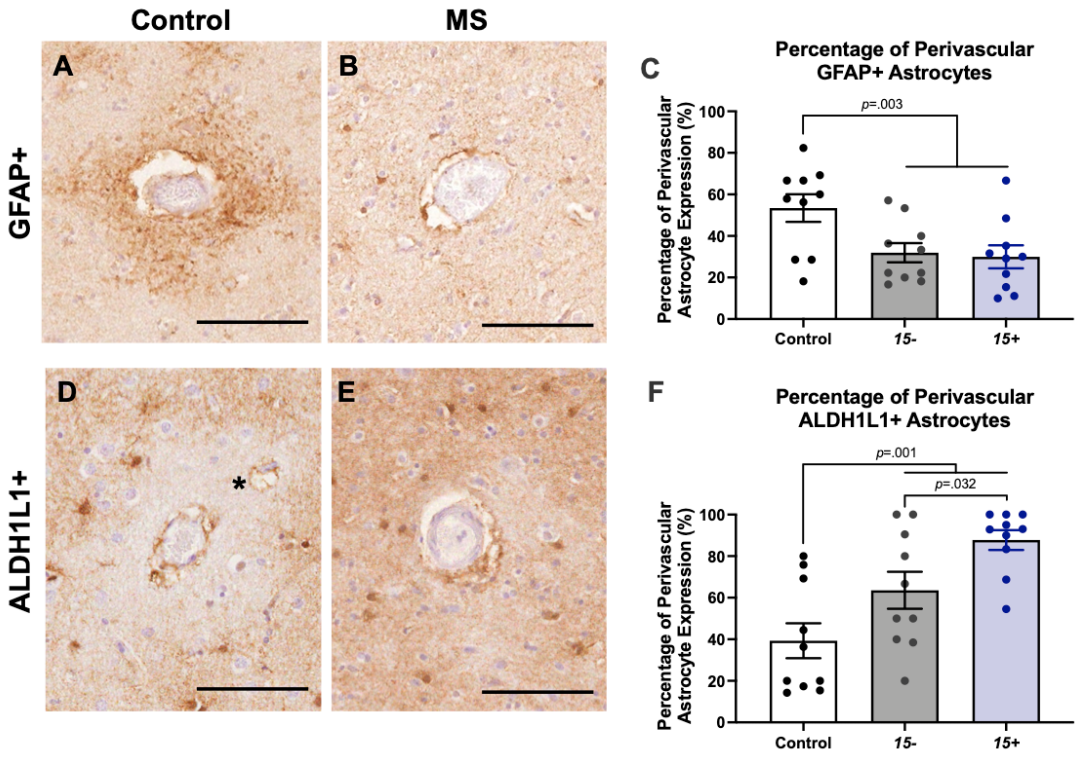


Figure 3.5. Changes to perivascular GFAP+ and ALDH1L1+ astrocyte expression in NAGM of the MS motor cortex. GFAP+ astrocyte expression around vessels was reduced in MS cases, which also displayed fewer GFAP+ endfeet relative to controls (**A-B**). The percentage of vessels with perivascular GFAP+ astrocyte expression was reduced in MS compared to controls regardless of *HLA-DRB1*15* genotype (**C**). In contrast, perivascular ALDH1L1+ astrocyte expression, which was typically immunonegative in controls (denoted by *), showed increased ALDH1L1+ expression in the endfeet and soma in MS (**D-E**). The percentage of vessels with perivascular ALDH1L1+ astrocyte expression was greater in MS than in controls, where within MS, the percentage of vessels with perivascular ALDH1L1+ astrocyte expression was also greater in *HLA-DRB1*15*+ than in *HLA-DRB1*15*- cases (**F**). Scale bar = 50µm. Error bars represent ±SEM.

3.3.3.2 Genotype influences perivascular astrocyte expression within MS

There was no effect of genotype status on the percentage of vessels with perivascular GFAP+ expression (p=.804; **Figure 3.5C**). However, genotype influenced the percentage of vessels with perivascular ALDH1L1+ expression such that the percentage was increased in *HLA-DRB1*15*+ than in *HLA-DRB1*15*- cases (*15*+: 87.8 ± 7.6%; *15*-: 63.6 ± 7.6%; p=.032; **Figure 3.5F**).

3.3.3.3 Vessel size does not influence presence of perivascular astrocyte expression in MS

To control for vessel size heterogeneity, we compared the size of vessels with and without perivascular astrocyte expression. The presence of perivascular GFAP+ or ALDH1L1+ astrocyte expression was not impacted by vessel size regardless of disease or genotype status (**Table 3.5**).

Table 3.5. The impact of vessel size on perivascular astrocyte expression in control, MS, *HLA-DRB1*15-*, and *HLA-DRB1*15+* cases. Comparisons were made between vessels with and without perivascular astrocyte expression (GFAP+; ALDH1L1+; AQP4+) to control for an influence of vessel size heterogeneity. Vessel size was calculated based on the mean luminal area (μm^2).

		Control	MS	*HLA-DRB1*15-*	*HLA-DRB1*15+*
GFAP+	**Present**	$1.2x10^3 \pm 8.2x10^2$	$9.1x10^2 \pm 4.9x10^2$	$8.7x10^2 \pm 4.9x10^2$	$7.9x10^2 \pm 3.8x10^2$
	Absent	$1.2x10^3 \pm 1.1x10^3$	$8.5x10^2 \pm 2.8x10^2$	$8.0x10^2 \pm 3.1x10^2$	$9.0x10^2 \pm 2.8x10^2$
	***p*-value**	**.942**	**.531**	**.652**	**.661**
ALDH1L1+	**Present**	$1.2x10^3 \pm 7.0x10^2$	$8.6x10^2 \pm 4.3x10^2$	$9.2x10^2 \pm 4.8x10^2$	$9.4x10^2 \pm 5.1x10^2$
	Absent	$1.2x10^3 \pm 7.4x10^2$	$8.4x10^2 \pm 3.4x10^2$	$7.9x10^2 \pm 3.9x10^2$	$8.9x10^2 \pm 2.5x10^2$
	***p*-value**	**.765**	**.930**	**.496**	**.613**
AQP4+	**Present**	$9.7x10^2 \pm 5.3x10^2$	$9.1x10^2 \pm 4.2x10^2$	$9.5x10^2 \pm 5.1x10^2$	$8.6x10^2 \pm 2.6x10^2$
	Absent	$1.2x10^3 \pm 4.0x10^2$	$9.4x10^2 \pm 2.9x10^2$	$9.1x10^2 \pm 3.2x10^2$	$9.7x10^2 \pm 2.7x10^2$
	***p*-value**	**.089**	**.851**	**.402**	**.782**

3.3.3.4 Perivascular GFAP+ astrocytes relate to AQP4+ astrocyte expression, whilst perivascular ALDH1L1+ astrocytes do not

To further evaluate the perivascular GFAP+ and ALDH1L1+ astrocyte changes observed in MS, we assessed the expression pattern of the astroglial water channel, AQP4+. As previously described[91], NAGM AQP4+ expression was concentrated in astrocyte processes, especially around vessel-related structures (**Figure 3.6**). Labelling of the soma was limited and punctate. Co-labelling of astrocyte markers revealed comparable perivascular patterning of the astrocyte endfeet between GFAP+ and AQP4+ expression (**Figure 3.6**). In contrast, there was minimal overlap of perivascular ALDH1L1+ and AQP4+ astrocyte expression as ALDH1L1+ was typically immunonegative around vessels (**Figure 3.6**).

As with perivascular GFAP+ astrocyte expression, the percentage of vessels with perivascular AQP4+ astrocyte expression was decreased in MS than in controls (MS: 13.1 ± 12.0%; Control: 26.2 ± 7.1%; p=.005; **Figure 3.6**). There was no effect of genotype status on the percentage of vessels with perivascular AQP4+ astrocyte expression (p=.616; **Figure 3.6**).

The presence of perivascular AQP4+ astrocyte expression was not influenced by vessel size regardless of disease or genotype status (**Table 3.5**).

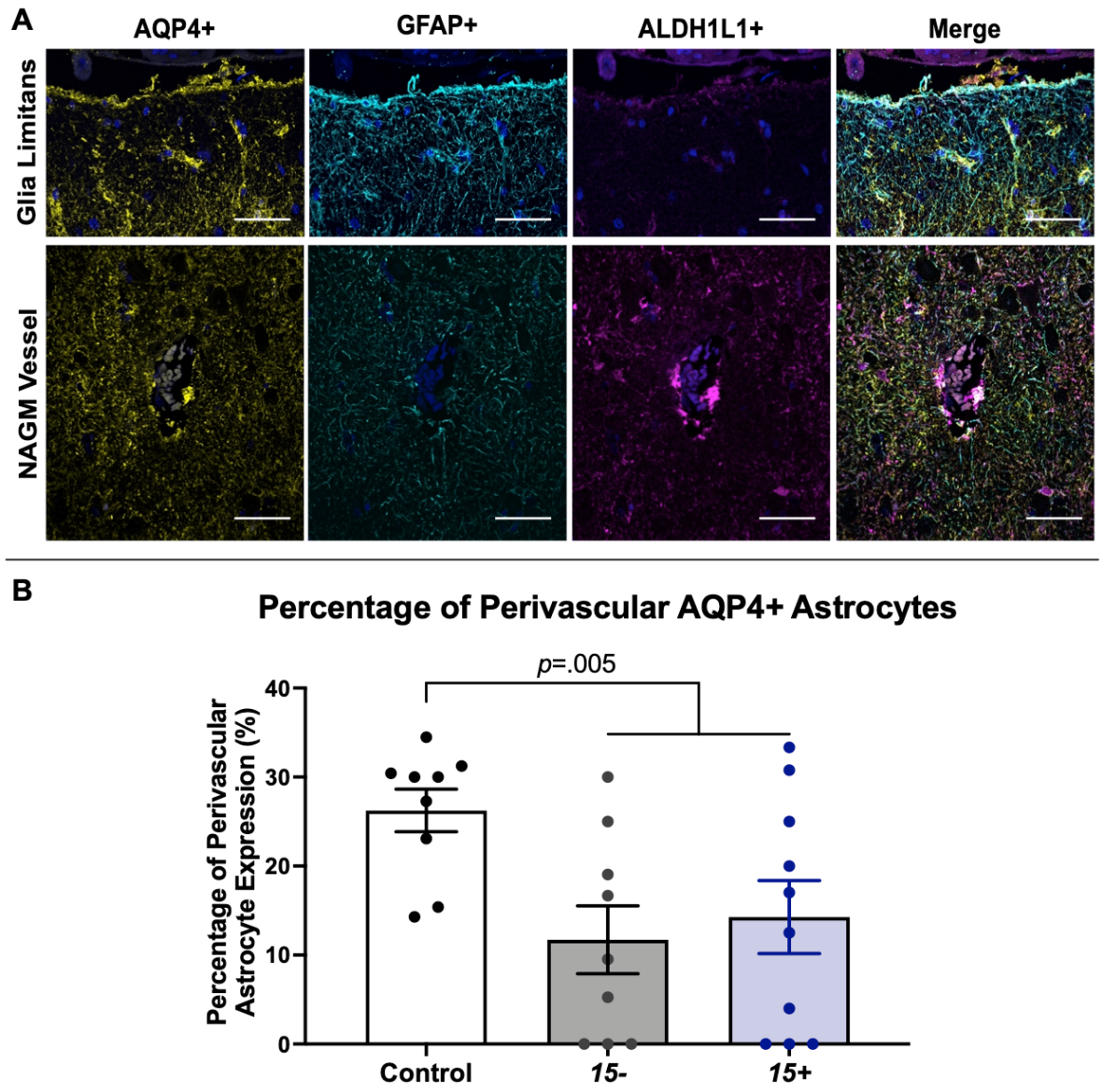


Figure 3.6. Perivascular AQP4+ astrocyte expression in the NAGM of the MS motor cortex. AQP4+ was localised to astrocyte processes, namely vessel-related structures such as the glia limitans and non-capillary vessels. Composite of AQP4+ (yellow), GFAP+ (cyan), and ALDH1L1+ (magenta) expression at the glia limitans and vasculature showed similar perivascular patterning between AQP4+ and GFAP+. In contrast, perivascular ALDH1L1+ expression minimally overlapped with perivascular AQP4+ and GFAP+ expression (**A**). Assessment of perivascular AQP4+ astrocyte expression revealed a decrease in the percentage of vessels with perivascular AQP4+ astrocyte expression in MS compared to controls regardless of *HLA-DRB1*15* status (**B**). Scale bar = 50µm. Nuclei were counterstained with Hoechst 33342 (blue). Error bars represent ±SEM.

3.3.4 Vascular landscape in NAGM

3.3.4.1 Endothelial expression differs between MS and controls

When considering all NAGM layers, CD31/34+ endothelial expression did not differ between MS and controls (MS: $2.7x10^3 \pm 3.3x10^2 \mu m^2$; Control: $2.7x10^3 \pm 2.2x10^2 \mu m^2$; p=.186; **Figure 3.7A**). However, CD31/34+ endothelial expression in supragranular layers was greater in MS compared to controls (MS: $2.8x10^3 \pm 3.5x10^2 \mu m^2$; Control: $2.7x10^3 \pm 3.1x10^2 \mu m^2$; p=.041; **Figure 3.7B**). In contrast, infragranular CD31/34+ endothelial expression was comparable between MS and controls (MS: $2.6x10^3 \pm 2.1x10^2 \mu m^2$; Control: $2.8x10^3 \pm 2.1x10^2 \mu m^2$; p=.464; **Figure 3.7C**).

CD31/34+ endothelial expression did not differ between NAGM supragranular and infragranular layers for MS and control cases (MS: p=.056; Control: p=.259; **Figure 3.7D-E**).

Moreover, CD31/34+ endothelial expression across all cortical GM layers was comparable between NAGM and corresponding lesional areas (NAGM: $2.8x10^3 \pm 2.5x10^2 \mu m^2$; Lesion: $2.7x10^3 \pm 2.2x10^2 \mu m^2$; p=.138).

3.3.4.2 Genotype does not impact endothelial expression

*HLA-DRB1*15* status did not influence CD31/34+ endothelial expression regardless of NAGM layer (All NAGM layers: p=.161; Supragranular: p=.102; Infragranular: p=.410; **Figure 3.7**).

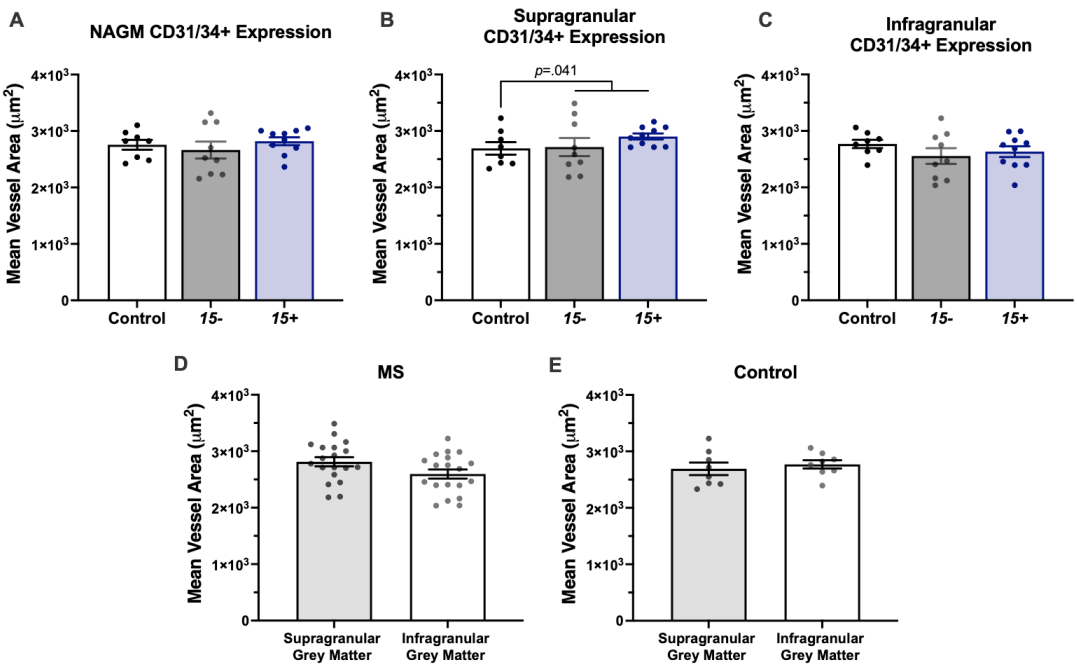


Figure 3.7. CD31/34+ endothelial expression in motor cortical NAGM. When considering all NAGM layers, there was no difference between CD31/34+ expression in MS and control cases (**A**). However, CD31/34+ expression in supragranular layers was greater in MS than in controls (**B**), which was not observed with infragranular layers (**C**). Genotype did not influence CD31/34+ expression (**A-C**). There was no difference in CD31/34+ expression between the supragranular and infragranular layers in MS and controls (**D**-**E**). Error bars represent ±SEM.

3.3.5 Vessel integrity in NAGM

3.3.5.1 Fibrinogen distribution is altered in MS compared to controls

The distribution of vascular leakage was based on the expression pattern of the large plasma protein fibrinogen. Intravascular fibrinogen+ expression showed cluster-like patterns within the confines of non-capillary and capillary walls (**Figure 3.8A-D**). Extravascular fibrinogen+ expression was observed in glial-like processes and surrounding neurons of non-capillary and capillary vessels (**Figure 3.8A-D**).

The proportion of extravascular to intravascular fibrinogen+ expression differed between MS and control cases when considering all vessel types and non-capillary vessels (All vessels: p=.021; Non-capillaries: p=.018; **Figure 3.8E-F**). MS cases showed relatively equal proportions of extravascular and intravascular fibrinogen+ expression, whilst fibrinogen+ expression was mostly intravascular in control cases. Capillary vessels had a comparable proportion of extravascular to intravascular fibrinogen+ expression between MS and controls (p=.053; **Figure 3.8G**).

Both control and MS cases had a similar proportion of extravascular to intravascular fibrinogen+ expression between supra- and infragranular NAGM layers regardless of vessel type (MS – All vessels: p=.054; Non-capillaries: p=.526, Capillaries: p=.059; Control – All vessels: p=.070; Non-capillaries: p=.277, Capillaries: p=.273).

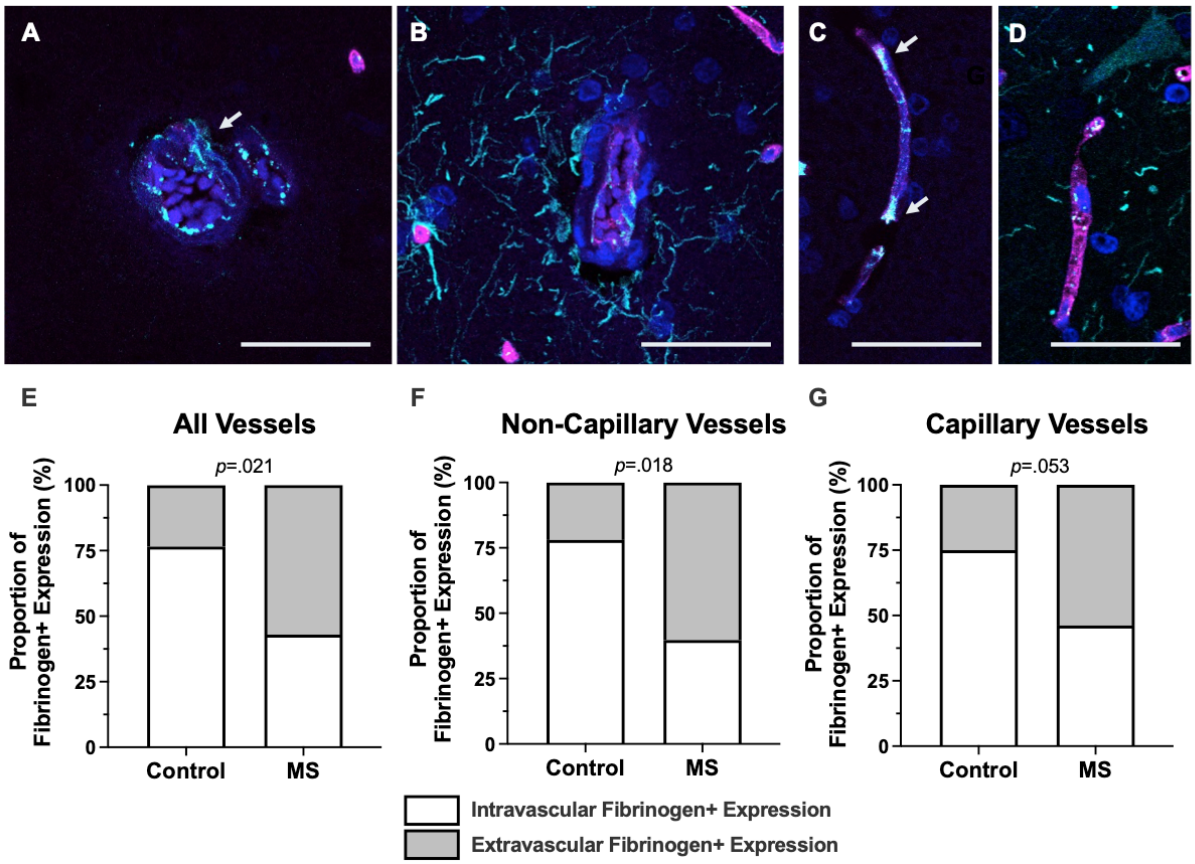


Figure 3.8. Extent and distribution of fibrinogen+ expression in motor cortical NAGM. Merge of fibrinogen+ (cyan) and UEA-1+ endothelium (magenta) non-capillary and capillary vessels (**A-D**). Intravascular fibrinogen+ expression showed clustering within the endothelial wall (arrows **A;C**), whilst extravascular fibrinogen+ expression was deposited in glial-like processes and neurons (**B;D**). All vessels, namely non-capillary vessels, had a greater proportion of extravascular to intravascular fibrinogen+ expression in MS than controls (**E-F**). The proportion of extravascular to intravascular fibrinogen+ expression in capillaries did not differ between MS and controls (**G**). Scale bar = 50μm. Nuclei were counterstained with Hoechst 33342 (blue).

3.3.5.2 Tight junction morphology is preserved in MS and controls

As outlined in the Materials and Methods, appropriate ZO-1+ expression showed mostly continuous immunopositivity, whereas aberrant ZO-1+ expression was discontinuous or absent along the endothelium (**Figure 3.2**). The proportion of continuous to discontinuous ZO-1+ tight junctional expression was comparable

between MS and control cases regardless of vessel type (All vessels: *p*=.452; Non-capillaries: *p*=.690, Capillaries: *p*=.985).

Moreover, MS cases had a similar proportion of continuous and discontinuous ZO-1+ expression between supragranular and infragranular NAGM layers for non-capillary and capillary vessels (All vessels: *p*=1.000; Non-capillaries: *p*=.811, Capillaries: *p*=1.000). This was also observed in control cases (All vessels: *p*=1.000; Non-capillaries: *p*=.663, Capillaries: *p*=1.000).

3.3.5.3 Relationships between metrics of vessel integrity differ in MS

When considering all vessel types, there was an association between fibrinogen+ expression and ZO-1+ expression in MS cases (*p*=.047; **Figure 3.9**). Continuous ZO-1+ expression mainly associated with extravascular fibrinogen+ expression, whereas discontinuous ZO-1+ expression had more equal association with either extravascular or intravascular fibrinogen+ expression. Although this relationship was not observed for non-capillary vessels, fibrinogen+ expression did relate to ZO-1+ expression for MS capillaries (Non-capillaries: *p*=.462; Capillaries: *p*=.032; **Figure 3.9**). Continuous ZO-1+ expression mostly associated with capillary extravascular fibrinogen+ expression, whilst discontinuous ZO-1+ expression typically related to capillary intravascular fibrinogen+ expression. The proportion of extravascular to intravascular fibrinogen+ expression was comparable between continuous and discontinuous ZO-1+ expression in control cases (All vessels: *p*=.722; Non-Capillary: *p*=.229; Capillary: *p*=.161).

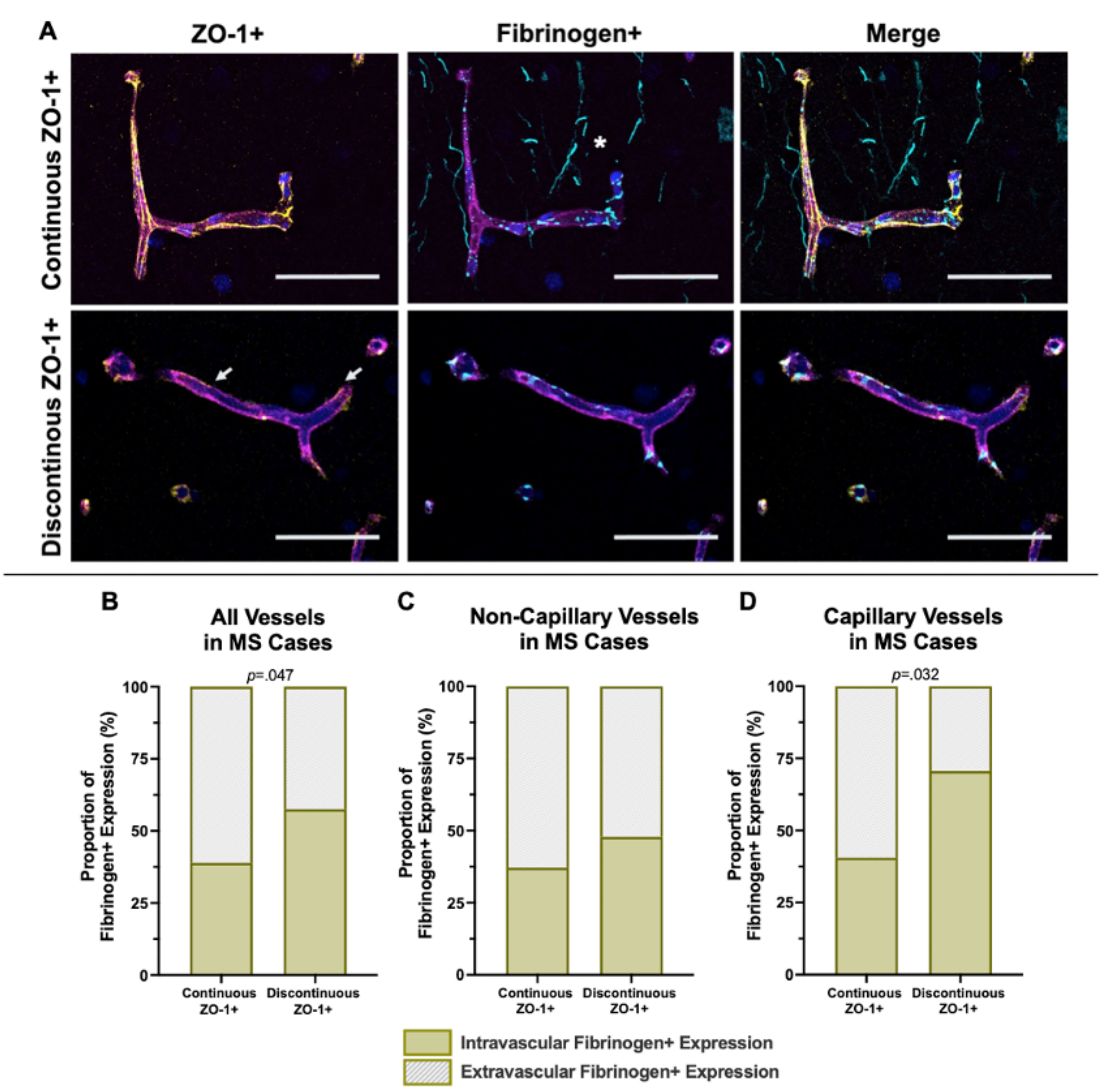


Figure 3.9. Relationship between ZO-1+ tight junctions and fibrinogen+ expression in MS cortical NAGM. Co-localisation of ZO-1+ tight junctions (yellow), fibrinogen+ (cyan), and UEA-1+ endothelium (magenta). Appropriate ZO-1+ expression was relatively continuous with the endothelium and often localised with extravascular fibrinogen+ expression (denoted by *). Aberrant ZO-1+ expression was discontinuous along the vessel (arrows) and typically localised with intravascular fibrinogen+ expression (**A**). When considering all vessel types, continuous ZO-1+ expression showed a correlation with extravascular fibrinogen+ expression, which was not seen for discontinuous ZO-1+ expression (**B**). Continuous and discontinuous ZO-1+ expression was similarly associated with extravascular and intravascular fibrinogen+ in non-capillary vessels (**C**). For MS capillary vessels, extravascular fibrinogen+ expression mostly related to continuous ZO-1+ expression, whereas intravascular fibrinogen+ expression associated with discontinuous ZO-1+ expression (**D**). Scale bar = 50μm. Nuclei were counterstained with Hoechst 33342 (blue).

3.3.6 Perivascular astrocyte relationships with markers of vessel integrity

Given the perivascular differences between GFAP+ and ALDH1L1+ astrocyte subpopulations, astrocytes were co-labelled with fibrinogen+ and ZO-1+ tight junction to evaluate the relationship between perivascular astrocytes and markers of vessel integrity in NAGM.

3.3.6.1 Perivascular astrocyte subpopulations differ in their relationships with fibrinogen deposition

The glial-like extravascular fibrinogen+ expression co-localised with GFAP+ and ALDH1L1+ astrocytes (**Figure 3.10A-D**). Although extravascular fibrinogen+ expression was present in a few perivascular ALDH1L1+ astrocytes, perivascular fibrinogen+ expression was predominantly localised with perivascular GFAP+ astrocytes.

In MS cases, there was no association between the presence or absence of perivascular GFAP+ astrocytes with intravascular and extravascular fibrinogen+ expression (p=.340; **Figure 3.10E**). However, perivascular ALDH1L1+ astrocytes were associated with fibrinogen+ expression (p=.015; **Figure 3.10F**). The absence of perivascular ALDH1L1+ astrocytes had a greater proportion of extravascular to intravascular fibrinogen+ expression than when perivascular ALDH1L1+ astrocytes were present. The presence or absence of perivascular GFAP+ or ALDH1L1+ astrocytes in control cases did not associate with fibrinogen+ expression (GFAP+: p=1.000; ALDH1L1+: p=1.000).

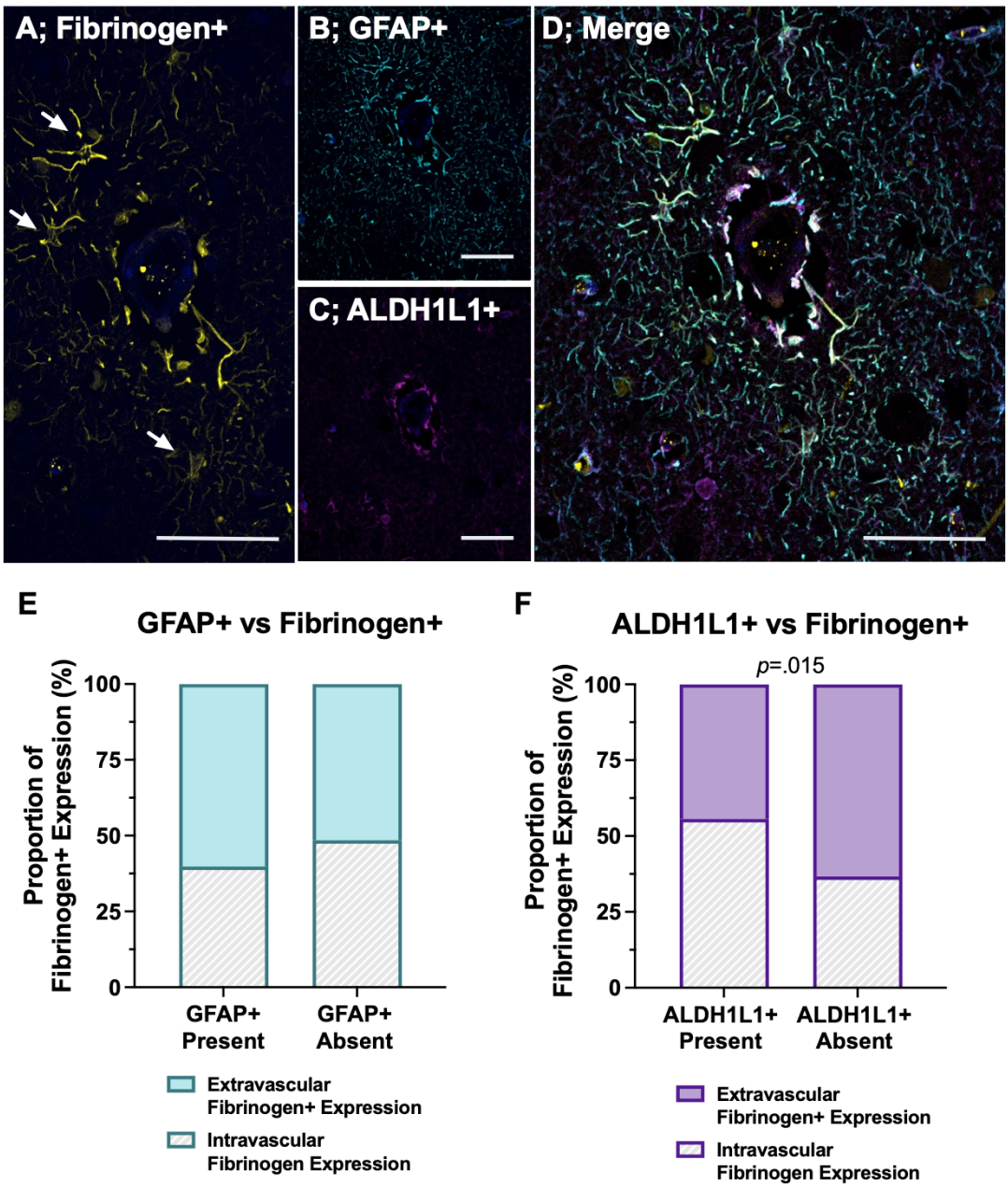


Figure 3.10. The relationship between perivascular astrocytes and fibrinogen deposition in the MS NAGM cortex. Extravascular fibrinogen+ expression was observed in glial-like processes (arrows; yellow; **A**). Merge with GFAP+ (cyan; **B**) and ALDH1L1+ (magenta; **C**) revealed co-localisation of extravascular fibrinogen+ with perivascular astrocytes, especially GFAP+ astrocytes (**D**). The presence or absence of perivascular GFAP+ astrocytes did not associate with extravascular and intravascular fibrinogen+ expression (**E**). However, the absence of perivascular ALDH1L1+ expression had a greater proportion of extravascular to intravascular fibrinogen+ expression than when perivascular ALDH1L1+ expression was present (**F**). Scale bar = 50μm. Nuclei were counterstained with Hoechst 33342 (blue).

3.3.6.2 Perivascular astrocyte subpopulations differ in their relationship with tight junctions

ZO-1+ tight junctional expression did not localise with perivascular astrocytes (**Figure 3.11A-D**). Any endfoot contacts appeared to be made with the endothelium and not ZO-1+.

In MS, the presence or absence of perivascular GFAP+ astrocyte expression did not associate with continuous or discontinuous ZO-1+ expression (p=.207; **Figure 3.11E**). In contrast, the absence of perivascular ALDH1L1+ astrocyte expression had a greater proportion of discontinuous to continuous ZO-1+ expression than when perivascular ALDH1L1+ astrocytes were present (p=.014; **Figure 3.11F**). There was no association of perivascular GFAP+ or ALDH1L1+ astrocytes with ZO-1+ expression in control cases (GFAP+: p=.716; ALDH1L1+: p=1.000).

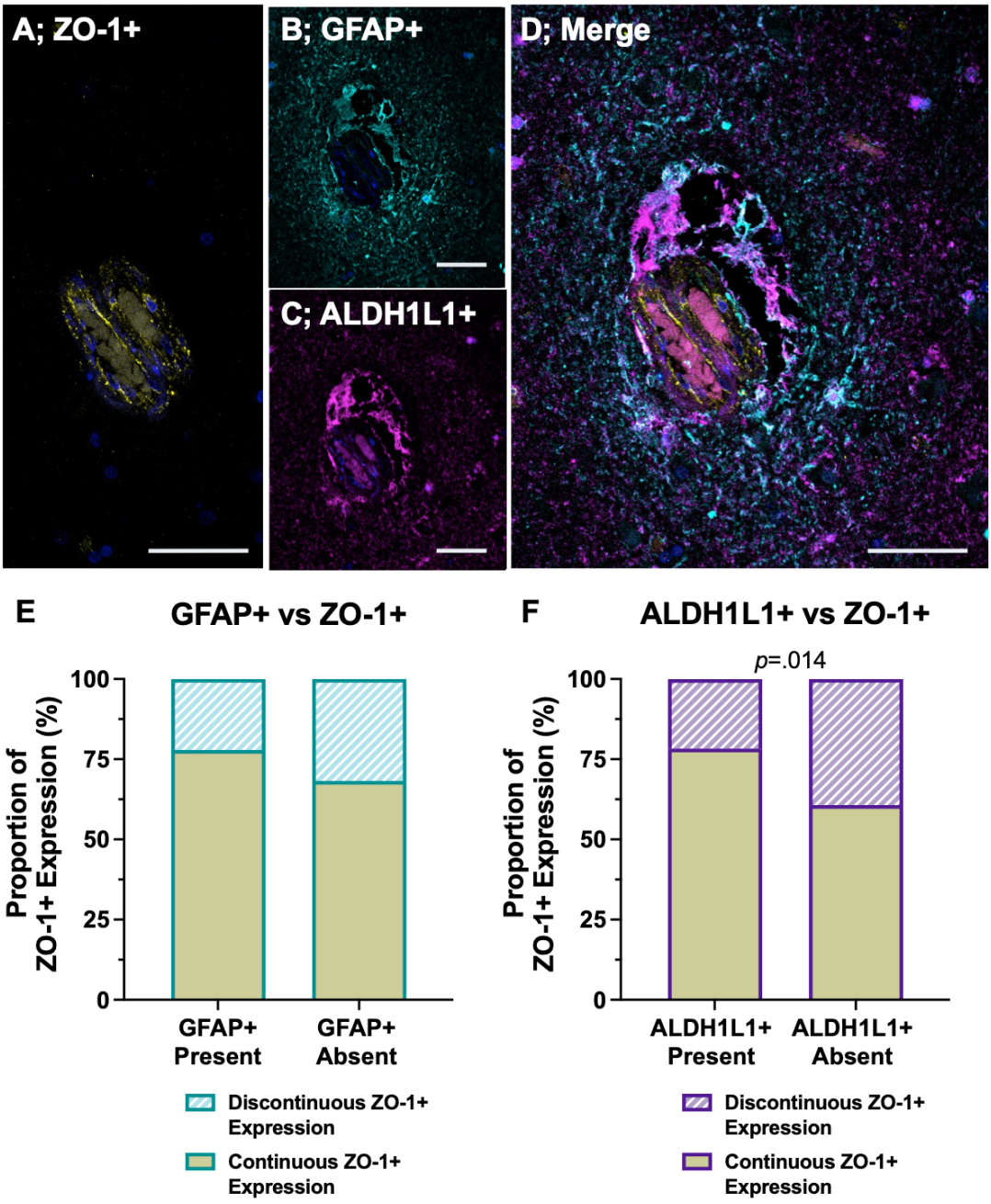


Figure 3.11. Relationship between perivascular astrocytes and ZO-1+ tight junctions in the MS NAGM cortex. Merge with ZO-1+ (yellow; **A**), GFAP+ (cyan; **B**) and ALDH1L1+ expression (magenta; **C-D**). There was no association between perivascular GFAP+ astrocyte expression and ZO-1+ expression (**E**). However, the absence of perivascular ALDH1L1+ astrocyte expression had a greater proportion of discontinuous to continuous ZO-1+ expression than when perivascular ALDH1L1+ expression was present (**F**). Scale bar = 50μm. Nuclei were counterstained with Hoechst 33342 (blue).

3.4 Discussion

Alteration in vascular integrity is an important contributor to MS pathological outcome[99,170]. In this chapter, we assess perivascular astrocyte subpopulations and their relationship with metrics of vessel integrity in the MS motor cortex. We provide evidence that perivascular astrocyte subpopulations have divergent relationships in MS, where GFAP+ astrocyte expression decreases and ALDH1L1+ astrocyte expression increases. We also observe that endothelial expression in the supragranular NAGM layers is greater in MS than in controls, indicating that changes occur in the MS vascular landscape. Our data show increased extravascular fibrinogen+ in the MS cortex, despite relative preservation of ZO-1+ tight junctions, suggesting that complex changes to MS vascular integrity are present. Moreover, the absence of ALDH1L1+ astrocytes relate to increased extravascular fibrinogen and disruption of tight junction morphology. These findings point to a role of astrocyte subpopulations in vessel integrity, which has implications on MS pathogenesis.

Astrocytes are known to be involved in specific interactions with blood vessels[183,184]. Our study reveals that perivascular astrocyte subpopulations have divergent relationships in MS. Perivascular GFAP+ expression show labelling of the astroglial endfeet and cell bodies. In contrast, there is a paucity of ALDH1L1+ astrocyte expression perivascularly (**Figure 3.5**). These findings highlight GFAP+, not ALDH1L1+ expression, as a major contributor to perivascular astrocyte expression. Our data are in line with transcriptomic studies on isolated perivascular astrocyte processes, which report that ALDH1L1+ expression in the endfeet can be negligible[185].

Further, we confirm that perivascular GFAP+ astrocytes co-localise with the water channel, AQP4, indicating that perivascular astrocytes can be comprised of AQP4+ and GFAP+ expression (**Figure 3.6**). AQP4 is highly localised to the astrocyte endfeet and is an important regulator of water homeostasis and vessel integrity[186,187]. Given the role AQP4+ astrocytes have on the structural integrity of vessels, we suggest that the GFAP+ expression in perivascular astrocytes also has similar functional relevance as AQP4+ expression[91,188]. Indeed, loss of GFAP+ expression has been linked to disrupted vessel integrity[171]. As an important constituent of the astrocyte cytoskeleton, GFAP may provide endfeet with the mechanical strength needed to support vasculature.

These perivascular expression patterns of astrocyte subpopulations also differ between MS and controls (**Figure 3.5**). Relative to control cases, we show that perivascular GFAP+ and AQP4+ astrocyte expression decreases, whilst perivascular ALDH1L1+ astrocyte expression increases in MS (**Figure 3.5**; **Figure 3.6**). Our data suggest that perivascular astrocytes, namely the endfeet, are compromised in MS, which is in line with previous work[91]. As described in Chapter 2, ALDH1L1+ astrocytes typically concentrate in neuronally dense regions and may provide neurotrophic support[147]. However, under pathological conditions such as MS, astrocytes can change phenotype or subpopulation composition[152,189]. Given the inverse changes to perivascular astrocyte subpopulations in MS, the upregulation of perivascular ALDH1L1+ astrocytes in MS may provide vascular support in areas of perivascular GFAP+ or AQP4+ astrocyte loss. The functional implications of this change in ALDH1L1+ expression remain undetermined and should be investigated further.

Changes to vessel integrity may explain the alteration to perivascular astrocyte expression observed in our MS cohort[99,100]. We show that NAGM CD31/34+ endothelial expression is greater in the supragranular layer of MS cases than in controls (**Figure 3.7**). Although there is limited understanding of the endothelial topography in the MS cortex, human neuropathologic studies have also reported upregulated endothelial expression in MS[190]. Work in EAE models suggests that increased vessel density may result from angiogenesis, which has been identified as a possible feature of neuroinflammatory and neurodegenerative disease[191,192]. Given the importance of meningeal inflammation in MS cortical pathology and meningeal proximity to the supragranular GM layers, our findings may result from an angiogenic response to inflammation[193].

As reported by others[99], extravascular fibrinogen was greater in MS than in controls, suggesting a breakdown of vessel integrity in the MS motor cortex (**Figure 3.8**). This challenges the idea that large serum proteins are not deposited in the MS cortex and that the GM vasculature is relatively preserved in MS[194]. Yet, surprisingly, our cohort shows no difference in NAGM ZO-1+ tight junction expression between MS and controls. Moreover, we report that NAGM extravascular fibrinogen is more likely to associate with continuous ZO-1+ tight junctions in MS cases (**Figure 3.9**). The contrasting expression patterns of barrier leakage and endothelial abnormality raises the possibility that in MS, components of the cerebral vascular change at different time points. Unlike fibrinogen, which is quickly converted into insoluble fibrin, tight junctional protein turnover occurs over several hours[195-197]. This may explain our findings and the findings of others who also observed abnormalities in endothelial tight junctions in non-neurological

disease[100]. The endothelial barrier also coordinates several other proteins, such as claudins and junctional adhesion molecules, which may contribute to vessel weakening independent of ZO-1+ tight junctions[198]. Further investigation on the relationship between fibrinogen leakage and the half-life of ZO-1+ tight junctions could help provide a greater understanding of the vascular changes in MS.

Our evaluation of the perivascular astrocytes with these metrics of vessel integrity indicates that ALDH1L1+ astrocytes, not GFAP+ astrocytes, mediate these interactions in MS. Perivascular GFAP+ astrocytes do not associate with fibrinogen+ or ZO-1+ tight junction expression in MS or controls (**Figure 3.10**; **Figure 3.11**). In contrast, the absence of perivascular ALDH1L1+ astrocytes associates with extravascular fibrinogen+ and discontinuous ZO-1+ tight junction expression, a finding solely present in MS cases (**Figure 3.10**; **Figure 3.11**). This finding, along with the increase in perivascular ALDH1L1+ astrocyte expression observed in our MS cohort (**Figure 3.5**), suggests that ALDH1L1+ astrocytes can provide endothelial support in MS, which leaves vessels without perivascular ALDH1L1+ astrocyte contacts vulnerable to damage. Indeed, not all astrocytes contribute to vessel breakdown and may protect vessels from further inflammatory insult in MS[94]. Given the highly dynamic and complex system required to maintain vessel integrity, functional analyses of perivascular astrocyte subpopulations, barrier proteins, and their interactive influence on vessel integrity are needed.

In summary, we find that MS astrocyte subpopulations show distinct perivascular relationships, where GFAP+ astrocyte expression is lost, and ALDH1L1+

astrocyte expression is increased. We provide evidence of changes to the vessel landscape by demonstrating greater supragranular endothelial expression in MS than in controls. The increased presence of extravascular fibrinogen deposition in the MS motor cortex, despite relative preservation of ZO-1+ tight junctional expression, also implicates that vessel integrity in MS is altered. Furthermore, only perivascular ALDH1L1+ astrocytes, not GFAP+ astrocytes, associate with metrics of vessel integrity, highlighting the potential functional differences of astrocyte subpopulations in MS. Future studies aimed at elucidating the mechanistic properties and behaviours of these two astrocyte subpopulations in relationship to vessel integrity may provide a better understanding of the role of vascular barriers in MS pathogenesis.

4 The distinct proteome profiles of astrocyte subpopulations in the multiple sclerosis motor cortex

4.1 Introduction

In the previous chapters, we have shown that astrocyte heterogeneity is an important feature in MS pathology. In particular, our data suggest that GFAP+ and ALDH1L1+ astrocyte subpopulations differ in their distribution and extent of expression in the MS motor cortex, and differentially relate to pathological outcomes in the parenchyma and perivasculature. These data point to key pathological differences of the GFAP+ and ALDH1L1+ astrocyte subpopulations in influencing the diversity of MS pathologies. The molecular profiles and associated mechanisms by which different astrocyte subpopulations contribute and respond to MS pathogenesis are poorly understood.

To better understand the contributions of GFAP+ and ALDH1L1+ astrocytes to MS pathology, we assess the proteome profiles of motor cortical GFAP+, ALDH1L1+, and GFAP+/ALDH1L1+ astrocyte subpopulations using LCM-directed mass spectrometry-based proteomics. By establishing a workflow capable of generating robust proteomic data from FFPE samples, we show that astrocyte subpopulations, especially GFAP+ and ALDH1L1+ astrocytes, have distinct proteome profiles irrespective of disease or MS *HLA-DRB1*15* genetic status. In comparison to ALDH1L1+ astrocytes, GFAP+ astrocytes are enriched in proteins related to haemostasis and immune processes. We also identify clear protein expression differences between MS and controls across all astrocyte subpopulations where GFAP+ astrocytes associate with immune-related proteins

and ALDH1L1+ astrocytes relate to synaptic vesicle clustering and voltage-gated potassium channels. To our knowledge, our data is the first to show an impact of MS *HLA-DRB1*15* status on the astrocyte proteome by identifying enrichment of immune-related proteins in GFAP+ and ALDH1L1+ astrocytes from *HLA-DRB1*15*+ samples. This work identifies the differentially expressed proteomes of astrocyte subpopulations in MS, with the aim of expanding our present knowledge of astrocyte subpopulation diversity in MS.

4.2 Materials and Methods

4.2.1 Study population

Based on the results of cortical NAGM GFAP+ astrocyte reactivity, which showed increased GFAP+ reactivity in MS than in controls, a subset of the cases in Chapter 2 was used (MS: *n*=20; Control: *n*=5). As previously mentioned, MS cases were genotyped at the *HLA-DRB1*15* locus (*15*-: *n*=10; *15*+: *n*=10) and all cases had fixed material available for detailed pathologic characterisation[99]. All autopsy material was derived from the UK MS tissue bank, Imperial College, London and obtained with relevant ethics committee approval according to regulations outlined in the UK Human Tissue Act 2006 (REC: 08/MRE09/31+5).

4.2.2 Optimisation of the formalin-fixed paraffin-embedded tissue workflow

Based on in-house methods for fresh frozen tissue in previous work[199], a titration of tissue area was used to determine the total NAGM tissue area required for adequate protein yield from laser capture in 10µm-thick FFPE tissues. We compared protein yields derived from FFPE and fixed frozen tissue to a fresh

frozen standard (provided by Simon Davis). In brief, 10-µm thick sections of FFPE or fixed frozen motor cortex were mounted onto PET membrane frame slides (Zeiss; 415190-9101-00). In place of xylene, FFPE sections were deparaffinised with 1.7% dishwasher soap to reduce protein loss using previously described methods[200-202]. Both FFPE and fixed frozen sections were counterstained with Harris Haematoxylin, air dried, and captured using an LMD7 laser microdissection microscope (Leica Microsystems, Germany) directly into lysis buffer (RIPA: Thermo Scientific; 89900). Titration areas ranged from $10^{2.5}$-10^{6}µm^2 and increased in increments of $10^{0.5}$µm^2 for each of the FFPE and fixed frozen tissue samples.

Refinement of the titration was carried out for areas $10^{4.5}$-$10^{5.5}$µm^2 for FFPE tissue. To mimic the capture of the average-sized astrocyte observed in our cohort, LCM selections were set to 130µm^2. Titration areas were achieved based on the sum of individual selections. Titrations were carried out on FFPE cortical tissue counterstained with Harris Haematoxylin. Due to the potential tissue loss from laser capture of small areas on membrane slides, sections were also mounted on EP-DIRECTOR® slides (Leica; 11600249). LMD7 laser settings were set to vaporise the energy transfer coating of EP-DIRECTOR® slides, which allowed the entire selected tissue to be collected.

All lysates were processed using a modified single-pot, solid-phase-enhanced sample preparation (SP3) method and underwent mass spectrometry analysis using the methods outlined below[203].

4.2.3 Immunohistochemistry

For LCM isolation, serial 10µm-thick motor cortical FFPE sections were double-labelled using a modified alkaline phosphatase (AP) and horseradish peroxidase (HRP) detection system[28,204]. Sections were deparaffinised with 1.7% dishwasher soap[200-202]. Sections underwent similar blocking and antigen retrieval methods, as described in Chapter 2. Primary antibodies for GFAP+ astrocytes (Dako) were visualised using ImmPACT® Vector® Red (Vector Labs; SK-5105) for AP detection, and primary antibodies for ALDH1L1+ astrocytes (ThermoFisher) were visualised using DAB (Agilent; K500711-2) for HRP detection (**Table 4.1**). Hoechst 33342 (ThermoFisher Scientific) was used as a positive nuclear stain. Sections were air-dried and stored at -80°C until use.

Table 4.1. Details of antibodies used in IHC methods for Chapter 4.

Primary Antibodies				
Name	**Manufacture**	**Catalogue Number**	**Host**	**Dilution**
ALDH1L1	ThermoFisher	UM500039	Mouse monoclonal	1/4000
GFAP	Dako	Z0334	Rabbit polyclonal	1/6000
Secondary Antibodies				
Name	**Manufacture**	**Catalog Number**	**Host**	**Dilution**
SignalStain® Boost IHC Detection Reagent (HRP, Mouse)	Cell Signalling	8125S	Goat anti-mouse	N/A
Horse Anti-Rabbit IgG Antibody (H+L), Biotinylated, R.T.U.	2bScientific	BP-1100-50	Horse anti-rabbit	N/A

4.2.4 Laser capture microdissection and SP3 digestion of astrocytes

Astrocytes were isolated using the IHC method outlined above. We used a dual brightfield and immunofluorescence microscopy approach to identify GFAP+, GFAP+/ALDH1L1+, and ALDH1L1+ astrocytes (**Figure 4.1**). Under brightfield conditions, GFAP+ was pink, GFAP+/ALDH1L1+ was pink-brown, and ALDH1L1+ was brown. Immunofluorescence of GFAP+ distinguished GFAP+ and GFAP+/ALDH1L1+ astrocytes from ALDH1L1+ astrocytes, which were absent under fluorescent conditions.

Approximately 1000 astrocyte somas (GFAP+; GFAP+/ALDH1L1+; ALDH1L1+) were isolated from each case using an LMD7 laser microdissection microscope (Lecia Biosystems). Tissue was captured directly into lysis buffer (radioimmunoprecipitation assay buffer [RIPA]) and stored as lysates at -80°C until processing. Proteins were purified and digested to peptides using a modified SP3 method[203]. In brief, lysates underwent heat and benzonase incubation to break formalin cross-links. Following dithiothreitol (DTT) reduction and iodoacetamide (IAA) alkylation, lysates were incubated with a 1:1 carboxylated-modified paramagnetic bead mix as described by[205] (Sera-Mag Speed Beads A: Thermo Scientific; 09-981-121; Sera-Mag Speed Beads B: Thermo Scientific; 09-981-123). Beads were isolated and then resuspended for overnight digestion at 37°C with trypsin. The supernatants containing eluted purified peptides were transferred to pre-slit glass vials containing 1% formic acid, to give a final concentration of 0.1% formic acid, until mass spectrometry analysis.

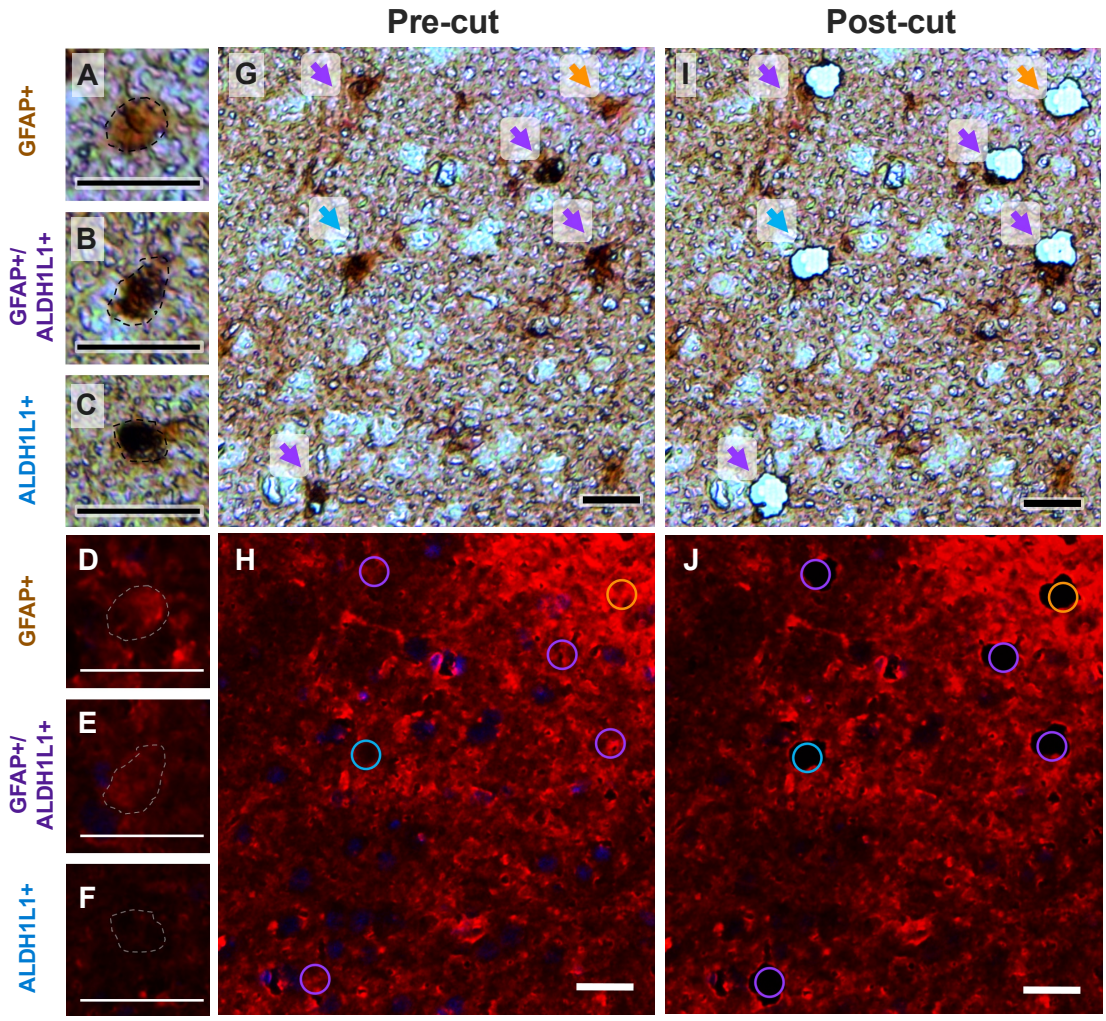


Figure 4.1. IHC directed LCM of GFAP+, GFAP+/ALDH1L1+, and ALDH1L1+ astrocytes in NAGM motor cortex. FFPE cortical tissue was labelled with GFAP and ALDH1L1 antibodies using a dual AP-HRP immunolabelling system. The GFAP antibody was visualised with ImmPACT® Vector® Red, which was pink in brightfield and red in fluorescent conditions. Brown DAB, which was absent under fluorescence, was used to visualise the ALDH1L1 antibody. Under brightfield conditions, GFAP+ was pink (**A**), GFAP+/ALDH1L1+ was pink-brown (**B**), and ALDH1L1+ was brown (**C**). GFAP+ and GFAP+/ALDH1L1+ were red (**D-E**), whilst ALDH1L1+ was absent (**F**) under fluorescent conditions. Around 1000 astrocyte somata per group (GFAP+; GFAP+/ALDH1L1+; ALDH1L1+) were isolated for each post-mortem case (**G-J**). Scale bar = 50μm.

4.2.5 Mass spectrometry data analyses

All mass spectrometry data analyses outlined in this section were kindly completed by Simon Davis.

4.2.5.1 Data-dependent acquisition workflow

For experiments related to FFPE optimisation, peptides were analysed by LC-MS/MS using a data-dependent acquisition (DDA) system. In brief, peptides were analysed by nano-UPLC-MS/MS using a Dionex Ultimate 3000 coupled to an Orbitrap Fusion Lumos (Thermo Scientific) using a 75µm x 500mm C18 EASY-Spray Columns with 2µm particles (Thermo Scientific) at a flow rate of 250nL/min. A 60-minute linear gradient from 2% buffer A to 35% buffer B (A: 5% DMSO, 0.1% formic acid in water; B: 5% DMSO, 0.1% formic acid in acetonitrile). MS1 scans were acquired in the Orbitrap between 400 and 1500 m/z with a resolution of 120,000 and an AGC target of 4×10^5. Precursor ions between charge state 2+ and 7+ and above the intensity threshold of 5×10^3 were selected for HCD fragmentation at a normalised collision energy of 28%, an AGC target of 4×10^3, a maximum injection time of 35ms and a dynamic exclusion window of 30s. MS/MS spectra were acquired in the ion trap using the rapid scan mode.

Protein identification and label-free quantification of raw data files were assessed using FragPipe (v16.0). Data files were searched against the Uniprot human database (20,421 sequences) using MSFragger (v3.3) within FragPipe, allowing for tryptic specificity with up to two missed cleavages[206]. Cysteine carbamidomethylation was set as a fixed modification. Methionine oxidation and protein N-terminal acetylation were set as variable modifications. Identifications were filtered to a 1% FDR on the peptide and protein levels[207]. Label-free quantification was performed using the MaxLFQ algorithm within IonQuant, and the “match between runs” option was enabled with an ion false discovery rate (FDR) of 1%[208].

4.2.5.2 Data-independent acquisition workflow

Peptides from the main astrocyte experiment were analysed by LC-MS/MS using a data-independent acquisition (DIA) system. Peptides were processed by nano-UPLC-MS/MS as described above. The instrument was operated in DIA mode, with 1 MS1 scan and 40 MS2 scans per cycle[209]. The MS1 scans were acquired in the Orbitrap between 350 – 1650m/z at a resolution of 120,000 and an AGC target of 4 x 10^5. MS2 scans were acquired in the Orbitrap between 200 – 2000m/z at a resolution of 30,000 and an AGC target of 1 x 10^6 and a maximum injection time of 60ms. The 40 DIA segment widths were adjusted to the precursor density (**Table S4.1**). The normalised HCD collision energy was set to 30%.

Proteins samples acquired using DIA were analysed using DIA-NN's (v1.8) deep learning spectral prediction to generate an *in-silico* spectral library[210]. The spectral prediction was based on the UniProt human database (20,421 sequences) with tryptic specificity allowing for two missed cleavages and a fixed modification of carbamidomethylation. Protein and peptide FDR were set to 1%, and the "match-between-runs" option was used. All remaining settings were left as default.

4.2.6 Statistical analyses

All hypotheses were carried out using two-sided tests, and analyses considered *p*-values ≤0.05 as significant (**Figure 4.2**). Statistical analyses were done using Perseus (v1.6.5.0), R-software (v4.1.2), SPSS (v27; IBM), and Prism software (v9; GraphPad).

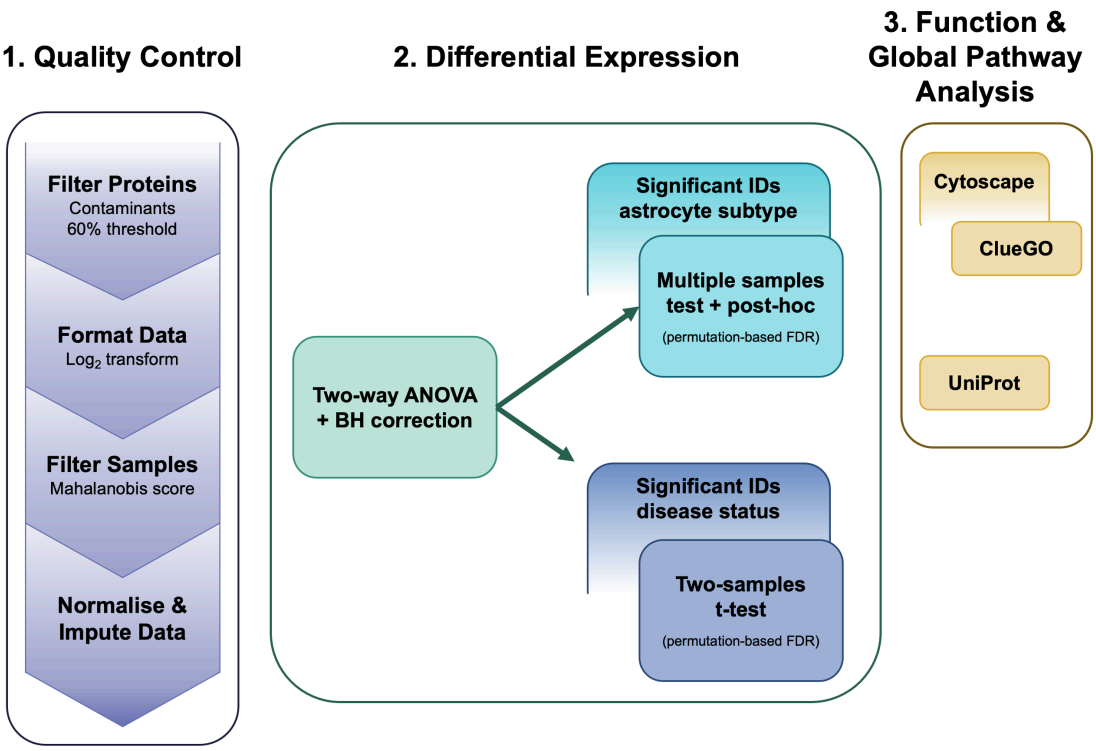


Figure 4.2. Summary of downstream proteomic analyses workflow. Data underwent quality control processing using the protein group matrix DIA-NN output file (**1**). Quality control processing included protein filtering, data formatting, sample filtering, normalisation, and imputation of missing values. Differential expression analyses were performed on cleaned data (**2**). We determined the global effects of astrocyte subtype, and disease or genotype status with BH corrected two-way ANOVA. Significant IDs for astrocyte subtype were carried forward for multiple samples test and posthoc analyses. Two-samples t-tests were performed on IDs significant for disease or genotype status. Protein groups called significant and met a $\log_2$ fold-change of ±1 were carried forward for function and global pathway analysis (**3**). Tools of analysis included ClueGO, a tool within Cytoscape, and UniProt.

4.2.6.1 Quality control processing

Downstream analyses were carried out on the protein group matrix DIA-NN output file. Data were filtered to remove potential contaminants. We only included proteins that were quantified in at least 60% of the samples. The proteins that met the threshold underwent $\log_2$ transformation. A Mahalanobis distance score was performed using R package pmartR (v0.9.0) to identify any samples that

were outliers[211,212]. Samples that met the threshold were median centred, and missing values were imputed with random numbers drawn from a normal distribution with a width of 0.3, and a downshift of 1.8 on a per-samples basis in Perseus software[213].

4.2.6.2 Differential expression analyses

Differential expression analysis was carried out in Perseus after quality control processing. Before performing statistical analysis of protein group IDs, we conducted an initial unsupervised principal component analysis (PCA) to evaluate the general clustering of samples. BH corrected two-way ANOVA was performed to determine the global effects of astrocyte subtype and disease or genotype status on protein group IDs.

Protein group IDs significant for astrocyte subtype were carried forward for multiple sample test and posthoc analyses. Multiple sample tests were corrected using a permutation-based FDR of 5%. Two-sample t-tests with permutation-based FDR to correct for multiple testing were performed on protein group IDs significant for disease or genotype status. All significant IDs were filtered based on a $\log_2$ fold-change of ±1.

4.2.6.3 Function and global pathway analyses

Protein groups called significant by differential expression analyses were taken forward for pathway analysis using ClueGO (v2.5.8), a tool within Cytoscape (v3.9.1), with *Homo Sapiens* set as the reference source[214-216]. The lists of significant protein groups were split based on the direction of the $\log_2$ fold-

change. Protein identifiers were tested for enrichment of the Gene Ontology Biological Process[217,218], KEGG pathways[219], and Reactome pathway terms[220] using the default settings, a two-sided hypergeometric test with Bonferroni step down. The predefined selection criteria required a minimum of three protein group IDs per functional pathway to be identified as a representative GO term. GO term fusion was also applied to merge parent-child terms of similar associated genes. All other ClueGO parameters were set to the default.

For protein group IDs that did not meet the predefined selection criteria, functional information of the protein group was carried out with UniProt Knowledgebase[221].

4.3 Results

4.3.1 Demographics

Clinical details of the cases used for the IHC analyses of this chapter are found in **Table 4.2**. 80% (16/20) of our MS cases were clinically classified as SPMS and 10% (2/20) as PPMS. The clinical course was unknown for 2 MS cases. The MS cases stratified by *HLA-DRB1*15* were matched on all demographic and clinical factors (**Table 4.2**).

Table 4.2. Clinical features of the cohort used in IHC analyses of Chapter 3. Covariates were assessed using Mann-Whitney (age; post-mortem interval; brain weight) and Fisher's Exact Test (sex).

	MS (*n*=20)	Control (*n*=5)	*p*-value	MS (*n*=20)		*p*-value
				HLA-DRB1*15- **(*n*=10)**	***HLA-DRB1*15+*** **(*n*=10)**	
Age of death (yrs)	63 (range: 42-82)	81 (range: 68-91)	.002	62 (range: 43-82)	63 (range: 42-73)	.971
Sex (F:M)	15:5	2:3	.283	8:2	7:3	1.000
Post-mortem interval (hrs)	18 (range: 8-38)	34 (range:22-52)	.015	17 (range: 8-28)	19 (range: 8-38)	.796
Brain weight (g)	1154 (range:950-1380)	1324 (range: 1090-1628)	.060	1160 (range:950-1380)	1148 (range: 1000-1350)	.796
Duration of disease (yrs)	29 (range: 12-47)	N/A	N/A	29 (range: 19-47)	28 (range: 12-46)	.780
Clinical course	PPMS=2 SPMS=16 Unknown=2	N/A	N/A	PPMS=1 SPMS=8 Unknown=1	PPMS=1 SPMS=8 Unknown=1	N/A

4.3.2 FFPE workflow

The titration analysis of FFPE tissue revealed that the total number of identified proteins was comparable to fixed frozen tissue (**Figure 4.3A**). At their maximum area of $10^6 \mu m^2$, FFPE tissue yielded 3100 proteins, whilst fixed frozen tissue yielded 3102 proteins. A fresh-frozen tissue reference standard from previous work had slightly higher outputs with a maximum yield of 3979 proteins (kindly provided by Simon Davis). Based on the curve plateau, a range of $10^{4.5}$-$10^{5.5} \mu m^2$ was determined to be optimal for FFPE tissue collection.

The titration refinement in the $10^{4.5}$-$10^{5.5} \mu m^2$ range on FFPE determined that a total area capture of $10^5 \mu m^2$ provided sufficient depth of protein identifications (**Figure 4.3B-C**). EP-DIRECTOR® slides also had a greater yield (2822 proteins) than membrane slides (464 proteins) at $10^5 \mu m^2$. Therefore, we used a total capture area of $10^5 \mu m^2$ from EP-DIRECTOR® slides for further experiments.

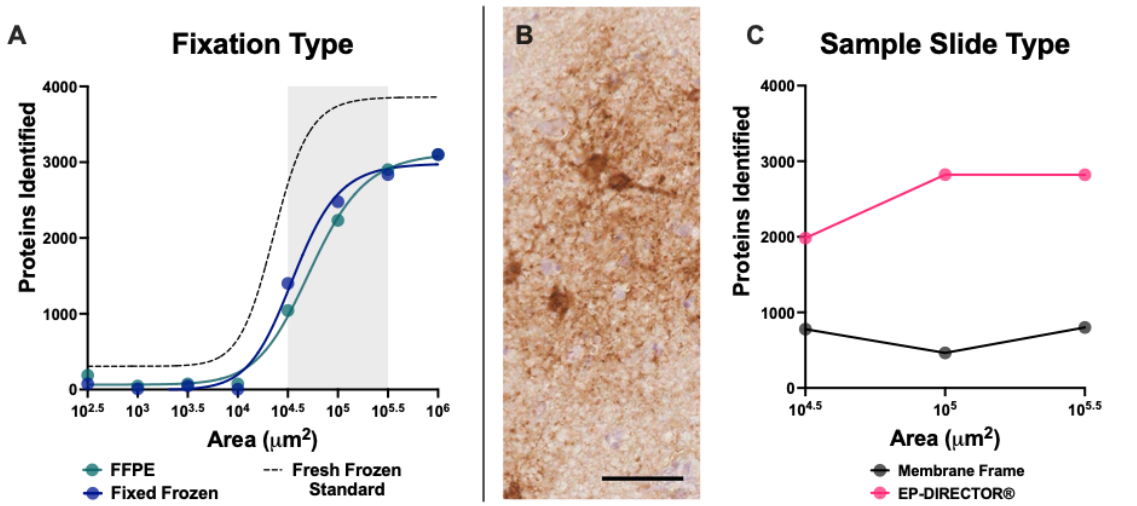


Figure 4.3. Influence of fixation and slide-type on the number of proteins identified with LCM-directed mass spectrometry. Across all areas, formalin fixation reduced the number of identified proteins compared to fresh frozen tissue. However, FFPE paraffin did not impact the number of identified proteins (**A**). A selection size of 130μm^2 was determined based on the approximate astrocyte size observed in our cohort (**B**). Further titration analysis revealed that a total capture area of 10^5μm^2 was sufficient for adequate numbers of identified proteins. EP-DIRECTOR® slides also identified more proteins than membrane frame slides (**C**). Scale bar = 50μm.

4.3.3 Proteomic quality control

Post-processing of mass spectrometry data with DIA-NN revealed that 6549 unique protein group IDs were present, where 5419 met the acceptable threshold of 60% across all samples.

Based on the Mahalanobis distance metrics, 85.3% (64/75) samples were carried forward for differential expression analyses (**Figure 4.4**). Specifically, quality control filtering removed 20% (1/5) from the GFAP+/ALDH1L1+ control group, 15% (3/20) from the GFAP+ MS group, 20% (4/20) from the GFAP+/ALDH1L1+ MS group, and 15% (3/20) from the ALDH1L1+ group.

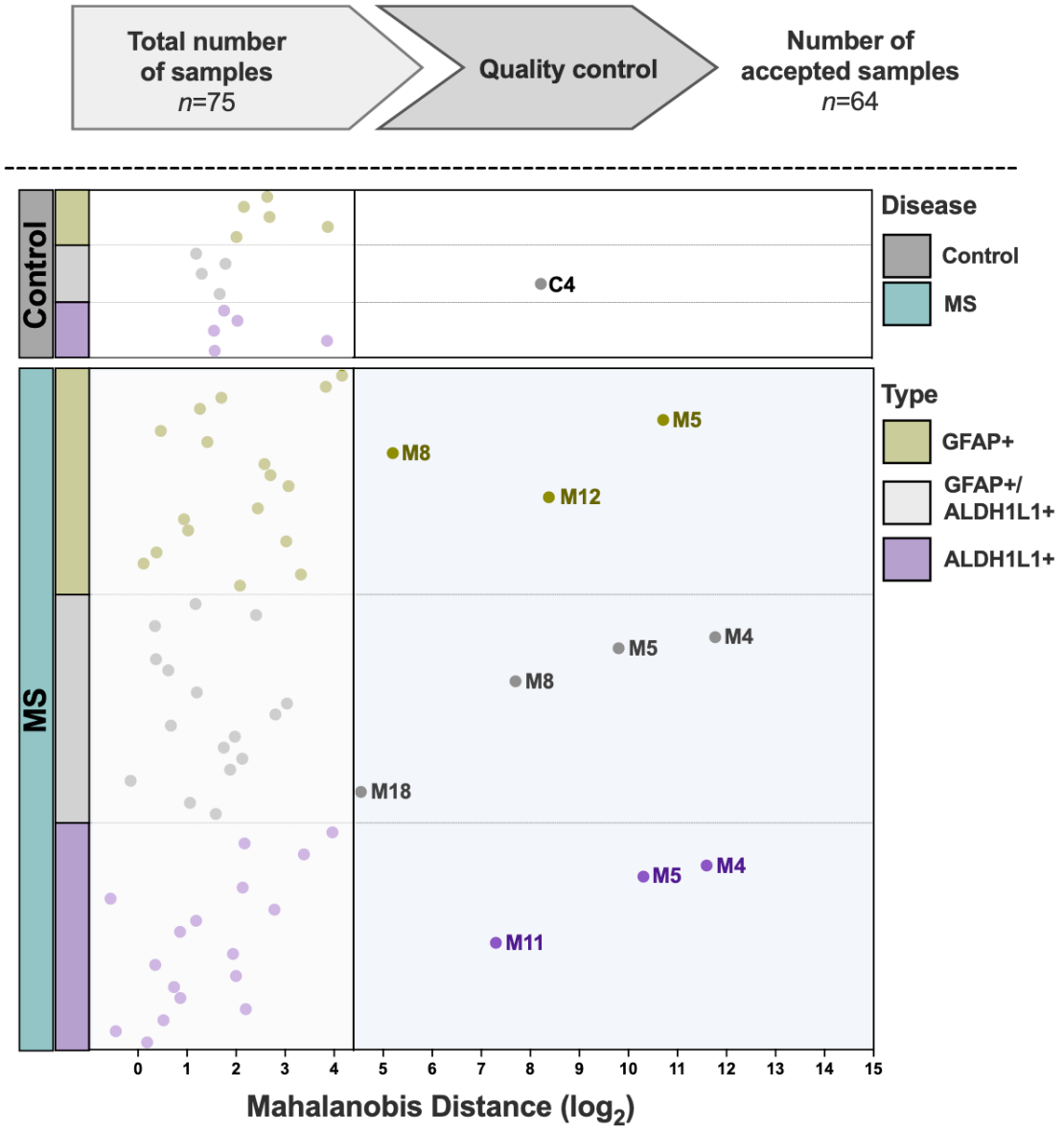


Figure 4.4. The number of samples for differential expression analysis after quality control filtering. Mahalanobis distance metrics were applied to all 75 samples, which identified 11 samples as potential outliers. Samples were from control (dark grey) and MS (teal) cases, which were pre-defined with LCM into GFAP+ (yellow); GFAP+/ALDH1L1+ (light grey); and ALDH1L1+ astrocytes (purple). A total of 64 samples were carried forward for differential expression analyses. Solid black line denotes $p \leq .05$. C = control sample; M = MS sample.

4.3.4 Influence of astrocyte subtype, disease, and genotype status on protein group IDs

4.3.4.1 Astrocyte subtype versus disease status

An unsupervised PCA was conducted to determine overall differential expression patterns present across all samples. PCA assessment of all samples revealed separation between disease status and astrocyte subtypes (**Figure 4.5A-C**). All samples showed separation of astrocyte subtypes where GFAP+ samples clustered towards the upper quadrants and ALDH1L1+ samples clustered towards the bottom quadrants. GFAP+/ALDH1L1+ samples clustered in between GFAP+ and ALDH1L1+ samples. Moreover, disease status appeared to separate across the x-axis. Control samples were clustered towards the negative x-axis, whilst MS samples clustered towards the positive x-axis.

A two-way ANOVA with BH correction showed that there was a significant effect of disease status and astrocyte subtype on protein group IDs (**Figure 4.5B**). There were 2,450 protein group IDs significant for disease status, with 1,931 IDs exclusive to disease status group. A total of 1,160 protein group IDs were significant for astrocyte subtype, of which 641 IDs were mutually exclusive to astrocyte subtype group. 519 protein group IDs were called significant for both disease status and astrocyte subtype. However, there was no interaction effect of disease status and astrocyte subtype on any protein group IDs.

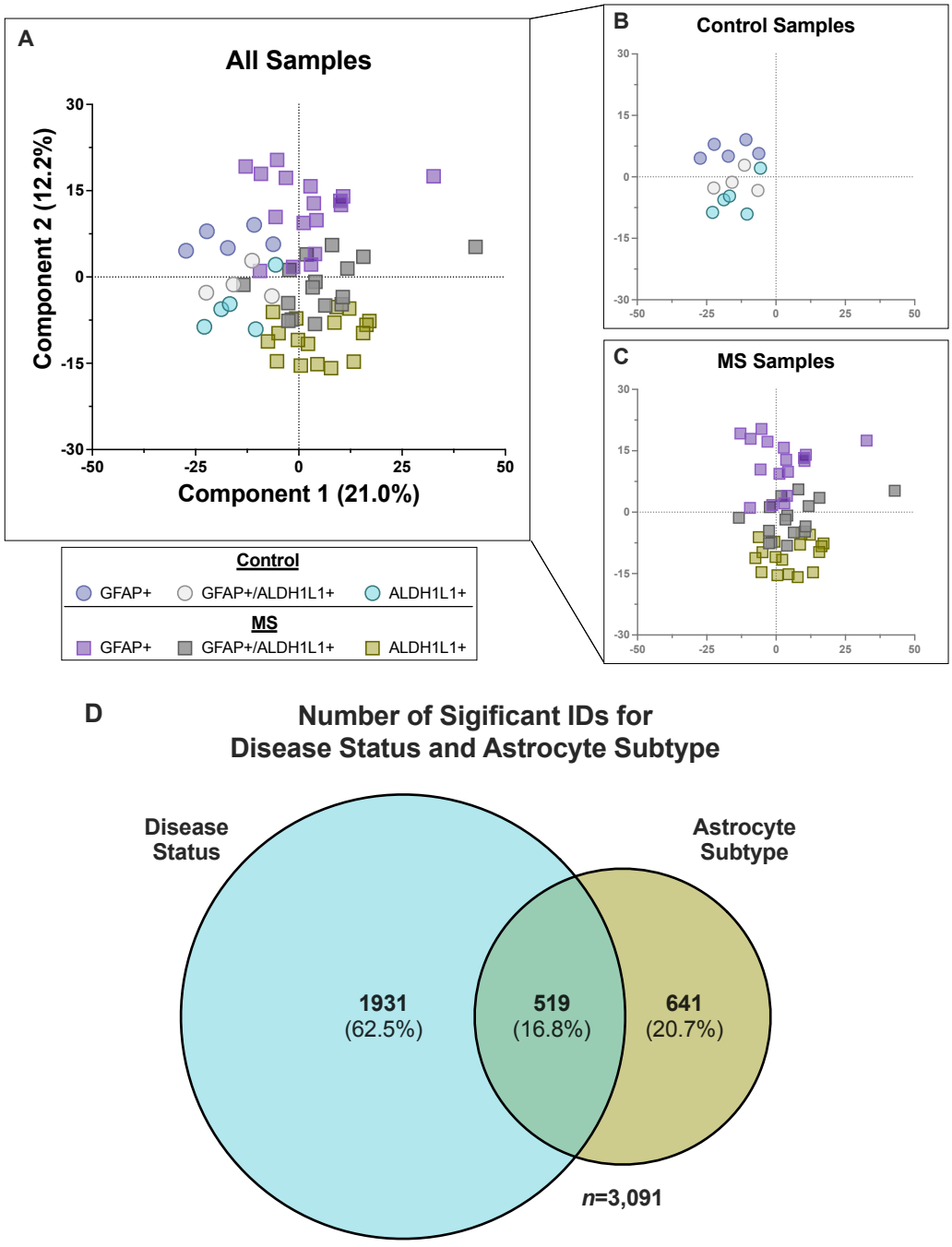


Figure 4.5. Influence of disease status and astrocyte subtype on the protein group IDs in all samples. Based on DIA-NN intensity values, PCA of all samples showed separation between disease status and astrocyte subtype (**A**). Separation was present between MS (**B**) and control samples (**C**), and between GFAP+, GFAP+/ALDH1L1+, and ALDH1L1+. A two-way ANOVA with BH correction revealed significant effects of disease status and astrocyte subtype (**D**). Disease status had 2,450 significant protein group IDs, where 1,931 IDs were exclusive to the disease status group (blue). Astrocyte subtype had 1,160 total significant protein group IDs with 641 IDs exclusive to astrocyte subtype group (yellow).

4.3.4.2 Astrocyte subtype versus genotype status

An initial assessment of MS samples with unsupervised PCA showed separation of astrocyte subtypes (**Figure 4.6A-C**). Regardless of genotype status, GFAP+ samples clustered towards the upper quadrants, whilst ALDH1L1+ samples clustered towards the lower quadrants. GFAP+/ALDH1L1+ samples clustered in between GFAP+ and ALDH1L1+ samples. PCA displayed minimal separation of genotype status, *as HLA-DRB1*15-* and *HLA-DRB1*15+* samples clustered at similar x-axis values (**Figure 4.6A-C**).

A two-way ANOVA with BH correction revealed significant effects of genotype status and astrocyte subtype on protein group IDs (**Figure 4.6D**). A total of 204 protein group IDs were significant for genotype status, with 176 IDs exclusive to genotype status group. There were 1,047 protein group IDs significant for astrocyte subtype, of which 1,019 IDs were mutually exclusive to astrocyte subtype group. 28 protein group IDs were called significant for both genotype status and astrocyte subtype. However, no interaction effect of genotype status and astrocyte subtype was present.

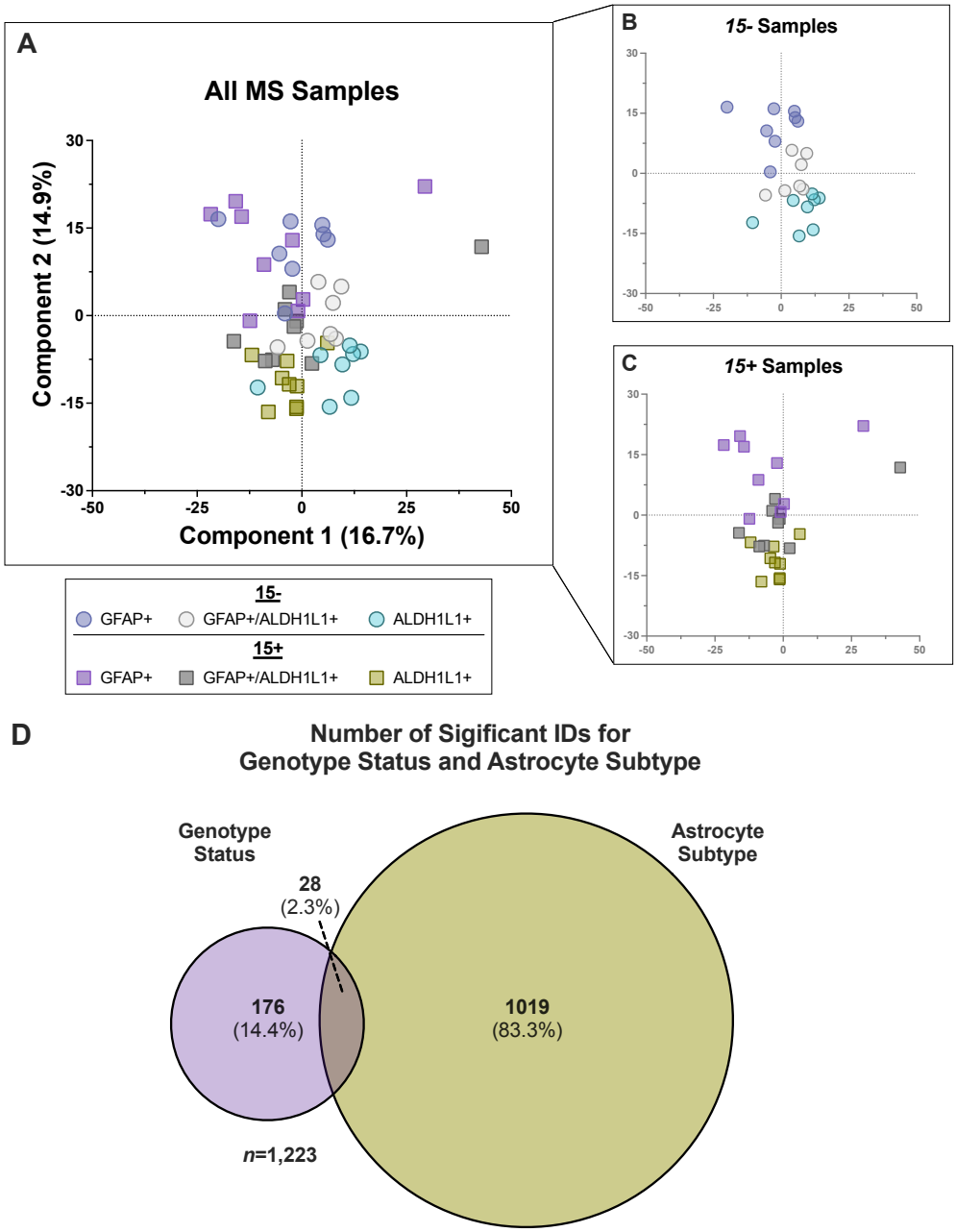


Figure 4.6. Influence of genotype status and astrocyte subtype on the protein group IDs in MS samples. PCA of DIA-NN intensity values in all MS samples showed separation between genotype status and astrocyte subtype (**A**). Both *HLA-DRB1*15-* (**B**) and *HLA-DRB1*15+* samples (**C**) displayed separation of astrocyte subtype groups GFAP+, GFAP+/ALDH1L1+, and ALDH1L1+, but the separation between genotype groups was minimal. A BH corrected two-way ANOVA revealed significant effects of genotype status and astrocyte subtype on protein group IDs (**D**). Genotype status had 204 significant protein group IDs, where 176 IDs were exclusive to the genotype status group (purple). Astrocyte subtype had 1,047 total significant protein group IDs with 1,019 IDs exclusive to astrocyte subtype group (yellow).

4.3.5 Proteome profiles of GFAP+ astrocytes differ from ALDH1L1+ astrocytes

4.3.5.1 Identification of astrocyte subtype proteomes

Of the 1,160 protein group IDs called significant for astrocyte subtype (**Figure 4.5B**), 344 IDs met the $\log_2$ fold-change of ±1 (**Figure 4.7A**). In control samples, astrocyte subtype was significant for 130 protein groups, where 50 IDs were exclusive to controls (**Figure 4.7A**; purple). MS samples had 294 protein groups significant for astrocyte subtype, of which 214 IDs were exclusive to MS (**Figure 4.7A**; blue). The intersection of control and MS samples revealed 80 protein group IDs.

We assessed the 80 protein group IDs shared between control and MS samples to identify core proteome profiles of astrocyte subtypes irrespective of disease status. Differential expression was greatest between GFAP+ and ALDH1L1+ astrocyte samples (**Figure 4.7B**). In contrast, differential expression between GFAP+ and GFAP+/ALDH1L1+ or ALDH1L1+ and GFAP+/ALDH1L1+ was minimal (**Figure 4.7B**).

Further assessment of the protein group IDs that intersected between GFAP+, ALDH1L1+, and GFAP+/ALDH1L1+ samples, showed general functions related to the regulation of the complement cascade, the Hippo signalling pathway, and the regulation of complement activation (**Figure 4.7C**). Protein groups that did not meet the preselected ClueGO criteria (GO terms absent) had UniProt functions associated with antioxidant pathways, acute inflammatory response, chaperone binding, and vitamin D binding (**Figure 4.7C**). The enrichment

direction of comparisons between GFAP+ and ALDH1L1+ or GFAP+ and GFAP+/ALDH1L1+ opposed the enrichment direction of ALDH1L1+ versus GFAP+/ALDH1L1+ samples (**Figure 4.7C**). Therefore, protein group IDs that were upregulated for GFAP+ samples were downregulated for ALDH1L1+ samples and vice versa.

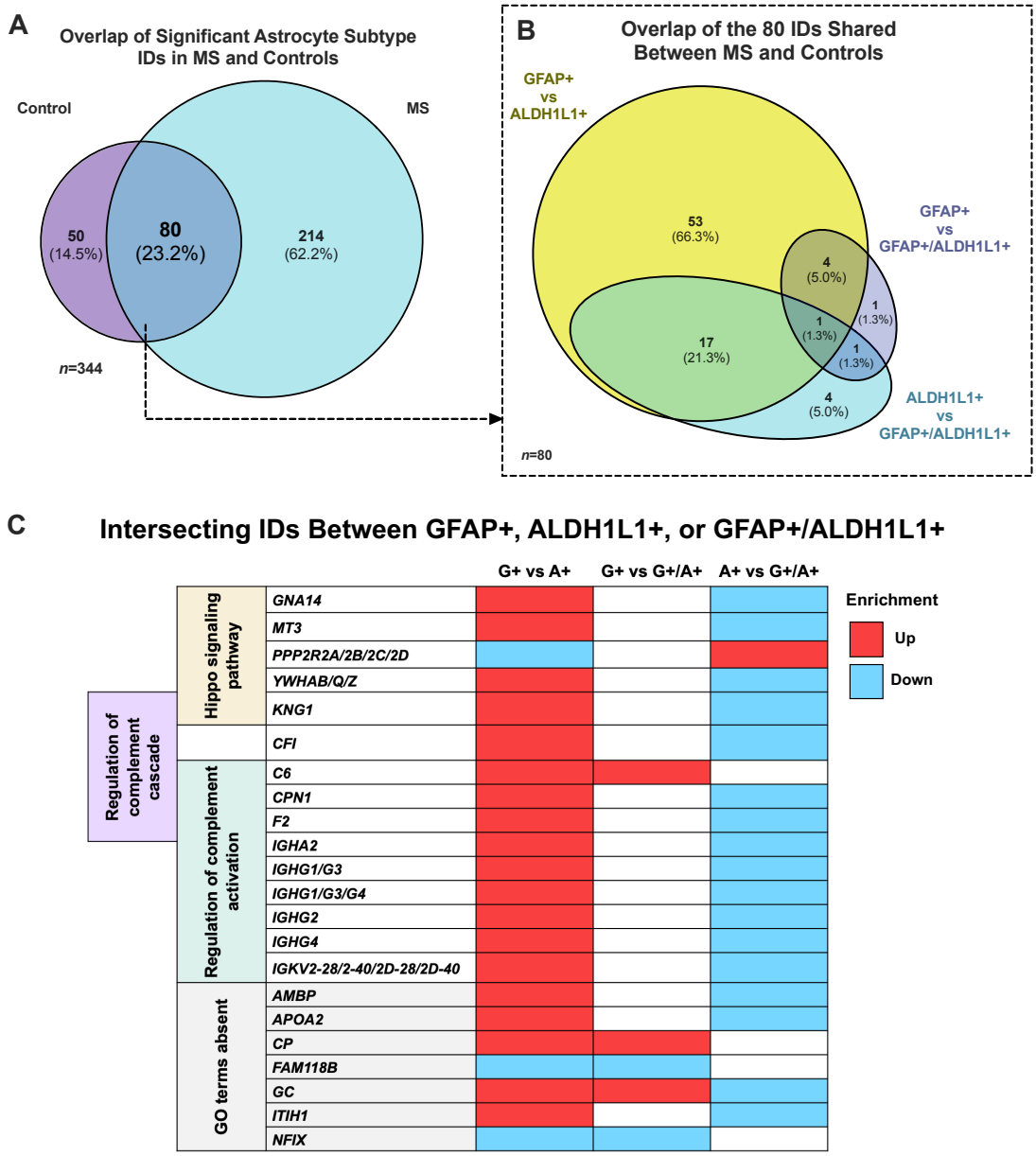


Figure 4.7. Differential expression of astrocyte subtypes in MS and control samples. Overlap of the 344 protein group IDs called significant with a $\log_2$ fold-change of ±1 revealed an intersect of 80 IDs between MS and control samples (**A**; Control = purple; MS = teal). Of these 80 IDs, differential expression was greatest between GFAP+ and ALDH1L1+ astrocyte samples (**B**; yellow). Differential expression between GFAP+ or ALDH1L1+ and GFAP+/ALDH1L1+ astrocyte samples was minimal. Protein group IDs that intersected between GFAP+, ALDH1L1+, and GFAP+/ALDH1L1+ samples showed functions related to complement cascade, hippo signalling, and regulation of complement activation (**C**). There was also an inverse relationship of enrichment direction for GFAP+ and ALDH1L1+ protein group IDs. G+ = GFAP+; A+ = ALDH1L1+; G+/A+ = GFAP+/ALDH1L1+; Red box = upregulation; Blue box = downregulation.

4.3.5.2 Protein expression differences between GFAP+ and ALDH1L1+ astrocytes

To identify core proteomes of GFAP+ and ALDH1L1+ astrocytes, we assessed the 53 protein group IDs that were only present between GFAP+ and ALDH1L1+ samples (**Figure 4.8; Table S4.2**). Functional network analysis between GFAP+ and ALDH1L1+ astrocyte samples showed relatively distinct clustering of down- and upregulated protein groups (**Figure 4.8**). Downregulated protein group IDs were related to nuclear envelope reassembly (**Figure 4.8**). For functional terms related to upregulated protein groups, haemostasis, humoral immune response, complement and coagulation cascades, endopeptidase inhibitor activity, and laminin interactions were present in the largest network cluster (**Figure 4.8**).

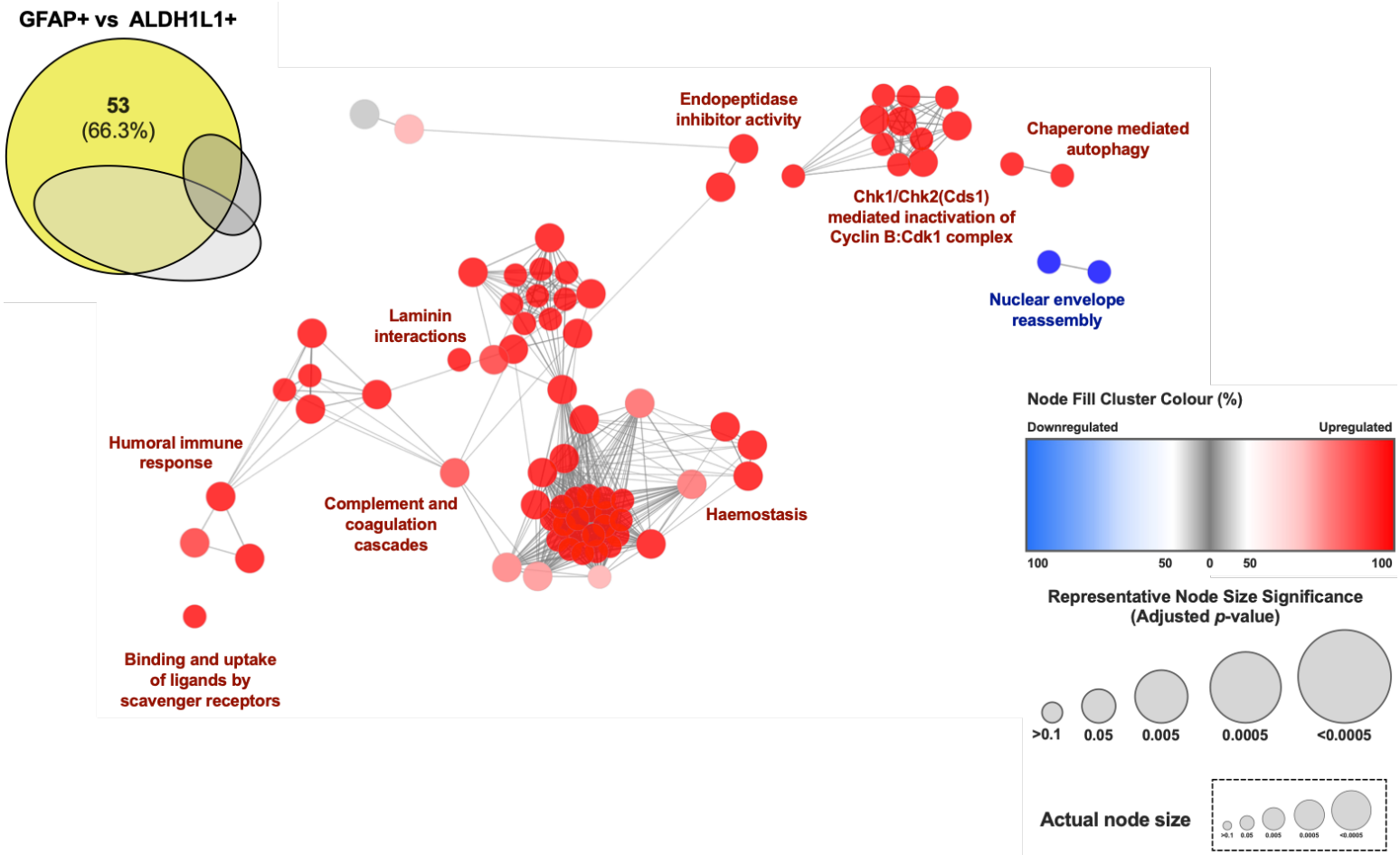


Figure 4.8. Differentially expressed protein groups between GFAP+ and ALDH1L1+ astrocytes in MS and controls. Functional network analysis of protein IDs only present between GFAP+ and ALDH1L1+ samples (yellow) demonstrated relatively distinct clustering of down- and upregulated protein group functions. Lines (edges) represent how many terms are in common between the two nodes. Blue = downregulated for GFAP+; Red = upregulated for GFAP+.

4.3.6 Proteome profiles differ between MS and controls in astrocyte subtypes

4.3.6.1 Proteome profile of GFAP+ astrocytes

The proteome profile of GFAP+ astrocytes differed between MS and control samples (**Figure 4.9; Table S4.3**). A two-sample t-test identified 94 downregulated protein groups, such as tubulin proteins (*TUBA4A/8; TUBB/2A/2B/4B/8; TUBB2A/2B/6*) in MS (**Figure 4.9A**). MS samples also had 53 identified upregulated protein groups, such as immunoglobulins (*IGHG1; IGHG2; IGHG3; IGHG4; IGHM; IGLV1-47; IGKV3-20/3D-20*) and major histocompatibility complex (MHC) class II (*HLA-DRA*) (**Figure 4.9A**). Functional analysis demonstrated distinct clustering of down- and upregulated protein groups (**Figure 4.9B**). Downregulated protein group IDs related to microtubule-dependent trafficking of connexons, resolution of sister chromatid cohesion, CLTA4 inhibitory signalling, and negative regulation of DDX58/IFIH2 signalling were among the most numerous (>5%; **Figure 4.9B**). For functional terms related to upregulated protein group IDs, mRNA 3'-end processing, myeloid leukocyte mediated immunity, signalling by BRAF and RAF1 fusions, and antimicrobial humoral response were the most frequent (>5%; **Figure 4.9B**).

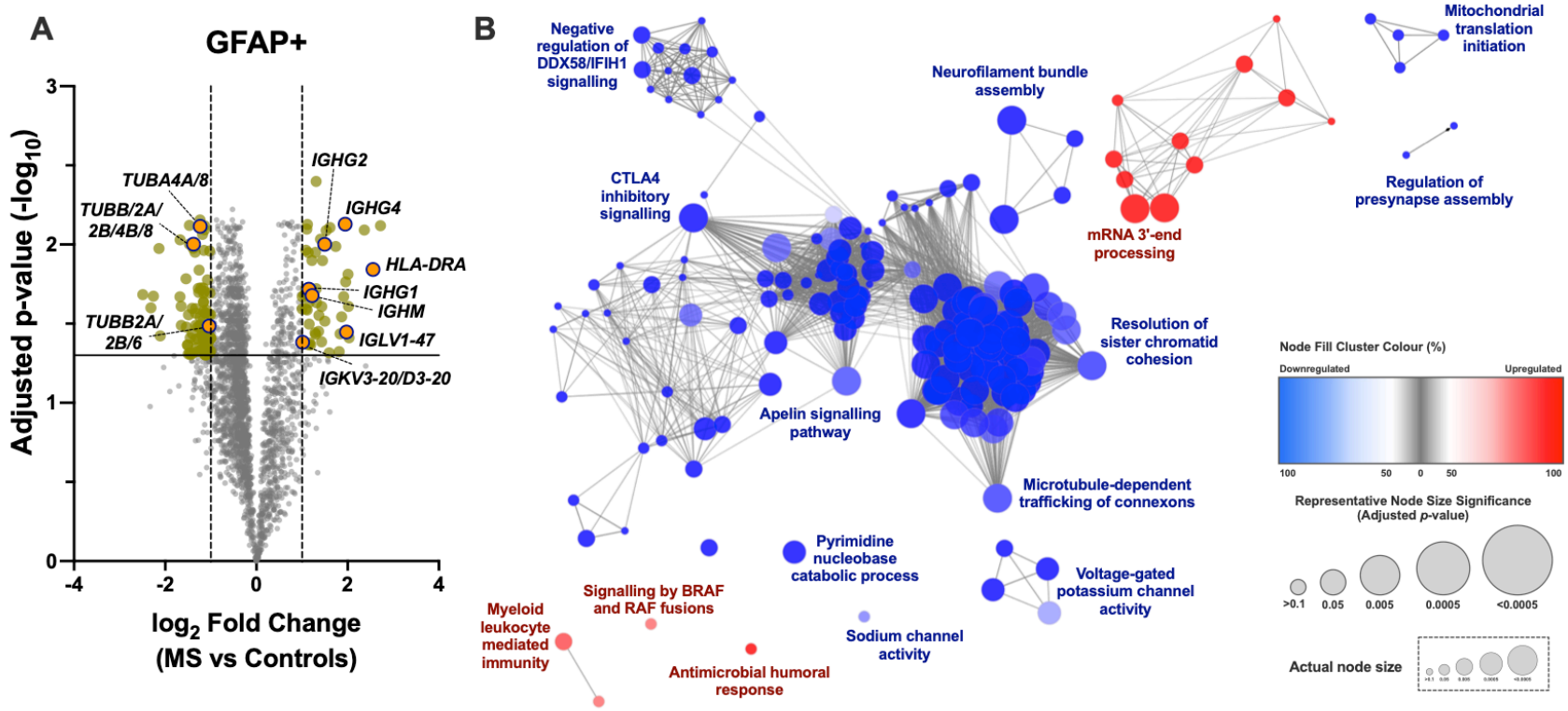


Figure 4.9. Differential expression of GFAP+ astrocytes in MS. A volcano plot of GFAP+ astrocytes between MS and control samples (**A**). Negative log_2 fold-change of protein groups such as tubulins (orange) represented downregulation, whilst positive log_2 fold-change of protein groups, including immunoglobulins and MHC class II (orange), signified upregulation in MS. Global pathway analysis showed distinct functional clustering of significantly down- and upregulated protein group IDs in MS (**B**). Volcano plot: horizontal solid line represents 5% FDR threshold, and vertical dashed lines represent ± 1-fold change. Network legend: Lines (edges) represent how many terms are in common between the two nodes. Blue = downregulated for MS; Red = upregulated for MS.

4.3.6.2 Proteome profile of ALDH1L1+ astrocytes

A two-sample t-test revealed that ALDH1L1+ astrocytes had differentially expressed protein groups between MS and controls (**Figure 4.10A; Table S4.4**). MS samples had 25 identified downregulated protein groups, such as voltage-gated potassium channels (*KCNA1/2/3/4/6*) and synaptic vesicle proteins (*SYN1/2/3*) (**Figure 4.10A**). 107 upregulated protein group IDs were detected, including mRNA splicing proteins (*CDC5L; DDX23; PTBP1; RBM14; U2AF1*) (**Figure 4.10A**). Functional analysis demonstrated that network clusters of down- and upregulated protein groups were mostly distinct (**Figure 4.10B**). Protein groups associated with cell-cell adhesion mediatory activity were present in both down- and upregulated protein groups (**Figure 4.10B**). For functional terms related to downregulated protein group IDs, voltage-gated potassium channels and synaptic vesicle clustering were numerous (>5%; **Figure 4.10B**). Upregulated protein group IDs related to RNA splicing, spliceosome, regulation of RNA splicing, mRNA export from the nucleus, and complement activation were most frequent (>5%; **Figure 4.10B**).

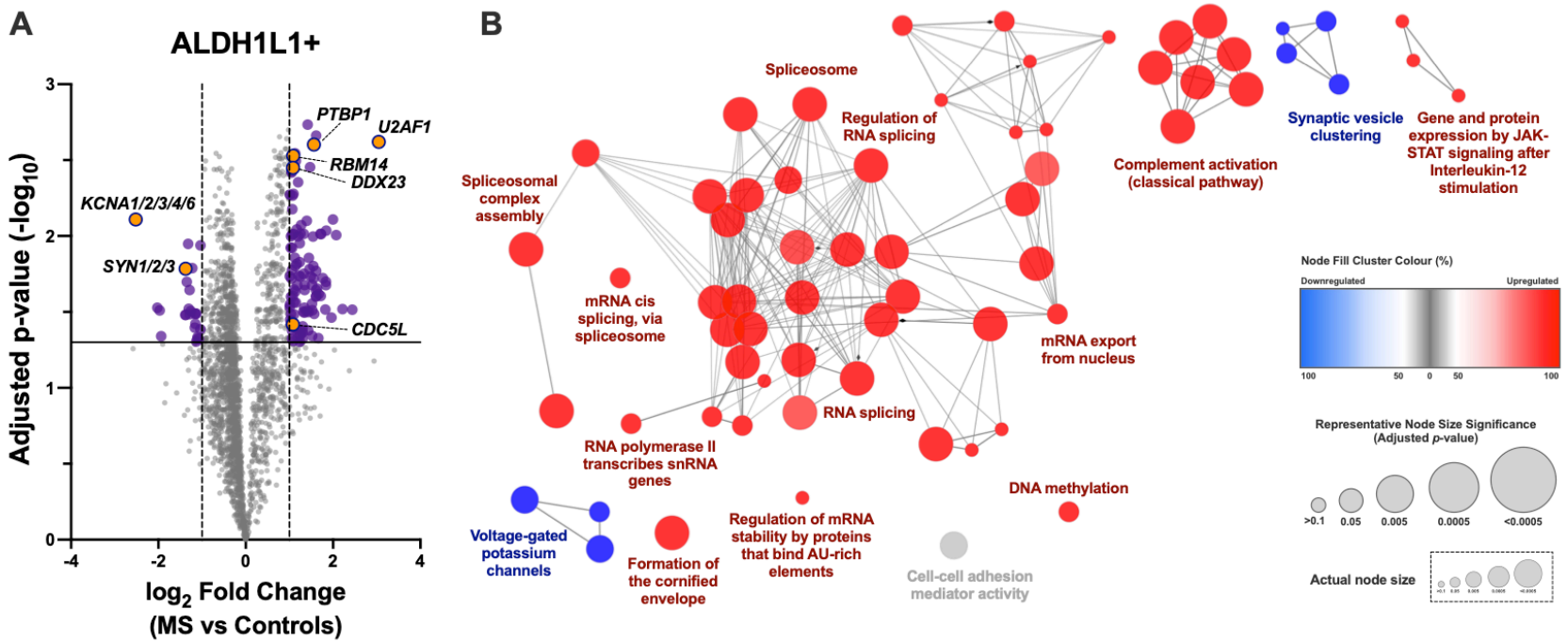


Figure 4.10. Differential expression of ALDH1L1+ astrocytes in MS. A volcano plot of ALDH1L1+ astrocytes between MS and control samples (**A**). Negative log_2 fold-change of protein groups, such as ion channels and synaptic vesicle proteins (orange), represented downregulation, whilst positive log_2 fold-change of protein groups, such as mRNA splicing proteins (orange), signified upregulation in MS. Global pathway analysis showed relatively distinct functional clustering of significantly down- and upregulated protein group IDs in MS (**B**). The function of cell-cell adhesion mediator activity was shared between down- and upregulated IDs (**B**; grey). Synaptic vesicle clustering was the dominant functional group for downregulated IDs in MS. Upregulated IDs mainly were related to functions associated with mRNA splicing in MS. Volcano plot: horizontal solid line represents 5% FDR threshold, and vertical dashed lines represent ± 1-fold change. Network legend: Lines (edges) represent how many terms are in common between the two nodes. Blue = downregulated for MS; Red = upregulated for MS.

4.3.6.3 Proteome profile of GFAP+/ALDH1L1+ astrocytes

The proteome profile of GFAP+/ALDH1L1+ astrocytes also differed between MS and control samples (**Figure 4.11A; Table S4.5**). A two-sample t-test identified 8 downregulated protein groups and 68 upregulated protein groups in MS (**Figure 4.11A**). Due to the limited number of downregulated protein group IDs, functional analysis could not be performed. However, some associated functions of downregulated protein groups included voltage-gated potassium channels (*KCND2*) and vesicle-fusing ATPases (*NSF*) (**Figure 4.11A**). For functional terms related to upregulated protein group IDs, nucleus organisation (*LMNA; LMNB1; NUMA1; NUP133; SMARCA5; SUN2*), chromatin remodelling, cellular response to zinc ion, mRNA splicing, regulation of RNA processing, positive regulation of histone modification, RNA polymerase transcription initiation, and ribonucleoprotein complex assembly were the most frequent (>5%; **Figure 4.11B**).

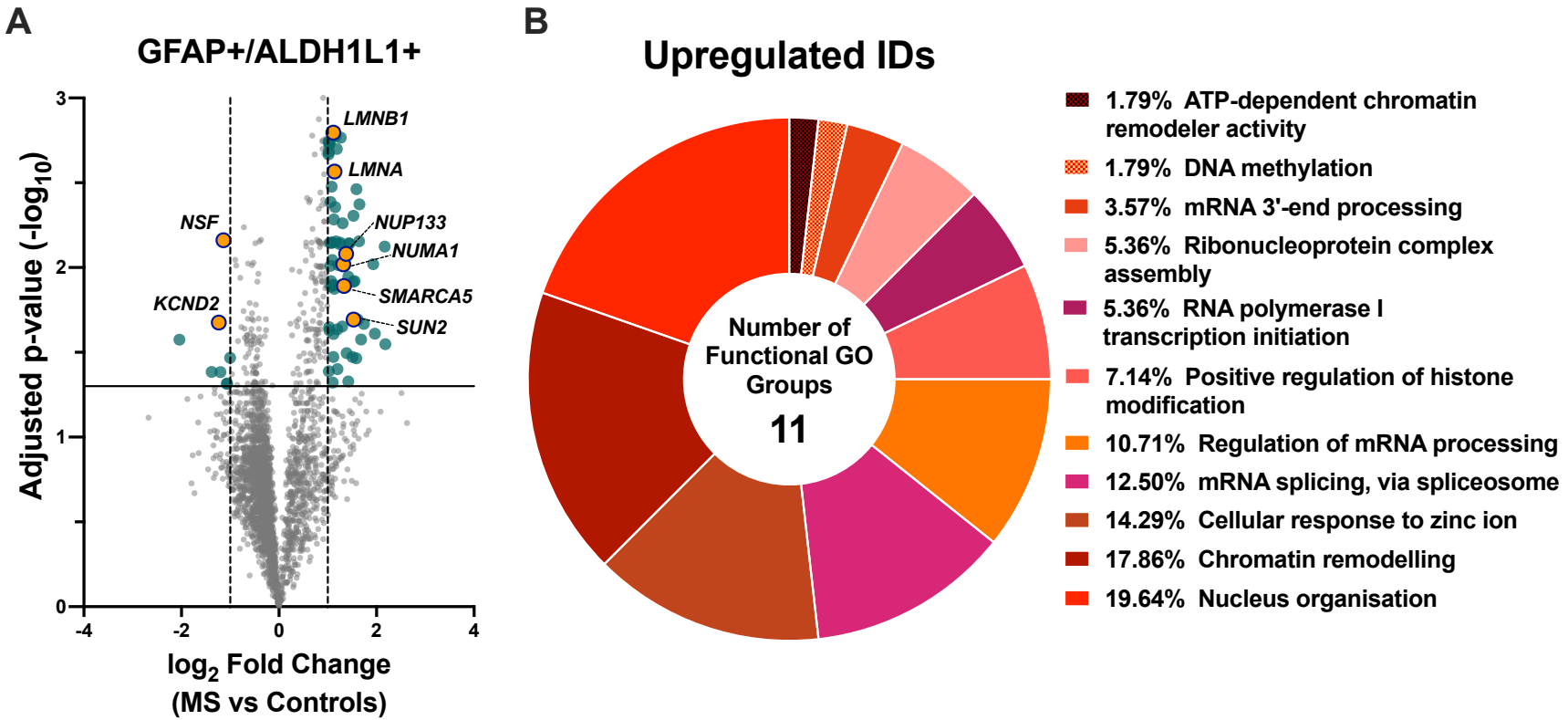


Figure 4.11. Differential expression of GFAP+/ALDH1L1+ astrocytes in MS. A volcano plot of GFAP+ALDH1L1+ astrocytes between MS and control samples (**A**). Negative log_2 fold-change of protein groups, such as voltage-gated potassium channels and vesicle-fusing ATPases (orange), represented downregulation, whilst positive log_2 fold-change of protein groups, such as nucleus organisation proteins (orange), signified upregulation in MS. Nucleus organisation was the largest functional term identified for upregulated IDs in MS (**B**). Volcano plot: horizontal solid line represents 5% FDR threshold, and vertical dashed lines represent ± 1-fold change.

4.3.7 *HLA-DRB1*15* status influences the proteome profiles of astrocyte subtypes

4.3.7.1 Proteome profile of GFAP+ astrocytes

A two-sample t-test revealed that GFAP+ astrocytes had differentially expressed protein groups between *HLA-DRB1*15*+ and *HLA-DRB1*15*- samples (**Figure 4.12A**). *HLA-DRB1*15*+ samples identified 3 downregulated and 7 upregulated protein groups. Due to the limited number of down- and upregulated protein group IDs, functional analysis could not be performed. However, downregulated protein group functions were related to glutathione metabolism (*GSTM1/5; GSTM1/4/5*), whilst some upregulated protein group functions were associated with HLA class I antigen presentation (*HLA-B/C/E*) (**Figure 4.12A**).

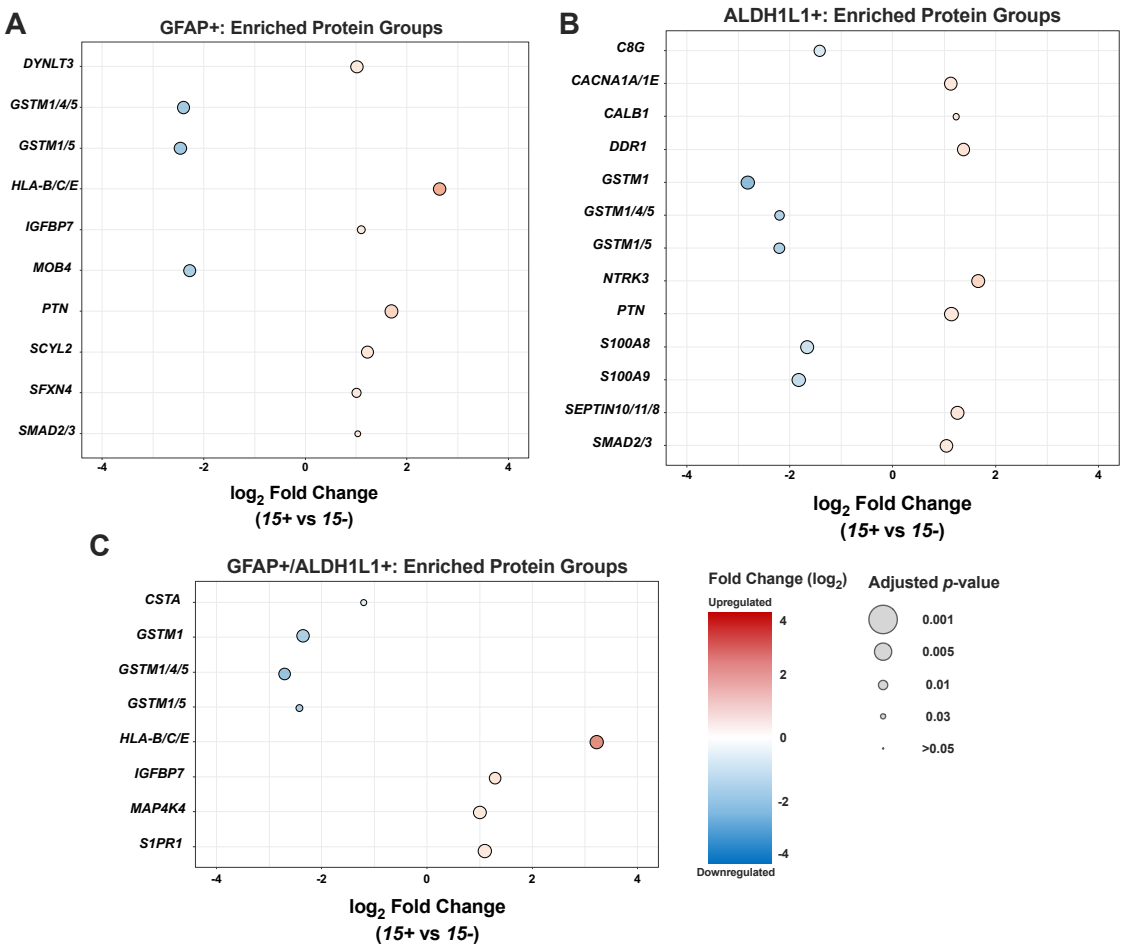


Figure 4.12. Enriched protein group IDs of astrocyte subtypes in *HLA-DRB1*15*+ compared to *HLA-DRB1*15*- samples. Dot plot of all down- and upregulated protein groups for GFAP+ (**A**), ALDH1L1+ (**B**), and GFAP+/ALDH1L1+ astrocyte subtypes in *HLA-DRB1*15*+ samples (**C**). Blue = downregulated for *HLA-DRB1*15*+; Red = upregulated for *HLA-DRB1*15*+.

4.3.7.2 Proteome profiles of ALDH1L1+ astrocytes

*HLA-DRB1*15* status also influenced the proteome profile of ALDH1L1+ astrocytes (**Figure 4.12B**). A two-sample t-test identified 6 downregulated and 7 upregulated protein group IDs. Although functional network analysis could not be performed, some downregulated protein group functions associated with antioxidant activity (*S100A8; S100A8*) and complement (*C8G*) (**Figure 4.12B**). Voltage-sensitive calcium channels proteins (*CACNA1A/E*) were amongst some of the functions associated with upregulated protein group IDs (**Figure 4.12B**).

4.3.7.3 Proteome profiles of GFAP+/ALDH1L1+ astrocytes

The proteome profile of GFAP+/ALDH1L1+ astrocytes was also influenced by *HLA-DRB1*15* status (**Figure 4.12C**). There were 4 downregulated and 4 upregulated protein groups identified by a two-sample t-test. Functional analysis was not performed due to the limited number of down- and upregulated protein group IDs. However, downregulated protein groups associated with glutathione metabolism (*GSTM1; GSTM1/5; GSTM1/4/5*), whilst some upregulated protein groups related to HLA class I antigen presentation (*HLA-B/C/E*) (**Figure 4.12C**).

4.3.8 Discussion

Understanding the molecular properties underlying astrocyte diversity is important to identify how astrocytes contribute to MS pathological outcomes. This chapter extends previous approaches that have characterised the molecular signatures of astrocytes in MS[33,155,159]. Although many studies describe changes to astroglial-related biomolecule expression in whole tissues, few have assessed the specific profiles of MS astrocytes[62,157]. Here, we provide for the first time evidence that astrocyte subpopulations, namely GFAP+ and ALDH1L1+ astrocytes, have distinct protein expression profiles regardless of MS disease or genotype status. In particular, we show that GFAP+ astrocytes are enriched in proteins related to haemostasis and immune processes, providing important insights into the role of the astrocyte on vessel integrity and CNS inflammation. Moreover, our novel data identify clear protein expression differences between MS and controls across all astrocyte subpopulations, such as enrichment of immune-related proteins in GFAP+ astrocytes and co-expression of synaptic vesicle clustering and voltage-gated potassium channels in ALDH1L1+

astrocytes. We also report proteome differences for MS *HLA-DRB1*15* status, which appear to impact the co-expression of inflammatory-related proteins on GFAP+ and ALDH1L1+ astrocytes.

Despite their immense morphological and functional diversity, little is known about the astroglial-specific properties of astrocyte subpopulations. Transcriptomic and genomic profiling of astrocytes has identified a wide range of molecular signatures suggestive of different astroglial subpopulations, which may underpin the differential responses seen in health and disease[130,131]. We identify distinct proteome profiles comparing GFAP+, ALDH1L1+, and GFAP+/ALDH1L1+ astrocytes, irrespective of disease status (i.e. MS or non-neurological disease; **Figure 4.7**). Differentially expressed protein patterns show inverse relationships between enriched GFAP+ and ALDH1L1+ protein groups, where upregulated GFAP+ protein groups are downregulated for ALDH1L1+ groups (**Figure 4.7**). Inverse relationships are also present for comparisons with GFAP+/ALDH1L1+ astrocytes, indicating that differential expression of astrocyte subtypes are driven by the pure GFAP+ and ALDH1L1+ astrocytes subgroups. Indeed, differential protein expression is greatest between GFAP+ and ALDH1L1+ astrocytes (**Figure 4.7**). These findings align with our histological observations described in Chapters 2-3 and provide further evidence of different astrocyte subpopulations in the motor cortex.

Our findings provide insights into the possible functional roles of distinct astrocyte subpopulations, namely GFAP+ astrocytes, under non-neurological conditions. Several of the upregulated protein groups enriched in GFAP+ astrocytes

compared to ALDH1L1+ astrocytes relate to haemostasis functions including fibrinogen subunits (*FGA; FGB; FGG*), coagulation factors (*F10; F13A1*), and plasminogen (*PLG*) (**Figure 4.8**). This finding extends our data from the previous chapters, which saw an exaggeration of GFAP+ expression around the vasculature (Chapter 2-3), by suggesting that the co-expression of haemostasis factors may be important for GFAP+ astrocyte and blood vessel interactions. Astrocytes are key regulators of vessel permeability[171], and their co-expression of numerous factors, including immune-related molecules, can influence the integrity of the CNS vasculature[56,150]. Indeed, we show that GFAP+ astrocytes are also enriched in protein groups related to inflammatory processes such as complement (*C1; C4A; C4B*), serine protease inhibitor (*SERPINA1*), and immunoglobulins (*IGKV2-29/D2-26/2D-29*) (**Figure 4.8**). We suggest that co-expression of both haemostasis and immune pathway proteins might relate to an essential role for GFAP+ astrocytes in regulating vascular-mediated inflammation under non-neurological conditions in the motor cortex. However, we also acknowledge that LCM cannot guarantee the pure isolation of cells. Therefore, we are unable to identify if protein group IDs arose from the surrounding environment, such as the endothelium, or from the astrocytes themselves. Future work aimed at using single-cell technologies to inform proteomic analysis alongside IHC validation of protein group IDs will provide further insight into the mechanisms underlying GFAP+ function.

Our results also highlight the molecular diversity of astrocytes in MS, which demonstrate differentially expressed protein groups from control astrocytes across all subpopulations (**Figure 4.9**; **Figure 4.10**; **Figure 4.11**). Our functional

enrichment analysis reveals that many of the upregulated protein groups in GFAP+, ALDH1L1+, and GFAP+/ALDH1L1+ astrocytes possess properties involved in mRNA processing and spliceosome activity. Although the overall functions of these spliceosome and mRNA processing-related protein groups were similar, we show that these protein groups are relatively distinct between astrocyte subtypes in MS. This suggests that the different expression changes undergone by distinct astrocyte subpopulations in MS are impacted at the protein level, not the global pathway level. Moreover, splicing, which is integral to gene regulation, is considered a key generator of protein diversity and may account for the diversity seen in astrocyte subpopulations[222,223]. In MS, aberrant spliceosome function has been implicated in the inappropriate reaction to self-antigens and protein aggregation, which may lead to harmful inflammation and breakdown of appropriate cell function[224,225]. However, little is known about the mechanisms underlying differential astrocyte expression in MS. Whilst our data suggest that MS astrocyte subpopulations undergo protein changes related to spliceosome and mRNA processing function, further investigation is required.

Functional enrichment analysis in MS GFAP+ astrocytes also identify major upregulated protein groups related to immune function, including immunoglobulins (*IGHG1; IGHG2; IGHG3; IGHG4; IGHM; IGLV1-47; IGKV3-20/3D-20*) and MHC class II (*HLA-DRA*) (**Figure 4.9**). Our data align with previous studies, which report increased antigen presentation and proteins related to the innate immune NF-κB pathways in astrocytes under inflammatory conditions[226]. This indicates that, even in MS regions where myelin is intact, GFAP+ astrocytes may undergo molecular changes that reflect a more

dysfunctional cytotoxic phenotype. Indeed, downregulated protein groups in GFAP+ astrocytes relate to cell division processes (*TUBA4A/8; TUBB/2A/2B/4B/8; TUBB2A/2B/6*) (**Figure 4.9**), suggesting possible dysregulation of the cell cycle and further indicates dysfunction of GFAP+ astrocytes. Whilst the role of dysregulated cell cycles on astrocyte function in MS has yet to be determined, our data highlights the potential functional roles of GFAP+ astrocytes, which relate to key outcomes of MS pathology, inflammation and neurodegeneration.

The proteome of ALDH1L1+ astrocytes also shows clear differences between MS and controls. Although the protein groups for ALDH1L1+ astrocytes were distinct from GFAP+ astrocytes, we report that the upregulated protein pathways in MS ALDH1L1+ astrocytes are broader, dominated by functions related to spliceosome and mRNA splicing (**Figure 4.10**). How the pathway changes in ALDH1L1+ astrocytes relate to MS pathogenesis is not clear. Therefore, evaluating the spliceosome mechanisms in ALDH1L1+ astrocytes would greatly improve our understanding of how ALDH1L1+ astrocyte changes contribute to MS pathology.

Given the data from the previous chapters demonstrating that ALDH1L1+ expression is biased to areas of greatest neuronal density (Chapter 2), we suggest that ALDH1L1+ astrocytes are important for neuronal support. The downregulated protein groups for ALDH1L1+ astrocytes relate to functions associated with synaptic vesicle clustering (*SYN1; SYN3; SYN3*) and voltage-gated potassium channels (*KCNA1; KCNA2; KCNA3; KCNA4; KCNA6*), in which

both relate to glia-neuron communication and support (**Figure 4.10**). Astroglial delivery of synaptic vesicles is important for cell-to-cell contact and exchange of soluble factors with neurons[227], impacting synaptic integrity under pathological conditions[228]. Moreover, astroglial regulation of potassium homeostasis is crucial for appropriate neuronal function with certain astroglial potassium channels considered neuroprotective in EAE models[229]. However, data on astroglial voltage-gated potassium channels in MS is complex, with reports of decreased potassium channel expression in active lesions and increased potassium expression in peri-lesional regions[230]. Although the role of ALDH1L1+ astroglial potassium channel expression in MS requires further investigation, these findings indicate a crucial astroglial-neuronal role for ALDH1L1+ astrocytes.

Our assessment of astroglial proteomes within MS reveals minimal differential protein expression between MS *HLA-DRB1*15*+ and *HLA-DRB1*15*- genotype groups (**Figure 4.12**). Although MS carriage of *HLA-DRB1*15* is associated with greater demyelination, inflammation, and neuronal loss, genotype alone does not influence global cortical astrocyte expression (Chapter 2). Our data suggest that whilst the extent of the astrocyte proteome is reduced between MS genotype groups compared to between MS and controls, astrocyte subpopulations still undergo distinct molecular changes based on genetic status.

We show that the top upregulated protein groups in GFAP+ astrocytes segregated by *HLA-DRB1*15* status relate to antigen presentation (*HLA-B; HLA-C; HLA-E*) (**Figure 4.12**). Antigen presentation is an important feature of the *HLA-DRB1*15* genotype due to its correlation with many MHC proteins, such as HLA-

DRB1[174]. Therefore, aberrant antigen presentation of GFAP+ astrocytes may act to recruit immune molecules, contributing to the greater inflammation and subsequent degeneration present in *HLA-DRB1*15*+ MS cases.

ALDH1L1+ astrocytes also show differential protein expression of the *HLA-DRB1*15* genotype (**Figure 4.12**). The downregulation of protein groups in MS *HLA-DRB1*15*+ samples associated with metal-binding proteins (*S100A8; S100A9*) is of particular interest due to their association with inflammatory functions. As important tenants of neuroinflammation[231], the downregulation of these metal-binding proteins suggests a possible neuroprotective effect on ALDH1L1+ astrocytes in response to the heightened inflammation present in *HLA-DRB1*15*+ samples. Future work characterising the co-expression of metal-binding proteins with ALDH1L1+ astrocytes may shed light on how *HLA-DRB1*15*+ genotype impacts ALDH1L1+ astrocyte function and, therefore, MS pathological outcome.

In summary, this chapter adds to our understanding of astrocyte diversity in MS. We show that astrocyte subpopulations express distinct proteome profiles and undergo subpopulation-specific changes in the MS motor cortex. Protein group differentiation was greatest between GFAP+ and ALDH1L1+ astrocytes, providing further evidence that these two astrocyte markers represent distinct astrocyte subpopulations. In addition, our data show MS-specific differences across all astrocyte subtypes, which may be a key contributor to MS heterogeneity. The co-expression of immune-related proteins with GFAP+ astrocytes may reflect a cytotoxic phenotype, whilst the association of synaptic

vesicle clustering and voltage-gated potassium channels with ALDH1L1+ astrocytes may signify a protective one. This work also highlights that MS carriage of *HLA-DRB1*15* impacts the co-expression of inflammatory-related proteins on GFAP+ and ALDH1L1+ astrocytes, providing insights into the astroglial mechanisms underpinning MS severity. Overall, the astrocyte proteomic data reported here are an important resource for future studies exploring the role of astrocytes in MS. Future studies investigating the functional role these astrocyte subpopulation proteins have on MS pathological outcomes may allow the identification of targets amenable to therapeutic modulation to halt the devastating consequences of the disease.

5 Overview and Future Perspectives

5.1 Thesis Summary

This thesis aims to assess astrocyte diversity and their relation to MS inflammatory neurodegeneration using quantitative neuropathology to instruct a targeted proteomic approach. We show that the human motor cortex has distinct subpopulations of astrocytes relevant to MS pathogenesis. In particular, we find that GFAP+ and ALDH1L1+ astrocyte subpopulations show diverging relationships with MS pathological outcomes, including demyelination, neuronal density, inflammation, and vascular breakdown. Proteome profiling of these astrocyte subpopulations identifies MS-specific protein group differences, which, coupled with our pathological observations, highlights the need to explore the functional mechanisms of astrocyte subpopulations in MS. We also report that astrocyte subpopulations are influenced by the primary genetic MS-risk factor *HLA-DRB1*15*, providing key insights into how genetic factors contribute to MS astrocyte diversity. Altogether, these findings advance our understanding of the nature of astrocyte diversity and their contribution to MS pathology, potentially influencing the design of future treatments and therapies modulating astrocytes in MS.

A summary of the principal findings of this thesis are provided below.

5.1.1 GFAP+ and ALDH1L1+ astrocytes represent distinct astroglial subpopulations, which differentially relate to MS pathological outcome

A principal finding of this thesis is that GFAP+ and ALDH1L1+ represent distinct astrocyte subpopulations in terms of distribution, relationship to MS pathology, and nature of protein expression. The conflation of findings suggests that GFAP+ astrocytes contribute to pathological harm, whilst ALDH1L1+ astrocytes contribute to neurotrophic support.

5.1.1.1 GFAP+ astrocytes act as perpetrators of MS pathology

Our characterisation of astrocytes in the motor cortex reveals a relationship between GFAP+ astrocytes and vasculature, irrespective of disease status. We find that GFAP+ astrocyte expression is greatest in vascularly-dense regions, including the subpial NAGM and subcortical NAWM (Chapter 2). GFAP+ expression is particularly exaggerated around NAGM vasculature, which in comparison to ALDH1L1+, is the predominant perivascular astrocyte subpopulation (Chapter 3). Vascular-related GFAP+ astrocyte relationships are also shown to be linked to immune response. Compared to ALDH1L1+ astrocytes, GFAP+ astrocytes are enriched for protein groups related to haemostasis and inflammatory processes (Chapter 4). Taken together, our findings implicate GFAP+ astrocyte as an important mediator of vessel permeability and inflammation. We suggest that GFAP+ astrocytes possess functional properties related to structural support, which is in line with its role as a cytoskeleton protein, and may explain why GFAP+ astrocytes correspond with cells, such as the endothelium, where barrier properties are important[150].

This thesis also provides evidence that GFAP+ astrocytes display phenotypic changes in MS related to pathological outcomes. Greater GFAP+ astrocyte reactivity is seen in MS than in controls and was especially increased in regions of demyelination (Chapter 2). We also find that perivascular GFAP+ astrocyte expression is reduced in MS compared to control cases (Chapter 3) and that MS GFAP+ astrocytes are enriched for protein groups related to immune function (Chapter 4). These findings highlight a possible link between GFAP+ astrocytes, inflammatory demyelination, and neurodegeneration in MS. Our results are consistent with the notion that GFAP+ astrocytes can contribute to pathological harm in disease states[55,150,232] and support that GFAP+ astrocyte dysfunction can be detrimental to MS pathology.

5.1.1.2 ALDH1L1+ astrocytes act as protectors of MS pathology

Although little is known about ALDH1L1+ astroglial function, our data implicate ALDH1L1+ astrocytes in an important relationship with cortical neurons. ALDH1L1+ astrocyte expression is most prominent in NAGM layers II-IV, corresponding to cortical regions of high neuronal density (Chapter 2). We also show that ALDH1L1+ astrocytes are positively associated with neuronal density in MS (Chapter 2), which suggests an interpretation that ALDH1L1+ astrocytes can have an important neurotrophic and protective role in MS. Indeed, differential protein analysis reveals an association of MS ALDH1L1+ astrocytes with protein groups related to synaptic vesicle clustering and voltage-gated potassium channels, both relevant to glia-neuron support (Chapter 4). Moreover, perivascular ALDH1L1+ astrocyte expression is greater in MS than in controls and is associated with extravascular fibrinogen deposition in the cortex (Chapter

3). This finding supports the notion that astrocytes can protect vessels from further breakdown in pathological conditions[94] and highlights a possible protective response of ALDH1L1+ astrocytes to areas of perivascular GFAP+ astrocyte loss.

5.1.1.3 Astrocyte subpopulation composition is important for astrocyte diversity in MS

A common mistake of pathological studies is considering astrocytes as a homogenous population, which can lead to misinterpretations[150]. In this thesis, we find no evidence of increased astrocyte density (Chapter 2), suggesting that changes to the composition of astrocyte subpopulations rather than astroglial proliferation occur in MS. Indeed, astrocyte subpopulations show inverse perivascular changes in MS, with the expression of GFAP+ astrocytes being decreased and ALDH1L1+ astrocyte being increased (Chapter 3). These subpopulations are also enriched for distinct protein groups related to spliceosome and mRNA processing, key pathways responsible for phenotypic diversity (Chapter 4). Therefore, our data indicate that changes to the phenotypic states of distinct astrocyte subpopulations may underlie the astroglial changes seen in MS, a finding consistent with others[152]. Critical next steps will be to understand how these phenotypic changes occur in astrocyte subpopulations and their specific contributions to MS pathogenesis.

5.1.2 *HLA-DRB1*15* influences GFAP+ and ALDH1L1+ astrocyte subpopulations in MS

Genetic susceptibility is a crucial contributor to MS heterogeneity, influencing clinical and pathological outcomes[26,28,52,99]. However, elucidating the impact of

*HLA-DRB1*15* status on CNS cell types has remained limited, with a poor understanding of its influence on astrocytes. Therefore, we sought to determine the impact of *HLA-DRB1*15* status on astrocyte subpopulations.

We find that genetic variation at the *HLA-DRB1*15* locus influences astrocyte subpopulations and their relationships in the MS motor cortex. GFAP+ astrocytes show increased reactivity in younger MS *HLA-DRB1*15*+ cases (Chapter 2), supporting the notion that younger age and MS carriage of *HLA-DRB1*15* leads to more severe MS pathologic outcomes[28]. Our data also identify enrichment of protein groups related to antigen presentation for GFAP+ astrocytes in *HLA-DRB1*15*+ cases (Chapter 4). The *HLA-DRB1*15* allele may impact antigen presentation of GFAP+ astrocytes, resulting in aberrant immune cell recruitment and subsequent inflammatory degeneration. Our findings highlight an impact of *HLA-DRB1*15* haplotype on GFAP+ astrocyte response with implications of enhanced phenotypic presentation of reactivity and cytotoxicity in GFAP+ astrocytes in *HLA-DRB1*15*+ cases.

*HLA-DRB1*15* genetic status also influences ALDH1L1+ astrocytes. We report that ALDH1L1+ astrocytes are positively associated with neuronal density, and macrophage/microglial inflammation, except in MS cases carrying the *HLA-DRB1*15* allele (Chapter 2). Our finding highlights that carriage of *HLA-DRB1*15* may impact appropriate ALDH1L1+ astrocytes response in MS. Specifically, ALDH1L1+ astrocytes may confer a protective role in MS *HLA-DRB1*15*+ cases to counteract the heightened inflammatory response associated with the *HLA-DRB1*15* allele. ALDH1L1+ astrocyte expression is also increased in the

perivascular area of *HLA-DRB1*15*+ cases (Chapter 3), which combined with its downregulation of immune-associated metal-binding protein groups, adds further support to a potential protective role (Chapter 4). This data therefore, suggest that ALDH1L1+ astrocytes, through neuron-astrocyte-microglia crosstalk, mediate the phenotypic differences between *HLA-DRB1*15*+ and *HLA-DRB1*15*- cases.

Overall, our results link genetic susceptibility to the phenotypic heterogeneity of astrocyte subpopulation response in MS, which provides important insights into the cellular mechanisms underlying the MS *HLA-DRB1*15* allele.

5.2 Study Limitations

The present findings put into perspective the critical role different astrocyte subpopulations have in MS. However, we acknowledge limitations intrinsic to using human post-mortem tissue. Autopsy material is biased towards more severe end-stage of disease, which may limit the generalisability of our findings. Moreover, pathological work can only provide a static view of a dynamic process, making it challenging to draw conclusions about the functional contributions different astrocyte subpopulations have in MS. However, given the unique features of human astrocytes, this thesis provides critical insight into disease-specific processes that animal models cannot capture. Human pathological studies also go beyond the resolution of current neuroimaging technologies, which allow for evaluating human astrocytes at the cellular and molecular levels. Other approaches used to study human systems, such as cell culture, have difficulty representing the spatial complexities of human astrocytes and their

relationships within the context of whole tissues. Therefore, despite these limitations, post-mortem studies are important to advance the field of astroglial biology and MS.

We also recognise that proteomic approaches to archival material have their challenges. However, our dual immunohistochemical and proteomics approach provides insights into the morphology, spatial features, and molecular signatures of distinct human astrocyte subpopulations in MS. Proteome profiling is important to understanding the molecular changes or potential pathogenic roles of particular cell types.

Human post-mortem material has several factors that can contribute to inconsistent proteomics results, including suboptimal tissue quality, genetic heterogeneity, agonal medication exposure or concomitant disease, cause of death, and post-mortem interval. In particular, formaldehyde-induced protein modifications hinder protein recovery, which makes extracting and identifying biomolecules from FFPE tissues, the primary source of archival material, difficult. Samples are often subject to harsh experimental conditions, such as prolonged heating at 95°C, and involve the removal of salt and detergent reagents, which can produce large variability and require more starting material than fresh tissues. We have addressed this limitation by implementing a DIA approach to mass spectrometry processing, which generally has fewer missing values than the more common DDA approach. Moreover, DIA has the advantage of untargeted and systematic sampling, producing a greater depth of analysis, quantitation, and reproducibility. In doing so, we have detected a high number of protein group IDs

comparable to fresh frozen tissue, thus generating robust data suitable for downstream proteomic analyses.

The processing and isolation of cell types from LCM can also be resource-intensive. Efforts to establish automated LCM systems continue to struggle with the complex and highly variable morphology of different cells making it challenging to accurately automate LCM isolation of astrocytes. Yet, LCM technologies can generate highly sensitive and robust data of particular cell types, reducing the competing effects of surrounding cell populations found in whole biological samples. The integration of machine learning techniques could streamline the identification of cell populations.

5.3 Future Work

Our findings in human post-mortem tissue have broadened our understanding of astrocyte diversity in health and MS. Future work is required to characterise the structure and function of astrocyte subpopulations. Initial approaches to decipher the role of GFAP+ and ALDH1L1+ astrocytes in MS pathogenesis are outlined below.

5.3.1 Pathological validation of astroglial subpopulation protein group IDs and their relationship with known pathological outcomes in MS

We identify several protein groups that distinguished GFAP+ and ALDH1L1+ astrocyte subpopulations and reveal that these astrocyte subpopulations show differential protein expression based on MS and controls. The next steps will be to perform orthogonal validation of significantly upregulated protein group IDs for

each astrocyte subpopulation using IHC and western blot methods. We could assess protein group IDs related to haemostasis (e.g. fibrinogen subunits) or inflammation (e.g. complement) to discriminate GFAP+ from ALDH1L1+ astrocytes in MS and controls. These protein group IDs could be co-labelled with each astrocyte subpopulation, which would provide insight into the localisation of these IDs within the astrocyte and identify the spatial distribution of these IDs across the cortex. We will also run similar validation steps for protein group IDs that were impacted by *HLA-DRB1*15*+ status (e.g. antigen presentation).

Our data is one of the first to perform a DIA assessment of LCM-targeted astrocyte subpopulations in human tissues directly linked to robust pathological parameters, making downstream data analysis highly informative and complex. Therefore, it will be pertinent to perform more comprehensive statistical analyses of our proteomics outputs to expand our current findings. Further statistical analysis of quantified astrocyte proteins from NAGM GFAP+, ALDH1L1+, and GFAP+/ALDH1L1+ astrocytes of MS and control cases could be modelled against pathological outcomes of MS pathology, including cortical demyelination, neuronal density, and macrophage/microglial inflammation, whilst taking into account the impact of genotype status. Additionally, full integration of clinical parameters, such as sex, age, and post-mortem interval, which we could not perform in our current findings due to computational constraints, would be informative.

Moreover, a limitation of this thesis is that non-neurological controls were not genotyped for genetic status, and thus, the impact of genotype on astrocyte

subpopulations outside of MS disease requires further investigation. Therefore, obtaining genotype data for non-neurological controls could clarify if the relationships reported in this thesis result from MS genetic status or are based on genetic status alone. We also suggest that adding several non-neurological controls to expand our existing cohort could also broaden the generalisability of our data.

5.3.2 Evaluate the cell-cell interactions of astrocyte subpopulations with neurons and microglia in MS

We show that astrocyte subpopulations associate differently with neurons and microglia in the MS motor cortex, suggesting that GFAP+ astrocytes contribute to cytotoxic processes, whilst ALDH1L1+ astrocytes contribute to protective responses. The assessment of spatial relationships between these astrocyte subpopulations, neurons, and macrophage/microglia subtypes through IF co-labelling or multiplex IHC would be helpful. Image analysis could also characterise changes in morphology to determine how phenotypic changes in astrocyte subpopulations relate to macrophage/microglia inflammation and neuronal loss. There could be particular consideration for the association of GFAP+, ALDH1L1+, or GFAP+/ALDH1L1+ astrocytes with neurons and macrophage/microglia subtypes, to determine if pure GFAP+ or ALDH1L1+ astrocyte subpopulations drive these astrocyte-neuron-microglia relationships.

Our functional enrichment analyses show that astrocyte subpopulations differentially relate to neurons and macrophages/microglia. However, it is not clear if co-expression of these protein groups with astrocyte subpopulations has

a causal or consequential impact on MS pathology. A complimentary assessment of our astroglial data with the investigation of the deep proteome in other cell types, including microglia and neurons, could be of interest. This could enable the comparison of protein group expression between different cell types, which may provide insight into how cell-cell interactions contribute to MS pathogenesis.

In vitro systems could also help elucidate the functional mechanisms underlying astrocyte subpopulation interactions with neurons and microglia. To achieve this, proteins related to inflammatory processes, which are enriched in MS GFAP+ astrocytes, not MS ALDH1L1+ astrocytes, could be individually added to human iPSC-derived astrocyte, neuronal, and microglia co- or tri-culture systems in MS and non-neurological controls. Functional validation in knockout/knock-in *in vivo* experimental models of MS, such as EAE, could also clarify the influence of these astroglial proteins on clinical and pathological outcomes.

5.3.3 Investigating the spatial relationships and functional mechanisms of perivascular astrocyte subpopulations with vessel integrity in MS

This thesis implicates perivascular astrocyte subpopulations in an important but complex relationship with NAGM MS vasculature, corresponding fibrinogen deposition, and its integrity of endothelial ZO-1+ tight junctions. Given this, future work should expand its focus to include other components of the cortical vasculature to provide a more in-depth understanding of how perivascular astrocytes influence and interact with the MS vascular interface. This could be achieved using multiplexing IHC of astrocyte subpopulations with endothelial proteins such as occludin, claudin, and junctional adhesion molecules, as well as

other vessel-related cells such as pericytes, in MS and non-neurological cases. We could assess both non-capillary and capillary vessels to account for the differences in perivascular astrocyte expression between the two vessel types. Moreover, the use of thicker tissue sections (>30μm) with this approach could better understand the spatial relationships and cellular composition of the entire MS astroglial-vascular system.

In vitro systems could also evaluate the perivascular properties of astrocyte subpopulations in MS. A possible avenue of investigation to measure the perivascular properties of astrocytes could be to use microfluidic devices, which allow for the integration of astrocytes with endothelium and other vascular-related components to mimic the CNS vasculature[233]. This could provide valuable insights into the differential barrier properties of human iPSC-derived astrocyte endfeet under MS-like conditions and identify possible targets to limit astroglial contributions to MS vessel permeability. Molecular analysis of the endfeet using approaches such as proteomics could identify common protein groups in GFAP+ and ALDH1L1+ astrocytes from our current proteomic dataset, which we could then assess in a comprehensive IF study. As iPSC and CRISPER-Cas9 technologies advance, future work could directly assess the functional properties of GFAP+ and ALDH1L1+ astrocyte subpopulations in human models.

5.4 Concluding Thoughts

In summary, this thesis undertook a quantitative neuropathological analysis of motor cortical GFAP+ and ALDH1L1+ astrocytes in a large cohort of post-mortem MS cases genotyped at the *HLA-DRB1*15* locus to inform a proteomic approach. This novel strategy has enabled us to find the following:

1. GFAP+ and ALDH1L1+ astrocytes represent distinct astrocyte subpopulations in the human motor cortex and differentially relate to MS pathological outcomes. The presence of these different astrocyte subpopulations, but lack of overall astrocyte proliferation, indicates that change to the composition of astrocyte subpopulations is a key contributor to astrocyte diversity in MS.
2. Proteomic data support the hypothesis that GFAP+ astrocytes may associate with MS pathological harm, whereas ALDH1L1+ astrocytes may relate to functions associated with protection and support in MS.
3. Primary MS genetic susceptibility factor, *HLA-DRB1*15*, influences GFAP+ and ALDH1L1+ astrocyte subpopulations in MS.

Altogether, this thesis highlights that astrocyte subpopulation diversity can contribute to MS heterogeneity. By deciphering the distribution and nature of astrocyte subpopulations in MS, we provide the foundation for further investigation of the astrocyte in MS pathology. In so doing, we may identify astroglial protein biomarkers that could be used for *in vivo* clinical research and eventually constitute target molecules for future treatments and therapies against the inflammatory and/or neurodegenerative responses in MS.

Appendix

Chapter 4

Table S4.1. The DIA segment widths used for mass-spectrometry analysis of LCM-targeted astrocytes. All segment widths were adjusted to the precursor density. Abbreviations: DIA = data-independent acquisition; LCM = laser capture microdissection.

Isolation Window Centre (m/z)	Isolation Width (m/z)
361.5	23
381.5	19
398.5	17
413.5	15
427	14
440	14
452.5	13
464	12
475.5	13
487.5	13
499.5	13
511	12
522.5	13
534.5	13
546.5	13
558	12
569.5	13
581.5	13
594.5	15
607.5	13
619.5	13
633	16
647.5	15
661.5	15
675.5	15
690	16
705.5	17
722.5	19
741	20
760.5	21
781	22

Continued…

Isolation Window Centre (m/z)	Isolation Width (m/z)
803	24
826.5	25
853	30
883	32
918.5	41
960.5	45
1013	62
1085	84
1388	524

Table S4.2. Differentially expressed protein groups between LCM-targeted GFAP+ and ALDH1L1+ astrocytes in MS and control samples. Identified protein groups are listed as their gene name. Circle colour represents log_2 fold change where blue denotes negative log_2 fold change (downregulation) and red denotes positive log_2 fold change (upregulation). Circle size represents adjusted *p*-value.

Identified Protein Groups (genes)	Disease Status	
	MS	Control
A1BG		
A2M		
APCS		
APOA1		
BGN		
BPNT2		
C18orf63		
C1S		
C4A		
C4A/B		
CD22		
CFB		
COL4A2		
COL6A1		

Continued...

Identified Protein Groups (genes)	Disease Status	
	MS	Control
COL6A2		
COL6A3		
DES;VIM		
EHD2		
F10		
F13A1		
FGA		
FGB		
FGF2		
FGG		
FLNA/B		
HMGN2/4		
HPX		
HRG		

1/2

***Table S4.2**. Continued…*

Identified Protein Groups (genes)	Disease Status	
	MS	Control
HSP90AA1/ AB1/AB2P		
IGHG2/3/4		
IGHV3-7		
IGKV2-29/ 2D-26/2D-29		
IGKV3-15/ 3-7/3D-7		
ITIH2		
ITIH4		
ITIH5		
LARP7		
LMNA/B1/B2		
NID1/2		
PECAM1		
PLG		
PRPF4		
RPL39		
SAP18		
SEH1L		

2/2

Continued…

Identified Protein Groups (genes)	Disease Status	
	MS	Control
SERPINA1		
SFN; YWHAG/H/Z		
SIGLEC15		
TAF15		
TAGLN		
TMSB4X		
TTR		
ZBTB20		

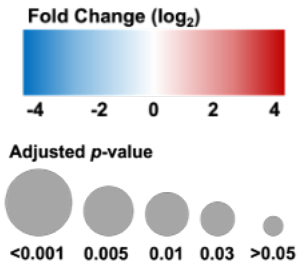
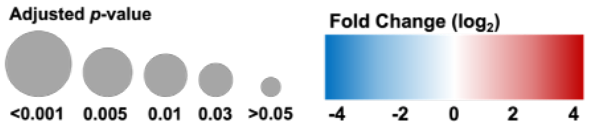


Table S4.3. Differential protein expression of LCM-targeted GFAP+ astrocytes between MS and control samples. Identified protein groups are listed as their gene name. Circle colour represents log_2 fold change where blue denotes negative log_2 fold change (downregulation) and red denotes positive log_2 fold change (upregulation). Circle size represents adjusted *p*-value.

Identified Protein Groups (genes)	MS vs Control
ABLIM3	
ACAN	
ADCY1	
ADCY8	
AKT1/3	
ANP32E	
AP4E1	
ATG5	
ATP6V0C	
AZGP1	
BTBD17	
C19orf12	
CAND2	
CAV1	
CD22	
CDC42EP4	
CEP97	

Continued...

Identified Protein Groups (genes)	MS vs Control
CHD4	
CHTOP	
CLCN6	
CLEC2L	
CNN3	
COPS7B	
COQ5	
CPEB2/4	
CPN1	
CREG1	
CSTA	
CTNNA1	
CYBRD1	
DDHD1	
DGKA	
DNAJB1/4	
DNAJB2/6	



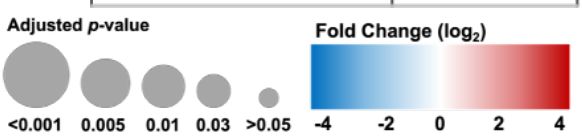
1/4

***Table S4.3**. Continued…*

Identified Protein Groups (genes)	MS vs Control
DOC2A	
DPYS	
DPYSL3/4	
DYNLT3	
DYSF	
EIF4G1/3	
ELANE	
FAM210B	
FDX1	
FGA	
FLAD1	
FN1	
GDPGP1	
GPC1	
GTPBP3	
HCN2	
HLA-DRA	
HMGN2	
HMGN4	

Continued…

Identified Protein Groups (genes)	MS vs Control
IGHG1	
IGHG1/3/4	
IGHG2	
IGHG2/3	
IGHG2/3/4	
IGHG4	
IGHM	
IGKV3-20/3D-20	
IGLV1-47	
IL1RAPL1	
INA/NEFH/L/M	
INA/L/M	
KCNA1/2/3/4/6	
KCTD16/8	
LMAN2L	
LMNA	
LRFN3	
LRRC14	
LRRTM4	



2/4

***Table S4.3**. Continued…*

Identified Protein Groups (genes)	MS vs Control
LSM4	
LYRM1	
MAP1LC3B/B2	
MARCHF5	
MGRN1	
MRPL11	
MRPL27	
MRPS17	
MRPS34	
MTMR7	
NAA25	
NAPRT	
NDUFAF5	
NEU2	
NFIX	
NOS1	
NR2C2	
NRGN	
NTNG1	

Continued…

Identified Protein Groups (genes)	MS vs Control
PABPN1	
PDK1/3	
PPP2R5B/5C/5D/5E	
PPP4R4	
PRKAA2	
PTBP1	
PTCD3	
PTRH2	
PXMP2	
RABL2B	
RAP1GAP/P2	
RBM25	
RGMA	
RNF123	
RTL8A/8C	
SCN3A	
SCN4B	
SERAC1	
SERPINH1	

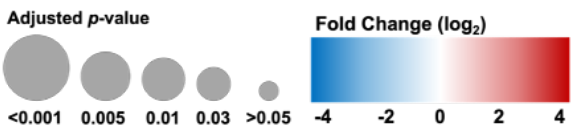
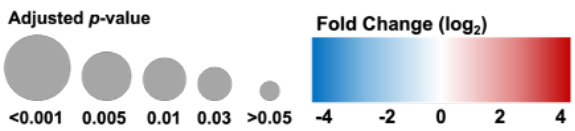


***Table S4.3**. Continued…*

Identified Protein Groups (genes)	MS vs Control
SHOC2	
SIGLEC15	
SIRPB1	
SLC25A52	
SLC4A3	
SLPI	
SMC3	
SON	
SPATA7	
SPHK2	
SRRM1	
SRSF4/5/6	
STAC2	
STAU1/2	
STX18	
STXBP1/2	
TAF15	
TAGLN	
TENM4	

Continued…

Identified Protein Groups (genes)	MS vs Control
THEMIS	
TIMM8A	
TMEM9B	
TTC39C	
TTYH3	
TUBA4A/8	
TUBB/2A/2B/3/ 4A/4B	
TUBB/2A/2B/4B/8	
TUBB2A/2B/6	
TUBGCP3	
U2AF1	
UBE2D1/2/3	
UBE3B	
UBR3	
UFM1	
USP32	
WDR20	
WDR54	



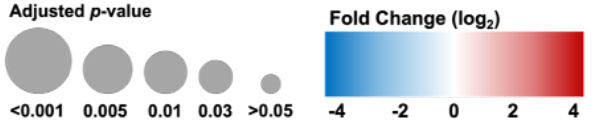
4/4

Table S4.4. Differential protein expression of LCM-targeted ALDH1L1+ astrocytes between MS and control samples. Identified protein groups are listed as their gene name. Circle colour represents log_2 fold change where blue denotes negative log_2 fold change (downregulation) and red denotes positive log_2 fold change (upregulation). Circle size represents adjusted *p*-value.

Identified Protein Groups (genes)	MS vs Control
ACAN	
AHNAK	
ANP32B	
ANP32E	
ANXA2	
ARG1	
ARL6IP1	
ASNS	
AZGP1	
BCLAF1	
BRD3/4	
CASP14	
CDC42EP4	
CDC5L	
CDH18	
CDH6	
CDSN	

Continued...

Identified Protein Groups (genes)	MS vs Control
CLSTN3	
CNN3	
CNTN4	
CPA4	
CST6	
CSTA	
CTNNA1	
CTNNBL1	
CYBRD1	
DAD1	
DDX18	
DDX21	
DDX23	
DGKQ	
DIS3	
DPYSL3/4	
DSC1	



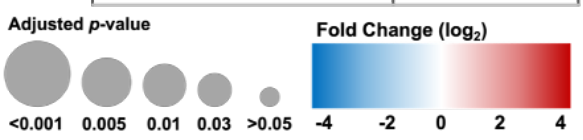
1/4

***Table S4.4**. Continued…*

Identified Protein Groups (genes)	MS vs Control
DSC3	
DSG1	
ECM1	
ETNPPL	
EXOSC10	
FABP5	
FGA	
FLG	
FLG2	
FOXRED1	
FUBP3	
GRIP1	
GSDMA	
GTF2I	
HAL	
HDGF/L2/L3/PSIP1	
HMGA1	
HNRNPA1/3	
HNRNPF/H1	

Continued…

Identified Protein Groups (genes)	MS vs Control
HSD17B11	
HSPB1	
HSPB8	
HTATSF1	
IGHG1/2/3	
IGHV3-7	
IGHV4-30-4/34/ 38-2/39/59/61	
IGKC	
IGKV3/7/D-7	
KCNA1/2/3/4/6	
KDELR1	
KHDRBS1	
KHDRBS1/2/3	
KLK10	
KLK7	
KPNA4	
LUC7L	
LUC7L2	
LUC7L3	



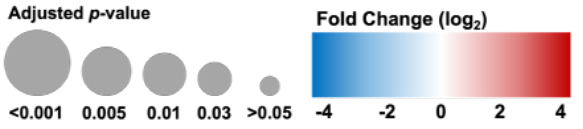
2/4

***Table S4.4**. Continued…*

Identified Protein Groups (genes)	MS vs Control
LYRM1	
MLLT11	
MRPL27	
MRPL50	
MTA2	
NAPRT	
NCBP1	
NCBP2AS2	
NCCRP1	
NCOA5	
NEU2	
NONO/PSPC1	
NUMA1	
OTUD6B	
PALLD	
PARP1	
PDZD11	
PIGT	
PNP	

Continued…

Identified Protein Groups (genes)	MS vs Control
PRPF4B	
PSMB8	
PTBP1	
PVALB	
RASGRF1/2	
RBM14	
RBM25	
RBM42	
RNASE7	
RPRD1A	
RPRD1B	
RTF1	
SBSN	
SERPINA12	
SERPINB2	
SIRPB1	
SLC16A1	
SLC4A1AP	
SLC4A3	



3/4

***Table S4.4**. Continued…*

Identified Protein Groups (genes)	MS vs Control
SMARCA1/5	
SMARCA5	
SMARCD3	
SRRM1	
SRSF3/7	
SRSF4;SRSF6	
SSB	
SUPT6H	
SUPV3L1	
SYN1/2/3	
TFB1M	
TGM1	
TGM3	
THOC2	
TMED5	
U2AF1	
YBX1	
YWHAB/G	
YY1	

4/4

Continued…

Identified Protein Groups (genes)	MS vs Control
ZNF326	
ZNF512	
ZSCAN18	

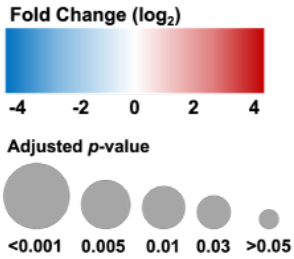
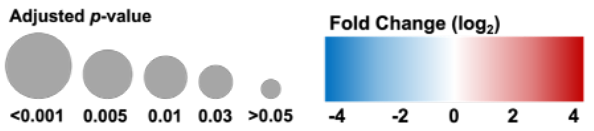


Table S4.5. Differential protein expression of LCM-targeted GFAP+/ ALDH1L1+ astrocytes between MS and control samples. Identified protein groups are listed as their gene name. Circle colour represents log_2 fold change where blue denotes negative log_2 fold change (downregulation) and red denotes positive log_2 fold change (upregulation). Circle size represents adjusted *p*-value.

Identified Protein Groups (genes)	MS vs Control
A2ML1	
ANP32E	
CBX1	
CDC42EP4	
CDC5L	
CENPV	
CHD4;CHD5	
CTNNA1	
CYBRD1	
DDX23	
DDX24	
DDX46	
DIS3	
DNPEP	
DPYSL3/4	
FUBP3	
GTF2I	

Continued…

Identified Protein Groups (genes)	MS vs Control
HNRNPC	
HNRNPH1	
HNRNPM	
HNRNPR	
HNRNPU	
HTATSF1	
IK	
IL1RAPL1	
KCND2	
LMNA	
LMNB1	
LUC7L/2	
LUC7L2	
LUC7L3	
MOBP	
MT1G/X/2A	
MTA1/2	



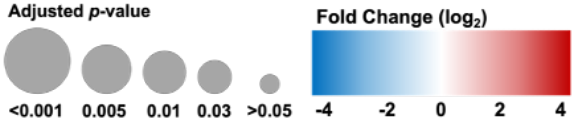
1/3

Table S4.5*. Continued…*

Identified Protein Groups (genes)	MS vs Control
NAPRT	
NRGN	
NSF/SMARCE1	
NUDT14	
NUMA1	
NUP133	
NUP98	
PARP1	
PHLDB1	
PNN	
POLR2A	
PPM1G	
PPTC7	
PRPF31	
PTBP1	
RALY	
RBM14	
RBM39	
RNF40	

Continued…

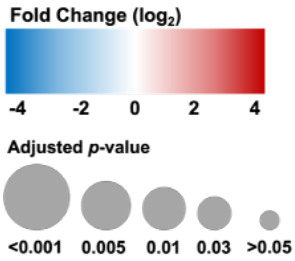
Identified Protein Groups (genes)	MS vs Control
RPRD1A	
RPRD1B	
RTF1	
SART3	
SERAC1	
SMARCA5	
SMARCC2	
SMARCD3	
SMARCE1	
SON	
SRRT	
SRSF3	
STAC2	
SUN2	
SUPT6H	
THOC2	
TRIM28	
U2AF1	
U2SURP	



2/3

***Table S4.5**. Continued…*

Identified Protein Groups (genes)	MS vs Control
UBTF	
XRCC5	
XRCC6	
ZFR	



3/3

References

1. Feigin, V.L.*, et al.* Global, regional, and national burden of neurological disorders during 1990–2015: a systematic analysis for the Global Burden of Disease Study 2015. *The Lancet Neurology* **16**, 877-897 (2017).
2. Wallin, M.T.*, et al.* Global, regional, and national burden of multiple sclerosis 1990–2016: a systematic analysis for the Global Burden of Disease Study 2016. *The Lancet Neurology* **18**, 269-285 (2019).
3. Belbasis, L., Bellou, V., Evangelou, E., Ioannidis, J.P.A. & Tzoulaki, I. Environmental risk factors and multiple sclerosis: an umbrella review of systematic reviews and meta-analyses. *The Lancet Neurology* **14**, 263-273 (2015).
4. Waubant, E.*, et al.* Environmental and genetic risk factors for MS: an integrated review. *Ann Clin Transl Neurol* **6**, 1905-1922 (2019).
5. Walton, C.*, et al.* Rising prevalence of multiple sclerosis worldwide: Insights from the Atlas of MS, third edition. *Mult Scler* **26**, 1816-1821 (2020).
6. Thompson, A.J.*, et al.* Diagnosis of multiple sclerosis: 2017 revisions of the McDonald criteria. *The Lancet Neurology* **17**, 162-173 (2018).
7. Gil-Gonzalez, I., Martin-Rodriguez, A., Conrad, R. & Perez-San-Gregorio, M.A. Quality of life in adults with multiple sclerosis: a systematic review. *BMJ Open* **10**, e041249 (2020).
8. Lublin, F.D. & Reingold, S.C. Defining the clinical course of multiple sclerosis: results of an international survey. National Multiple Sclerosis Society (USA) Advisory Committee on Clinical Trials of New Agents in Multiple Sclerosis. *Neurology* **46**, 907-911 (1996).
9. Patzold, U. & Pocklington, P.R. Course of multiple sclerosis. First results of a prospective study carried out of 102 MS patients from 1976-1980. *Acta Neurol Scand* **65**, 248-266 (1982).
10. Kremenchutzky, M., Rice, G.P., Baskerville, J., Wingerchuk, D.M. & Ebers, G.C. The natural history of multiple sclerosis: a geographically based study 9: observations on the progressive phase of the disease. *Brain* **129**, 584-594 (2006).
11. Scalfari, A.*, et al.* The natural history of multiple sclerosis: a geographically based study 10: relapses and long-term disability. *Brain* **133**, 1914-1929 (2010).
12. Ziemssen, T.*, et al.* A mixed methods approach towards understanding key disease characteristics associated with the progression from RRMS to SPMS: Physicians' and patients' views. *Mult Scler Relat Disord* **38**, 101861 (2020).
13. Polman, C.H.*, et al.* Diagnostic criteria for multiple sclerosis: 2010 revisions to the McDonald criteria. *Ann Neurol* **69**, 292-302 (2011).
14. Scalfari, A.*, et al.* The relationship of age with the clinical phenotype in multiple sclerosis. *Mult Scler* **22**, 1750-1758 (2016).
15. Ebers, G.C. Natural history of primary progressive multiple sclerosis. *Mult Scler* **10 Suppl 1**, S8-13; discussion S13-15 (2004).
16. Lublin, F.D.*, et al.* Defining the clinical course of multiple sclerosis: the 2013 revisions. *Neurology* **83**, 278-286 (2014).

17. Bjornevik, K.*, et al.* Longitudinal analysis reveals high prevalence of Epstein-Barr virus associated with multiple sclerosis. *Science* **375**, 296-301 (2022).
18. Olsson, T., Barcellos, L.F. & Alfredsson, L. Interactions between genetic, lifestyle and environmental risk factors for multiple sclerosis. *Nat Rev Neurol* **13**, 25-36 (2017).
19. Vukusic, S., Van Bockstael, V., Gosselin, S. & Confavreux, C. Regional variations in the prevalence of multiple sclerosis in French farmers. *J Neurol Neurosurg Psychiatry* **78**, 707-709 (2007).
20. Willer, C.J.*, et al.* Timing of birth and risk of multiple sclerosis: population based study. *BMJ* **330**, 120 (2005).
21. Harirchian, M.H., Fatehi, F., Sarraf, P., Honarvar, N.M. & Bitarafan, S. Worldwide prevalence of familial multiple sclerosis: A systematic review and meta-analysis. *Mult Scler Relat Disord* **20**, 43-47 (2018).
22. Compston, A. & Coles, A. Multiple sclerosis. *The Lancet* **359**, 1221-1231 (2002).
23. International Multiple Sclerosis Genetics, C. Multiple sclerosis genomic map implicates peripheral immune cells and microglia in susceptibility. *Science* **365**, eaav7188-eaav7188 (2019).
24. Masterman, T.*, et al.* HLA-DR15 is associated with lower age at onset in multiple sclerosis. *Ann Neurol* **48**, 211-219 (2000).
25. Watanabe, M.*, et al.* HLA genotype-clinical phenotype correlations in multiple sclerosis and neuromyelitis optica spectrum disorders based on Japan MS/NMOSD Biobank data. *Sci Rep* **11**, 607 (2021).
26. Okuda, D.T.*, et al.* Genotype-Phenotype correlations in multiple sclerosis: HLA genes influence disease severity inferred by 1HMR spectroscopy and MRI measures. *Brain* **132**, 250-259 (2009).
27. DeLuca, G.C.*, et al.* Casting light on multiple sclerosis heterogeneity: the role of HLA-DRB1 on spinal cord pathology. *Brain* **136**, 1025-1034 (2013).
28. Yates, R.L., Esiri, M.M., Palace, J., Mittal, A. & DeLuca, G.C. The influence of HLA-DRB1*15 on motor cortical pathology in multiple sclerosis. *Neuropathol Appl Neurobiol* **41**, 371-384 (2015).
29. Stys, P.K., Zamponi, G.W., van Minnen, J. & Geurts, J.J. Will the real multiple sclerosis please stand up? *Nat Rev Neurosci* **13**, 507-514 (2012).
30. Lassmann, H. Mechanisms of white matter damage in multiple sclerosis. *Glia* **62**, 1816-1830 (2014).
31. Attfield, K.E., Jensen, L.T., Kaufmann, M., Friese, M.A. & Fugger, L. The immunology of multiple sclerosis. *Nat Rev Immunol* (2022).
32. van der Valk, P. & Amor, S. Preactive lesions in multiple sclerosis. *Curr Opin Neurol* **22**, 207-213 (2009).
33. van Wageningen, T.A.*, et al.* Distinct gene expression in demyelinated white and grey matter areas of patients with multiple sclerosis. *Brain Commun* **4**, fcac005 (2022).
34. Zhang, Z.*, et al.* Parenchymal accumulation of CD163+ macrophages/microglia in multiple sclerosis brains. *J Neuroimmunol* **237**, 73-79 (2011).
35. Lassmann, H. Pathogenic Mechanisms Associated With Different Clinical Courses of Multiple Sclerosis. *Front Immunol* **9**, 3116 (2018).

36. Prins, M.*, et al.* Pathological differences between white and grey matter multiple sclerosis lesions. *Ann N Y Acad Sci* **1351**, 99-113 (2015).
37. Frischer, J.M.*, et al.* The relation between inflammation and neurodegeneration in multiple sclerosis brains. *Brain* **132**, 1175-1189 (2009).
38. Kuhlmann, T.*, et al.* An updated histological classification system for multiple sclerosis lesions. *Acta Neuropathol* **133**, 13-24 (2017).
39. Holley, J.E., Gveric, D., Newcombe, J., Cuzner, M.L. & Gutowski, N.J. Astrocyte characterization in the multiple sclerosis glial scar. *Neuropathol Appl Neurobiol* **29**, 434-444 (2003).
40. Williams, A., Piaton, G. & Lubetzki, C. Astrocytes--friends or foes in multiple sclerosis? *Glia* **55**, 1300-1312 (2007).
41. Bø, L. The histopathology of grey matter demyelination in multiple sclerosis. *Acta Neurol Scand Suppl*, 51-57 (2009).
42. Bö, L., Vedeler, C.A., Nyland, H.I., Trapp, B.D. & Mork, S.J. Subpial demyelination in the cerebral cortex of multiple sclerosis patients. *J Neuropathol Exp Neurol* **62**, 723-732 (2003).
43. Vercellino, M.*, et al.* Grey matter pathology in multiple sclerosis. *J Neuropathol Exp Neurol* **64**, 1101-1107 (2005).
44. Gilmore, C.P.*, et al.* Spinal cord gray matter demyelination in multiple sclerosis-a novel pattern of residual plaque morphology. *Brain Pathol* **16**, 202-208 (2006).
45. Bevan, R.J.*, et al.* Meningeal inflammation and cortical demyelination in acute multiple sclerosis. *Ann Neurol* **84**, 829-842 (2018).
46. Tallantyre, E.C.*, et al.* Clinico-pathological evidence that axonal loss underlies disability in progressive multiple sclerosis. *Mult Scler* **16**, 406-411 (2010).
47. DeLuca, G.C., Williams, K., Evangelou, N., Ebers, G.C. & Esiri, M.M. The contribution of demyelination to axonal loss in multiple sclerosis. *Brain* **129**, 1507-1516 (2006).
48. Klaver, R.*, et al.* Neuronal and Axonal Loss in Normal-Appearing Gray Matter and Subpial Lesions in Multiple Sclerosis. (2015).
49. van der Poel, M.*, et al.* Transcriptional profiling of human microglia reveals grey-white matter heterogeneity and multiple sclerosis-associated changes. *Nat Commun* **10**, 1139 (2019).
50. DeLuca, G.C., Ebers, G.C. & Esiri, M.M. Axonal loss in multiple sclerosis: a pathological survey of the corticospinal and sensory tracts. *Brain* **127**, 1009-1018 (2004).
51. Trapp, B.D.*, et al.* Cortical neuronal densities and cerebral white matter demyelination in multiple sclerosis: a retrospective study. *The Lancet Neurology* **17**, 870-884 (2018).
52. Yates, R.L.*, et al.* The influence of HLA-DRB1*15 on the relationship between microglia and neurons in multiple sclerosis normal appearing cortical grey matter. *Brain Pathol*, e13041 (2021).
53. Carassiti, D.*, et al.* Neuronal loss, demyelination and volume change in the multiple sclerosis neocortex. *Neuropathology and Applied Neurobiology* **44**, 377-390 (2018).
54. Schirmer, L.*, et al.* Neuronal vulnerability and multilineage diversity in multiple sclerosis. *Nature* **573**, 75-82 (2019).

55. Healy, L.M., Stratton, J.A., Kuhlmann, T. & Antel, J. The role of glial cells in multiple sclerosis disease progression. *Nat Rev Neurol* **18**, 237-248 (2022).
56. Liddelow, S.A.*, et al.* Neurotoxic reactive astrocytes are induced by activated microglia. *Nature* **541**, 481-487 (2017).
57. Bsibsi, M.*, et al.* Toll-like receptor 3 on adult human astrocytes triggers production of neuroprotective mediators. *Glia* **53**, 688-695 (2006).
58. Moore, C.S.*, et al.* Astrocytic tissue inhibitor of metalloproteinase-1 (TIMP-1) promotes oligodendrocyte differentiation and enhances CNS myelination. *J Neurosci* **31**, 6247-6254 (2011).
59. Rao, V.T.*, et al.* MicroRNA Expression Patterns in Human Astrocytes in Relation to Anatomical Location and Age. *J Neuropathol Exp Neurol* **75**, 156-166 (2016).
60. Rao, V.T.S.*, et al.* Astrocytes in the Pathogenesis of Multiple Sclerosis: An In Situ MicroRNA Study. *J Neuropathol Exp Neurol* **78**, 1130-1146 (2019).
61. Argaw, A.T.*, et al.* Astrocyte-derived VEGF-A drives blood-brain barrier disruption in CNS inflammatory disease. *J Clin Invest* **122**, 2454-2468 (2012).
62. Waller, R.*, et al.* Gene expression profiling of the astrocyte transcriptome in multiple sclerosis normal appearing white matter reveals a neuroprotective role. *J Neuroimmunol* **299**, 139-146 (2016).
63. Absinta, M.*, et al.* A lymphocyte-microglia-astrocyte axis in chronic active multiple sclerosis. *Nature* (2021).
64. Somjen, G.G. Nervenkitt: notes on the history of the concept of neuroglia. *Glia* **1**, 2-9 (1988).
65. Andriezen, W.L. The Neuroglia Elements in the Human Brain. *Br Med J* **2**, 227-230 (1893).
66. Gorshkov, K., Aguisanda, F., Thorne, N. & Zheng, W. Astrocytes as targets for drug discovery. *Drug Discov Today* **23**, 673-680 (2018).
67. Oberheim, N.A., Goldman, S.A. & Nedergaard, M. Heterogeneity of astrocytic form and function. *Methods Mol Biol* **814**, 23-45 (2012).
68. Oberheim, N.A.*, et al.* Uniquely hominid features of adult human astrocytes. *J Neurosci* **29**, 3276-3287 (2009).
69. Falcone, C.*, et al.* Redefining varicose projection astrocytes in primates. *Glia* (2021).
70. Falcone, C.*, et al.* Cortical Interlaminar Astrocytes Are Generated Prenatally, Mature Postnatally, and Express Unique Markers in Human and Nonhuman Primates. *Cereb Cortex* **31**, 379-395 (2021).
71. Oberheim, N.A., Wang, X., Goldman, S. & Nedergaard, M. Astrocytic complexity distinguishes the human brain. *Trends Neurosci* **29**, 547-553 (2006).
72. Colombo, J.A. & Reisin, H.D. Interlaminar astroglia of the cerebral cortex: a marker of the primate brain. *Brain Res* **1006**, 126-131 (2004).
73. Escartin, C., Guillemaud, O. & Carrillo-de Sauvage, M.A. Questions and (some) answers on reactive astrocytes. *Glia* **67**, 2221-2247 (2019).
74. Garman, R.H. Histology of the central nervous system. *Toxicol Pathol* **39**, 22-35 (2011).
75. Popescu, B.F. & Lucchinetti, C.F. Pathology of demyelinating diseases. *Annu Rev Pathol* **7**, 185-217 (2012).

76. Popescu, B.F., Pirko, I. & Lucchinetti, C.F. Pathology of multiple sclerosis: where do we stand? *Continuum (Minneap Minn)* **19**, 901-921 (2013).
77. Ludwin, S.K., Rao, V., Moore, C.S. & Antel, J.P. Astrocytes in multiple sclerosis. *Mult Scler* **22**, 1114-1124 (2016).
78. Black, J.A., Newcombe, J. & Waxman, S.G. Astrocytes within multiple sclerosis lesions upregulate sodium channel Nav1.5. *Brain* **133**, 835-846 (2010).
79. Ponath, G.*, et al.* Myelin phagocytosis by astrocytes after myelin damage promotes lesion pathology. *Brain* **140**, 399-413 (2017).
80. Cohen-Salmon, M.*, et al.* Astrocytes in the regulation of cerebrovascular functions. *Glia* **69**, 817-841 (2021).
81. Heithoff, B.P.*, et al.* Astrocytes are necessary for blood-brain barrier maintenance in the adult mouse brain. *Glia* **69**, 436-472 (2021).
82. Appelt-Menzel, A.*, et al.* Establishment of a Human Blood-Brain Barrier Co-culture Model Mimicking the Neurovascular Unit Using Induced Pluri- and Multipotent Stem Cells. *Stem Cell Reports* **8**, 894-906 (2017).
83. Herland, A.*, et al.* Distinct Contributions of Astrocytes and Pericytes to Neuroinflammation Identified in a 3D Human Blood-Brain Barrier on a Chip. *PLoS One* **11**, e0150360 (2016).
84. Fu, J.*, et al.* Astrocyte-Derived TGFbeta1 Facilitates Blood-Brain Barrier Function via Non-Canonical Hedgehog Signaling in Brain Microvascular Endothelial Cells. *Brain Sci* **11**(2021).
85. Alvarez, J.I.*, et al.* The Hedgehog pathway promotes blood-brain barrier integrity and CNS immune quiescence. *Science* **334**, 1727-1731 (2011).
86. Saadoun, S., Papadopoulos, M.C. & Krishna, S. Water transport becomes uncoupled from K+ siphoning in brain contusion, bacterial meningitis, and brain tumours: immunohistochemical case review. *J Clin Pathol* **56**, 972-975 (2003).
87. Wang, M.X., Ray, L., Tanaka, K.F., Iliff, J.J. & Heys, J. Varying perivascular astroglial endfoot dimensions along the vascular tree maintain perivascular-interstitial flux through the cortical mantle. *Glia* **69**, 715-728 (2021).
88. Takai, Y.*, et al.* Staging of astrocytopathy and complement activation in neuromyelitis optica spectrum disorders. *Brain* (2021).
89. Zeppenfeld, D.M.*, et al.* Association of Perivascular Localization of Aquaporin-4 With Cognition and Alzheimer Disease in Aging Brains. *JAMA Neurol* **74**, 91-99 (2017).
90. Medici, V., Frassoni, C., Tassi, L., Spreafico, R. & Garbelli, R. Aquaporin 4 expression in control and epileptic human cerebral cortex. *Brain Res* **1367**, 330-339 (2011).
91. Prineas, J.W. & Lee, S. Multiple Sclerosis: Destruction and Regeneration of Astrocytes in Acute Lesions. *J Neuropathol Exp Neurol* **78**, 140-156 (2019).
92. Alvarez, J.I., Cayrol, R. & Prat, A. Disruption of central nervous system barriers in multiple sclerosis. *Biochim Biophys Acta* **1812**, 252-264 (2011).
93. Bö, L.*, et al.* Induction of nitric oxide synthase in demyelinating regions of multiple sclerosis brains. *Ann Neurol* **36**, 778-786 (1994).

94. Mizee, M.R.*, et al.* Astrocyte-derived retinoic acid: a novel regulator of blood-brain barrier function in multiple sclerosis. *Acta Neuropathol* **128**, 691-703 (2014).
95. Roemer, S.F.*, et al.* Pattern-specific loss of aquaporin-4 immunoreactivity distinguishes neuromyelitis optica from multiple sclerosis. *Brain* **130**, 1194-1205 (2007).
96. Matsuoka, T., Suzuki, S.O., Suenaga, T., Iwaki, T. & Kira, J. Reappraisal of aquaporin-4 astrocytopathy in Asian neuromyelitis optica and multiple sclerosis patients. *Brain Pathol* **21**, 516-532 (2011).
97. Sinclair, C., Kirk, J., Herron, B., Fitzgerald, U. & McQuaid, S. Absence of aquaporin-4 expression in lesions of neuromyelitis optica but increased expression in multiple sclerosis lesions and normal-appearing white matter. *Acta Neuropathol* **113**, 187-194 (2007).
98. Miyamoto, K., Nagaosa, N., Motoyama, M., Kataoka, K. & Kusunoki, S. Upregulation of water channel aquaporin-4 in experimental autoimmune encephalomyeritis. *J Neurol Sci* **276**, 103-107 (2009).
99. Yates, R.L.*, et al.* Fibrin(ogen) and neurodegeneration in the progressive multiple sclerosis cortex. *Ann Neurol* **82**, 259-270 (2017).
100. Leech, S., Kirk, J., Plumb, J. & McQuaid, S. Persistent endothelial abnormalities and blood-brain barrier leak in primary and secondary progressive multiple sclerosis. *Neuropathol Appl Neurobiol* **33**, 86-98 (2007).
101. Vos, C.M.*, et al.* Blood-brain barrier alterations in both focal and diffuse abnormalities on postmortem MRI in multiple sclerosis. *Neurobiol Dis* **20**, 953-960 (2005).
102. Golanov, E.V.*, et al.* Fibrinogen Chains Intrinsic to the Brain. *Front Neurosci* **13**, 541 (2019).
103. Conforti, P.*, et al.* Fibrinogen regulates lesion border-forming reactive astrocyte properties after vascular damage. *Glia* (2022).
104. Vainchtein, I.D.*, et al.* Astrocyte-derived interleukin-33 promotes microglial synapse engulfment and neural circuit development. *Science* **359**, 1269-1273 (2018).
105. Coggan, J.S.*, et al.* Norepinephrine stimulates glycogenolysis in astrocytes to fuel neurons with lactate. *PLoS Comput Biol* **14**, e1006392 (2018).
106. Sugama, S.*, et al.* Stress-induced microglial activation occurs through beta-adrenergic receptor: noradrenaline as a key neurotransmitter in microglial activation. *J Neuroinflammation* **16**, 266 (2019).
107. Liddelow, S.A., Marsh, S.E. & Stevens, B. Microglia and Astrocytes in Disease: Dynamic Duo or Partners in Crime? *Trends Immunol* **41**, 820-835 (2020).
108. Mayo, L.*, et al.* Regulation of astrocyte activation by glycolipids drives chronic CNS inflammation. *Nat Med* **20**, 1147-1156 (2014).
109. Yiangou, Y.*, et al.* COX-2, CB2 and P2X7-immunoreactivities are increased in activated microglial cells/macrophages of multiple sclerosis and amyotrophic lateral sclerosis spinal cord. *BMC Neurol* **6**, 12 (2006).
110. Narcisse, L., Scemes, E., Zhao, Y., Lee, S.C. & Brosnan, C.F. The cytokine IL-1beta transiently enhances P2X7 receptor expression and function in human astrocytes. *Glia* **49**, 245-258 (2005).

111. Jacobsen, C*., et al.* Brain atrophy and disability progression in multiple sclerosis patients: a 10-year follow-up study. *J Neurol Neurosurg Psychiatry* **85**, 1109-1115 (2014).
112. Dougherty, K.D., Dreyfus, C.F. & Black, I.B. Brain-derived neurotrophic factor in astrocytes, oligodendrocytes, and microglia/macrophages after spinal cord injury. *Neurobiology of disease* **7**, 574-585 (2000).
113. Taylor, A.R*., et al.* Astrocyte and muscle-derived secreted factors differentially regulate motoneuron survival. *J Neurosci* **27**, 634-644 (2007).
114. Pfrieger, F.W. & Barres, B.A. Synaptic efficacy enhanced by glial cells in vitro. *Science* **277**, 1684-1687 (1997).
115. Johnson, M.A., Weick, J.P., Pearce, R.A. & Zhang, S.C. Functional neural development from human embryonic stem cells: Accelerated synaptic activity via astrocyte coculture. *Journal of Neuroscience* **27**, 3069-3077 (2007).
116. Hartley, R.S., Margulis, M., Fishman, P.S., Lee, V.M. & Tang, C.M. Functional synapses are formed between human NTera2 (NT2N, hNT) neurons grown on astrocytes. *J Comp Neurol* **407**, 1-10 (1999).
117. Tang, X*., et al.* Astroglial cells regulate the developmental timeline of human neurons differentiated from induced pluripotent stem cells. *Stem Cell Res* **11**, 743-757 (2013).
118. Anderson, C.M. & Swanson, R.A. Astrocyte glutamate transport: Review of properties, regulation, and physiological functions. Vol. 32 1-14 (2000).
119. Spampinato, S.F., Copani, A., Nicoletti, F., Sortino, M.A. & Caraci, F. Metabotropic glutamate receptors in glial cells: A new potential target for neuroprotection? , Vol. 11 414-414 (Frontiers Media S.A., 2018).
120. Pierre, K. & Pellerin, L. Monocarboxylate transporters in the central nervous system: Distribution, regulation and function. Vol. 94 1-14 (2005).
121. Suzuki, A*., et al.* Astrocyte-neuron lactate transport is required for long-term memory formation. *Cell* **144**, 810-823 (2011).
122. Liu, J.S.H., Zhao, M.-L., Brosnan, C.F. & Lee, S.C. Expression of Inducible Nitric Oxide Synthase and Nitrotyrosine in Multiple Sclerosis Lesions. *The American Journal of Pathology* **158**, 2057-2066 (2001).
123. Baranzini, S.E*., et al.* Genetic variation influences glutamate concentrations in brains of patients with multiple sclerosis. *Brain* **133**, 2603-2611 (2010).
124. Perriot, S*., et al.* Human Induced Pluripotent Stem Cell-Derived Astrocytes Are Differentially Activated by Multiple Sclerosis-Associated Cytokines. *Stem Cell Reports* **11**, 1199-1210 (2018).
125. Ponath, G*., et al.* Enhanced astrocyte responses are driven by a genetic risk allele associated with multiple sclerosis. *Nature Communications* **9**(2018).
126. Waubant, E*., et al.* A randomized controlled phase II trial of riluzole in early multiple sclerosis. *Annals of Clinical and Translational Neurology* **1**, 340-347 (2014).
127. Chataway, J*., et al.* Efficacy of three neuroprotective drugs in secondary progressive multiple sclerosis (MS-SMART): a phase 2b, multiarm,

double-blind, randomised placebo-controlled trial. *The Lancet Neurology* **19**, 214-225 (2020).
128. Chao, C.C.*, et al.* Metabolic Control of Astrocyte Pathogenic Activity via cPLA2-MAVS. *Cell* **179**, 1483-1498.e1422 (2019).
129. Zhang, W.*, et al.* Lactate Is a Natural Suppressor of RLR Signaling by Targeting MAVS. *Cell* **178**, 176-189.e115 (2019).
130. Moulson, A.J., Squair, J.W., Franklin, R.J.M., Tetzlaff, W. & Assinck, P. Diversity of Reactive Astrogliosis in CNS Pathology: Heterogeneity or Plasticity? *Front Cell Neurosci* **15**, 703810 (2021).
131. Guttenplan, K.A. & Liddelow, S.A. Astrocytes and microglia: Models and tools. *J Exp Med* **216**, 71-83 (2019).
132. Garwood, C.J.*, et al.* Review: Astrocytes in Alzheimer's disease and other age-associated dementias: a supporting player with a central role. *Neuropathol Appl Neurobiol* **43**, 281-298 (2017).
133. Eidsvaag, V.A., Enger, R., Hansson, H.A., Eide, P.K. & Nagelhus, E.A. Human and mouse cortical astrocytes differ in aquaporin-4 polarization toward microvessels. *Glia* **65**, 964-973 (2017).
134. Moretto, G., Xu, R.Y. & Kim, S.U. CD44 expression in human astrocytes and oligodendrocytes in culture. *J Neuropathol Exp Neurol* **52**, 419-423 (1993).
135. Vis, J.C.*, et al.* Connexin expression in Huntington's diseased human brain. *Cell Biol Int* **22**, 837-847 (1998).
136. Sofroniew, M.V. & Vinters, H.V. Astrocytes: biology and pathology. *Acta Neuropathol* **119**, 7-35 (2010).
137. Fadul, M.M.*, et al.* NDRG2 Expression Correlates with Neurofibrillary Tangles and Microglial Pathology in the Ageing Brain. *Int J Mol Sci* **21**(2020).
138. Mitchelmore, C.*, et al.* NDRG2: a novel Alzheimer's disease associated protein. *Neurobiol Dis* **16**, 48-58 (2004).
139. Flugge, G., Araya-Callis, C., Garea-Rodriguez, E., Stadelmann-Nessler, C. & Fuchs, E. NDRG2 as a marker protein for brain astrocytes. *Cell Tissue Res* **357**, 31-41 (2014).
140. Steiner, J.*, et al.* Evidence for a wide extra-astrocytic distribution of S100B in human brain. *BMC Neurosci* **8**, 2 (2007).
141. Roberts, R.C., Roche, J.K. & McCullumsmith, R.E. Localization of excitatory amino acid transporters EAAT1 and EAAT2 in human postmortem cortex: a light and electron microscopic study. *Neuroscience* **277**, 522-540 (2014).
142. Lee, T.S.*, et al.* GAT1 and GAT3 expression are differently localized in the human epileptogenic hippocampus. *Acta Neuropathol* **111**, 351-363 (2006).
143. Sun, W.*, et al.* SOX9 Is an Astrocyte-Specific Nuclear Marker in the Adult Brain Outside the Neurogenic Regions. *J Neurosci* **37**, 4493-4507 (2017).
144. O'Leary, L.A.*, et al.* Characterization of Vimentin-Immunoreactive Astrocytes in the Human Brain. *Frontiers in Neuroanatomy* **14**(2020).
145. Eng, L.F., Vanderhaeghen, J.J., Bignami, A. & Gerstl, B. An acidic protein isolated from fibrous astrocytes. *Brain Res* **28**, 351-354 (1971).

146. Bushong, E.A., Martone, M.E., Jones, Y.Z. & Ellisman, M.H. Protoplasmic astrocytes in CA1 stratum radiatum occupy separate anatomical domains. *J Neurosci* **22**, 183-192 (2002).
147. Cahoy, J.D.*, et al.* A transcriptome database for astrocytes, neurons, and oligodendrocytes: a new resource for understanding brain development and function. *J Neurosci* **28**, 264-278 (2008).
148. Hol, E.M.*, et al.* Neuronal expression of GFAP in patients with Alzheimer pathology and identification of novel GFAP splice forms. *Mol Psychiatry* **8**, 786-796 (2003).
149. Zwirner, J.*, et al.* GFAP positivity in neurons following traumatic brain injuries. *Int J Legal Med* **135**, 2323-2333 (2021).
150. Escartin, C.*, et al.* Reactive astrocyte nomenclature, definitions, and future directions. *Nat Neurosci* **24**, 312-325 (2021).
151. Srinivasan, R.*, et al.* New Transgenic Mouse Lines for Selectively Targeting Astrocytes and Studying Calcium Signals in Astrocyte Processes In Situ and In Vivo. *Neuron* **92**, 1181-1195 (2016).
152. Serrano-Pozo, A., Gomez-Isla, T., Growdon, J.H., Frosch, M.P. & Hyman, B.T. A phenotypic change but not proliferation underlies glial responses in Alzheimer disease. *Am J Pathol* **182**, 2332-2344 (2013).
153. Yu, X., Nagai, J. & Khakh, B.S. Improved tools to study astrocytes. *Nat Rev Neurosci* **21**, 121-138 (2020).
154. Jakel, S. & Williams, A. What Have Advances in Transcriptomic Technologies Taught us About Human White Matter Pathologies? *Front Cell Neurosci* **14**, 238 (2020).
155. Jafari, A., Babajani, A. & Rezaei-Tavirani, M. Multiple Sclerosis Biomarker Discoveries by Proteomics and Metabolomics Approaches. *Biomark Insights* **16**, 11772719211013352 (2021).
156. Sen, M.K., Almuslehi, M.S.M., Shortland, P.J., Mahns, D.A. & Coorssen, J.R. Proteomics of Multiple Sclerosis: Inherent Issues in Defining the Pathoetiology and Identifying (Early) Biomarkers. *Int J Mol Sci* **22**(2021).
157. Elkjaer, M.L., Rottger, R., Baumbach, J. & Illes, Z. A Systematic Review of Tissue and Single Cell Transcriptome/Proteome Studies of the Brain in Multiple Sclerosis. *Front Immunol* **13**, 761225 (2022).
158. Herrera, J.A.*, et al.* Laser capture microdissection coupled mass spectrometry (LCM-MS) for spatially resolved analysis of formalin-fixed and stained human lung tissues. *Clin Proteomics* **17**, 24 (2020).
159. Farias, A.S., Pradella, F., Schmitt, A., Santos, L.M. & Martins-de-Souza, D. Ten years of proteomics in multiple sclerosis. *Proteomics* **14**, 467-480 (2014).
160. Han, M.H.*, et al.* Proteomic analysis of active multiple sclerosis lesions reveals therapeutic targets. *Nature* **451**, 1076-1081 (2008).
161. Ly, L.*, et al.* Comprehensive tissue processing strategy for quantitative proteomics of formalin-fixed multiple sclerosis lesions. *J Proteome Res* **10**, 4855-4868 (2011).
162. Rai, N.K.*, et al.* Comparative Proteomic Profiling Identifies Reciprocal Expression of Mitochondrial Proteins Between White and Gray Matter Lesions From Multiple Sclerosis Brains. *Front Neurol* **12**, 779003 (2021).
163. Borggrewe, M.*, et al.* Regionally diverse astrocyte subtypes and their heterogeneous response to EAE. *Glia* **69**, 1140-1154 (2021).

164. Calabrese, M.*, et al.* Cortical lesion load associates with progression of disability in multiple sclerosis. *Brain* **135**, 2952-2961 (2012).
165. Eshaghi, A.*, et al.* Progression of regional grey matter atrophy in multiple sclerosis. *Brain* **141**, 1665-1677 (2018).
166. Benjamini, Y. & Hochberg, Y. Controlling the False Discovery Rate: A Practical and Powerful Approach to Multiple Testing. *Journal of the Royal Statistical Society: Series B (Methodological)* **57**, 289-300 (1995).
167. Templeton, G.F. A Two-Step Approach for Transforming Continuous Variables to Normal: Implications and Recommendations for IS Research. *Communications of the Association for Information Systems* **28**(2011).
168. Linnet, K. Two-stage transformation systems for normalization of reference distributions evaluated. *Clin Chem* **33**, 381-386 (1987).
169. Boyd, J.C. & Lacher, D.A. A multi-stage Gaussian transformation algorithm for clinical laboratory data. *Clin Chem* **28**, 1735-1741 (1982).
170. Spencer, J.I., Bell, J.S. & DeLuca, G.C. Vascular pathology in multiple sclerosis: reframing pathogenesis around the blood-brain barrier. *J Neurol Neurosurg Psychiatry* **89**, 42-52 (2018).
171. Liedtke, W.*, et al.* GFAP is necessary for the integrity of CNS white matter architecture and long-term maintenance of myelination. *Neuron* **17**, 607-615 (1996).
172. Yang, C.K.*, et al.* Aldehyde dehydrogenase 1 (ALDH1) isoform expression and potential clinical implications in hepatocellular carcinoma. *PLoS One* **12**, e0182208 (2017).
173. O'Leary, L.A. & Mechawar, N. Implication of cerebral astrocytes in major depression: A review of fine neuroanatomical evidence in humans. *Glia* (2021).
174. Enz, L.S.*, et al.* Increased HLA-DR expression and cortical demyelination in MS links with HLA-DR15. *Neurol Neuroimmunol Neuroinflamm* **7**(2020).
175. Weber, F.*, et al.* Human astrocytes are only partially competent antigen presenting cells. Possible implications for lesion development in multiple sclerosis. *Brain* **117 (Pt 1)**, 59-69 (1994).
176. Ransohoff, R.M. & Estes, M.L. Astrocyte expression of major histocompatibility complex gene products in multiple sclerosis brain tissue obtained by stereotactic biopsy. *Arch Neurol* **48**, 1244-1246 (1991).
177. Morcos, Y., Lee, S.M. & Levin, M.C. A role for hypertrophic astrocytes and astrocyte precursors in a case of rapidly progressive multiple sclerosis. *Mult Scler* **9**, 332-341 (2003).
178. van Wageningen, T.A.*, et al.* Regulation of microglial TMEM119 and P2RY12 immunoreactivity in multiple sclerosis white and grey matter lesions is dependent on their inflammatory environment. *Acta Neuropathol Commun* **7**, 206 (2019).
179. Brambilla, R. The contribution of astrocytes to the neuroinflammatory response in multiple sclerosis and experimental autoimmune encephalomyelitis. *Acta Neuropathol* **137**, 757-783 (2019).
180. Bankhead, P.*, et al.* QuPath: Open source software for digital pathology image analysis. *Sci Rep* **7**, 16878 (2017).

181. Duvernoy, H.M., Delon, S. & Vannson, J.L. Cortical blood vessels of the human brain. *Brain Res Bull* **7**, 519-579 (1981).
182. Reina-De La Torre, F., Rodriguez-Baeza, A. & Sahuquillo-Barris, J. Morphological characteristics and distribution pattern of the arterial vessels in human cerebral cortex: a scanning electron microscope study. *Anat Rec* **251**, 87-96 (1998).
183. Abbott, N.J., Ronnback, L. & Hansson, E. Astrocyte-endothelial interactions at the blood-brain barrier. *Nat Rev Neurosci* **7**, 41-53 (2006).
184. Pivoriunas, A. & Verkhratsky, A. Astrocyte-Endotheliocyte Axis in the Regulation of the Blood-Brain Barrier. *Neurochem Res* **46**, 2538-2550 (2021).
185. Boulay, A.C.*, et al.* Translation in astrocyte distal processes sets molecular heterogeneity at the gliovascular interface. *Cell Discov* **3**, 17005 (2017).
186. Nicchia, G.P.*, et al.* The role of aquaporin-4 in the blood-brain barrier development and integrity: studies in animal and cell culture models. *Neuroscience* **129**, 935-945 (2004).
187. Wolburg-Buchholz, K.*, et al.* Loss of astrocyte polarity marks blood-brain barrier impairment during experimental autoimmune encephalomyelitis. *Acta Neuropathol* **118**, 219-233 (2009).
188. Oklinski, M.K.*, et al.* Immunolocalization of Water Channel Proteins AQP1 and AQP4 in Rat Spinal Cord. *J Histochem Cytochem* **62**, 598-611 (2014).
189. Willis, C.L.*, et al.* Focal astrocyte loss is followed by microvascular damage, with subsequent repair of the blood-brain barrier in the apparent absence of direct astrocytic contact. *Glia* **45**, 325-337 (2004).
190. Holley, J.E., Newcombe, J., Whatmore, J.L. & Gutowski, N.J. Increased blood vessel density and endothelial cell proliferation in multiple sclerosis cerebral white matter. *Neurosci Lett* **470**, 65-70 (2010).
191. Macmillan, C.J., Starkey, R.J. & Easton, A.S. Angiogenesis is regulated by angiopoietins during experimental autoimmune encephalomyelitis and is indirectly related to vascular permeability. *J Neuropathol Exp Neurol* **70**, 1107-1123 (2011).
192. Girolamo, F., Coppola, C., Ribatti, D. & Trojano, M. Angiogenesis in multiple sclerosis and experimental autoimmune encephalomyelitis. *Acta Neuropathol Commun* **2**, 84 (2014).
193. Magliozzi, R.*, et al.* A Gradient of neuronal loss and meningeal inflammation in multiple sclerosis. *Ann Neurol* **68**, 477-493 (2010).
194. van Horssen, J., Brink, B.P., de Vries, H.E., van der Valk, P. & Bo, L. The blood-brain barrier in cortical multiple sclerosis lesions. *J Neuropathol Exp Neurol* **66**, 321-328 (2007).
195. Fallon, R.F. & Goodenough, D.A. Five-hour half-life of mouse liver gap-junction protein. *J Cell Biol* **90**, 521-526 (1981).
196. Chen, Y., Lu, Q., Schneeberger, E.E. & Goodenough, D.A. Restoration of tight junction structure and barrier function by down-regulation of the mitogen-activated protein kinase pathway in ras-transformed Madin-Darby canine kidney cells. *Mol Biol Cell* **11**, 849-862 (2000).
197. Willis, C.L. Glia-induced reversible disruption of blood-brain barrier integrity and neuropathological response of the neurovascular unit. *Toxicol Pathol* **39**, 172-185 (2011).

198. Tietz, S. & Engelhardt, B. Brain barriers: Crosstalk between complex tight junctions and adherens junctions. *J Cell Biol* **209**, 493-506 (2015).
199. Davis, S., Scott, C., Ansorge, O. & Fischer, R. Development of a Sensitive, Scalable Method for Spatial, Cell-Type-Resolved Proteomics of the Human Brain. *J Proteome Res* **18**, 1787-1795 (2019).
200. Falkeholm, L., Grant, C.A., Magnusson, A. & Moller, E. Xylene-free method for histological preparation: a multicentre evaluation. *Lab Invest* **81**, 1213-1221 (2001).
201. Pandey, P., Dixit, A., Tanwar, A., Sharma, A. & Mittal, S. A comparative study to evaluate liquid dish washing soap as an alternative to xylene and alcohol in deparaffinization and hematoxylin and eosin staining. *J Lab Physicians* **6**, 84-90 (2014).
202. Prema, V.*, et al.* Biofriendly Substitutes for Xylene in Deparaffinization. *J Pharm Bioallied Sci* **12**, S623-S630 (2020).
203. Sielaff, M.*, et al.* Evaluation of FASP, SP3, and iST Protocols for Proteomic Sample Preparation in the Low Microgram Range. *J Proteome Res* **16**, 4060-4072 (2017).
204. Habibi, H.*, et al.* Expression and function of FGF9 in the hypertrophied ligamentum flavum of lumbar spinal stenosis patients. *Spine J* **21**, 1010-1020 (2021).
205. Hughes, C.S.*, et al.* Ultrasensitive proteome analysis using paramagnetic bead technology. *Mol Syst Biol* **10**, 757 (2014).
206. Kong, A.T., Leprevost, F.V., Avtonomov, D.M., Mellacheruvu, D. & Nesvizhskii, A.I. MSFragger: ultrafast and comprehensive peptide identification in mass spectrometry-based proteomics. *Nat Methods* **14**, 513-520 (2017).
207. da Veiga Leprevost, F.*, et al.* Philosopher: a versatile toolkit for shotgun proteomics data analysis. *Nat Methods* **17**, 869-870 (2020).
208. Yu, F., Haynes, S.E. & Nesvizhskii, A.I. IonQuant Enables Accurate and Sensitive Label-Free Quantification With FDR-Controlled Match-Between-Runs. *Mol Cell Proteomics* **20**, 100077 (2021).
209. Muntel, J.*, et al.* Comparison of Protein Quantification in a Complex Background by DIA and TMT Workflows with Fixed Instrument Time. *J Proteome Res* **18**, 1340-1351 (2019).
210. Demichev, V., Messner, C.B., Vernardis, S.I., Lilley, K.S. & Ralser, M. DIA-NN: neural networks and interference correction enable deep proteome coverage in high throughput. *Nat Methods* **17**, 41-44 (2020).
211. Stratton, K.G.*, et al.* pmartR: Quality Control and Statistics for Mass Spectrometry-Based Biological Data. *J Proteome Res* **18**, 1418-1425 (2019).
212. Matzke, M.M.*, et al.* Improved quality control processing of peptide-centric LC-MS proteomics data. *Bioinformatics* **27**, 2866-2872 (2011).
213. Tyanova, S.*, et al.* The Perseus computational platform for comprehensive analysis of (prote)omics data. *Nat Methods* **13**, 731-740 (2016).
214. Shannon, P.*, et al.* Cytoscape: a software environment for integrated models of biomolecular interaction networks. *Genome Res* **13**, 2498-2504 (2003).

215. Bindea, G.*, et al.* ClueGO: a Cytoscape plug-in to decipher functionally grouped gene ontology and pathway annotation networks. *Bioinformatics* **25**, 1091-1093 (2009).
216. Mlecnik, B., Galon, J. & Bindea, G. Comprehensive functional analysis of large lists of genes and proteins. *J Proteomics* **171**, 2-10 (2018).
217. Ashburner, M.*, et al.* Gene ontology: tool for the unification of biology. The Gene Ontology Consortium. *Nat Genet* **25**, 25-29 (2000).
218. Gene Ontology, C. The Gene Ontology resource: enriching a GOld mine. *Nucleic Acids Res* **49**, D325-D334 (2021).
219. Kanehisa, M. & Goto, S. KEGG: kyoto encyclopedia of genes and genomes. *Nucleic Acids Res* **28**, 27-30 (2000).
220. Gillespie, M.*, et al.* The reactome pathway knowledgebase 2022. *Nucleic Acids Res* **50**, D687-D692 (2022).
221. UniProt, C. UniProt: the universal protein knowledgebase in 2021. *Nucleic Acids Res* **49**, D480-D489 (2021).
222. Liu, Y.*, et al.* Impact of Alternative Splicing on the Human Proteome. *Cell Rep* **20**, 1229-1241 (2017).
223. Zhang, Y.*, et al.* An RNA-sequencing transcriptome and splicing database of glia, neurons, and vascular cells of the cerebral cortex. *J Neurosci* **34**, 11929-11947 (2014).
224. Ren, P.*, et al.* Alternative Splicing: A New Cause and Potential Therapeutic Target in Autoimmune Disease. *Front Immunol* **12**, 713540 (2021).
225. Hecker, M.*, et al.* Aberrant expression of alternative splicing variants in multiple sclerosis - A systematic review. *Autoimmun Rev* **18**, 721-732 (2019).
226. Dozio, V. & Sanchez, J.C. Profiling the proteomic inflammatory state of human astrocytes using DIA mass spectrometry. *J Neuroinflammation* **15**, 331 (2018).
227. Wang, S.*, et al.* Synapsin I is an oligomannose-carrying glycoprotein, acts as an oligomannose-binding lectin, and promotes neurite outgrowth and neuronal survival when released via glia-derived exosomes. *J Neurosci* **31**, 7275-7290 (2011).
228. Taylor, X.*, et al.* Activated endothelial cells induce a distinct type of astrocytic reactivity. *Communications Biology* **5**(2022).
229. Jukkola, P.I., Lovett-Racke, A.E., Zamvil, S.S. & Gu, C. K+ channel alterations in the progression of experimental autoimmune encephalomyelitis. *Neurobiol Dis* **47**, 280-293 (2012).
230. Schirmer, L.*, et al.* Differential loss of KIR4.1 immunoreactivity in multiple sclerosis lesions. *Ann Neurol* **75**, 810-828 (2014).
231. Denstaedt, S.J.*, et al.* S100A8/A9 Drives Neuroinflammatory Priming and Protects against Anxiety-like Behavior after Sepsis. *J Immunol* **200**, 3188-3200 (2018).
232. Petzold, A.*, et al.* Markers for different glial cell responses in multiple sclerosis: clinical and pathological correlations. *Brain* **125**, 1462-1473 (2002).
233. Lauranzano, E.*, et al.* A Microfluidic Human Model of Blood-Brain Barrier Employing Primary Human Astrocytes. *Adv Biosyst* **3**, e1800335 (2019).